広島大学学位請求論文

Bulky substituents and solvent effects on the lifetime of singlet cyclopentane-1,3-diyls with π single bond character

(π単結合性をもつ一重項シクロペンタン-1, 3-ジラジカルの寿命に及ぼす嵩高い置換基と溶媒効果)

２０２１年

広島大学大学院理学研究科

化学専攻

秋坂　陸生

目　次

Hiromichi Aihara, Rikuo Akisaka, Toshiyuki Morikawa, Takeshi Fujita, Kie Yamakawa, Toshihiro Shimada, Junji Ichikawa, *J. Fluor. Chem.* 2017, *203*, 173-184.

③ Kinetic Stabilization of Localized Singlet Diradicaloids With π Single Bonding Character. Rikuo Akisaka and Manabu Abe, In *Kinetic Control in Synthesis and Self-Assembly*; Elsevier, 2019; 1-20.

④ Impact of the macrocyclic structure and dynamic solvent effect on the reactivity of a localised singlet diradicaloid with π-single bonding character. Zhe Wang, Rikuo Akisaka, Sohshi Yabumoto, Tatsuo Nakagawa, Sayaka Hatano and Manabu Abe, *Chem. Sci.* 2021. *12*, 613-625.

主論文

Bulky substituents and solvent effects on the lifetime of singlet cyclopentane-1,3-diyls with π single bond character

Department of Chemistry,

Graduate School of Science,

Hiroshima University

Rikuo, Akisaka

Contents

Chapter 1.
General Introduction

Section 1.1. Influence of the novel π functional system; π single bond

Organic functional molecules generally have specific π electron systems. For example, fullerene C_{60}, which is also called a buckminsterfullerene ball, has bent π bonds, although π bond is generally planer bonding character (Figure 1.1a). This curved bonding stabilized the molecular orbitals with the anti-bonding character because of low orbital interaction and sp^3 hybridization (Figure 1.1b).[1] So, fullerenes have low LUMO (lowest unoccupied molecular orbital) energy. They were applied to reactant as an electrophile,[2,3] organic semiconductor in material science,[4,5] and guest molecule with electron-rich host molecule for supramolecular chemistry.[6,7] Linearly fused benzene rings, acenes, are another example which is actively studying in physical organic chemistry (Figure 1.1c). Increasing the benzene conjugation increases the HOMO (highest occupied molecular orbital) energy and decrease the LUMO energy. From this feature, analogs of acene were used in material science like p-type semiconductor[8,9] or singlet oxygen sensor.[10] Because the π systems are essential for a characteristic of the organic molecule. It is crucial to create a new concept of the π electron system and investigate the electronic character of that to develop organic materials.

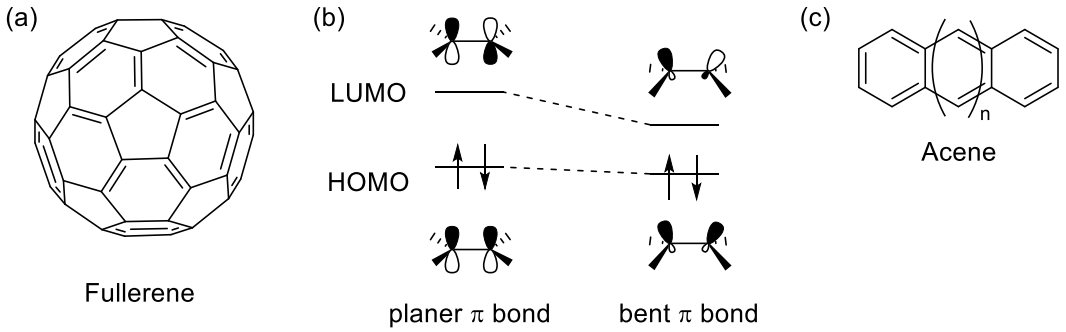

Figure 1.1. Selected example of functional π systems. (a) Molecular structure of fullerene. (b) Bending effect on the frontier orbital. (c) General formula of acene.

The smallest π system, ethylene, has two types of bond: σ bond, which is along with the bond axis, and π bond, which is perpendicular to ethylene's plane. The C-C bond length in ethylene and its analogs was around 1.3 angstroms because there is a rigid σ bond.[11] If we can generate the π bond without a σ bond, which is called π single bonding, it should be a new concept for organic chemistry. A smaller HOMO-LUMO gap would be achieved in a π single bond than a π bond with a σ bond in the same carbon number because the overlap of orbital was weakened (Figure 1.2).[12]

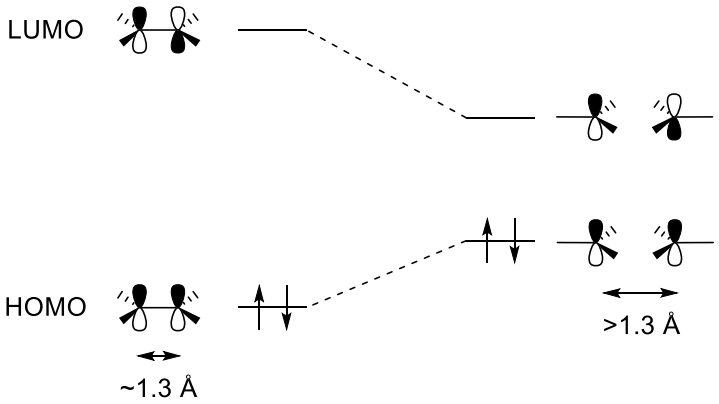

Figure 1.2. The concept of π single bonding.

Section 1.2. The chemistry of localized diradicals

The π single bond species were regarded as two methyl radicals with bonding character in HOMO and anti-bonding character in LUMO. So, localized diradicals, which have two radicals in one molecule, would be the π single bonding molecule candidate. In localized diradical species, there are three types of electron configuration (Figure 1.3), triplet species, singlet species having bonding character in HOMO (Type-1), and singlet species having anti-bonding character in HOMO (Type-2).[13]

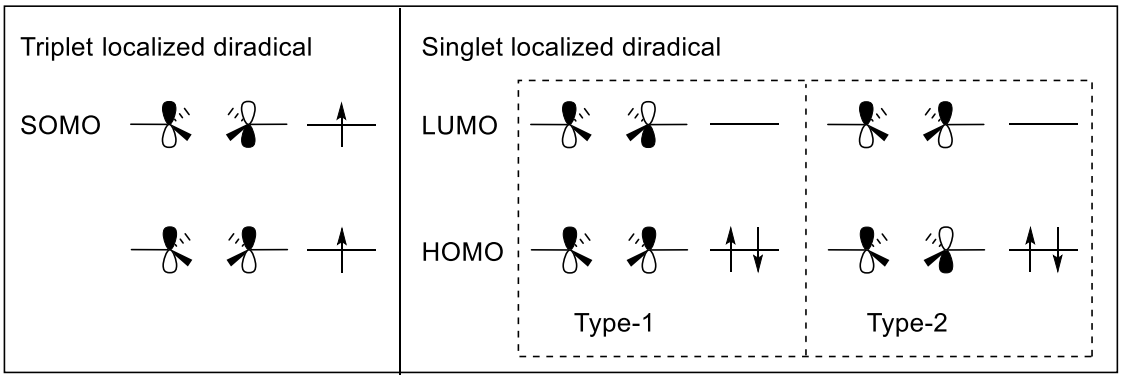

Figure 1.3. Most stable electronic configuration of three types of localized diradicals.

There are many studies on the manipulation of electron configuration in the ground state of localized diradical in both theoretical and experimental chemistry.[14–19] In particular, 1,3-diradical in four or five-membered cyclic systems were studied by many chemists. When two p orbitals on radical carbons of 1,3-diradical interact, the molecular orbitals were divided into two types (Figure 1.4a), bonding character orbital (ψ_s) and anti-bonding character orbital (ψ_a). By through-space interaction, ψ_s was stabilized than p orbital of isolated carbon radical, and ψ_a was destabilized. If we only consider through space interaction, all 1,3-diradical were regarded as Type-1 singlet ground state. However, there is another type of interaction, through bond interaction. If we introduce the electron-donating group (EDG) at C2 carbon, ψ_s orbital interacted with

pseudo p orbital formed by $\sigma_{C\text{-}EDG}$, and it is destabilized. The energy level of ψ_s increased, and two electrons from the p orbital of two radicals were selectively entered in ψ_a orbitals. So, Type-2 singlet diradical, which has an anti-bonding character in HOMO, was generated by introducing strong EDG, such as silicon, at C2 carbon. If we introduce the weak EDG groups, like hydrogen or carbon, the destabilization of ψ_s was small. And diradical would have triplet ground state. Introducing the electron-withdrawing group (EWG) at C2 carbon, ψ_s orbital was stabilized by the interaction with pseudo p orbital consisting of $\sigma^*_{C\text{-}EWG}$ orbital (Figure 1.4b). Because of this, 1,3-diradicals having EWGs at C2 position are Type-1 singlet ground state and candidate for the π single bond molecules.

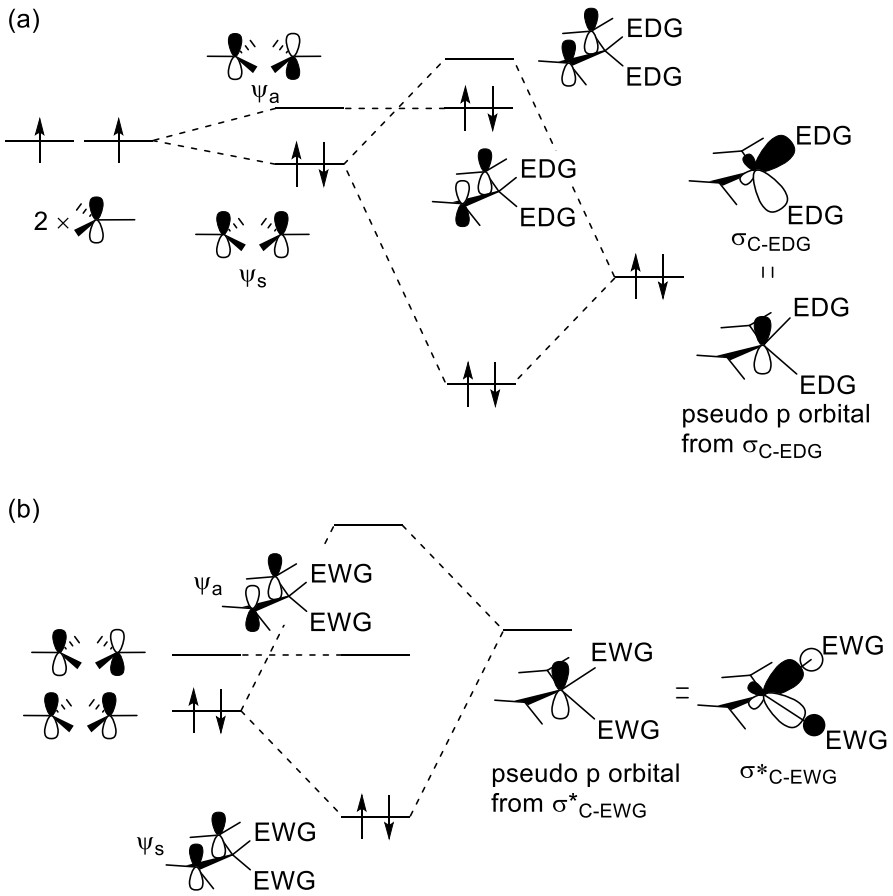

Figure 1.4. The energy diagram for molecular orbital of 1,3-diradical explaining (a) through space interaction and through-bond interaction with $\sigma_{C\text{-}EDG}$ (b) through bond interaction with $\sigma^*_{C\text{-}EWG}$.

These theoretical understandings were experimentally demonstrated. Closs and Dougherty detected triplet 1,3-diradical under low matrix condition (Figure 1.5a).[20,21] The generation of Type-2 singlet diradical was conducted by not only the introduction of an electron-donating group at C2 position but also the replacement of C2 carbon to hetero atom, such as phosphorus. Same to pseudo p orbital, the lone pair of hetero atom interacts with ψ_s orbital, and the energy level of ψ_s was risen up (Figure 1.5c). Finally, 1,3-diradicals **A** with phosphorus atom at 2nd and 4th position in cyclobutene-1,3-diyls became singlet ground state diradical in Type-2, isolated by Niecke for the first time (Figure 1.5b).[22] By the almost same concept, isolable Type-2 singlet diradicals were synthesized by Yoshifuji, Sekiguchi, Power, Lappert, and Schulz.[23–30]

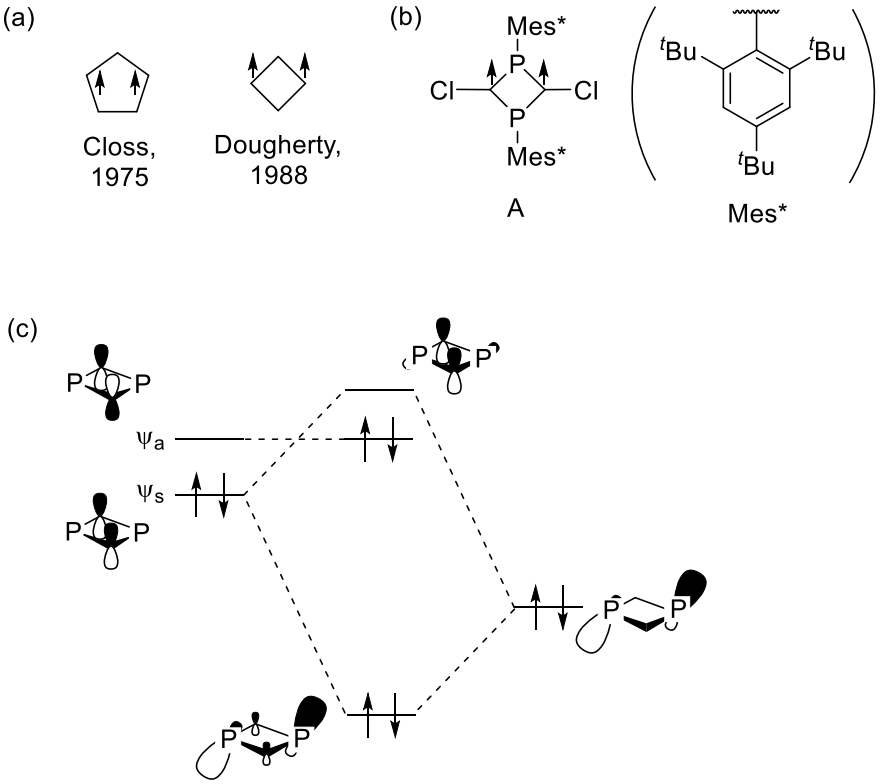

Figure 1.5. (a) Detected example of 1,3-diradicals as triplet ground state. (b) The first example of isolable localized singlet diradical: 1,3-dipphospha-cyclobutane-2,4-diyls **A**. (c) The energy diagram of molecular orbital for **A**.

Several groups, including our laboratory, also studied the singlet diradicals of Type-1. The isolation of Type-1 diradical was challenging because the bond formation process of 1,3-diradical in Type-1 is the allowed disrotatory motion.[17] In contrast to Type-1 diradical, the closing motion was suppressed for Type-2 diradical structurally because it should be the conrotatory ring-closing reaction. Against this backdrop, Bertrand and his co-worker succeeded in synthesizing 1,3-dibora-2,4-diphospha-cyclobutane-1,3-diyls **B** (Figure 1.6a) using phosphonium cation and borate radical, which is isoelectronic to carbon radical.[31] In this molecule, pseudo p orbital from $\sigma^*_{P\text{-}C}$ makes the 1,3-diradical to Type-1 singlet (Figure 1.6b). Bulky substituents at boron and phosphine atoms and the minus charge localized at boron atoms suppressed the bond formation between boron atoms. From this report, the Type-1 diradical species, Al_2P_2, Ge_2Ga_2, and Si_4 were discovered (Figure 1.6c).[32–36] Nevertheless, the radical atoms were changed to hetero atom in all the isolable compounds, so isolation of the ethylene's pure π single bond is not succeeded.

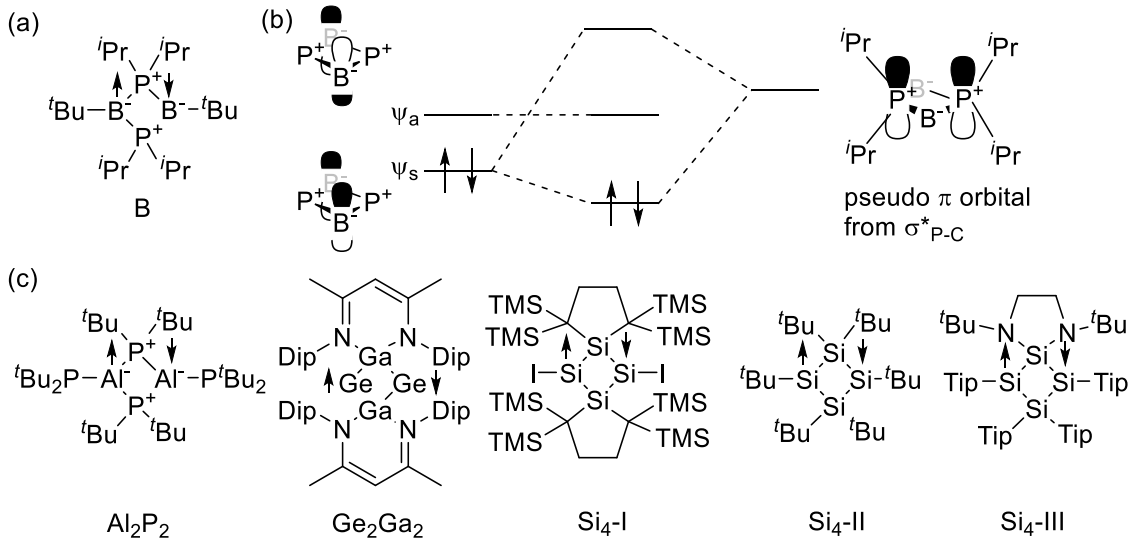

Figure 1.6. (a) The first example of isolable Type-1 singlet diradical, 1,3-dibora-2,4-diphospha-cyclobutane-1,3-diyls **B**. (b) The energy diagram of the molecular orbital for compounds **B**. (c) Isolable singlet diradicals which has bonding interaction between radical centers in HOMO. (Dip: 2,6-diisopropyl phenyl, TMS: trimethylsilyl, Tip: 2,4,6-triisopropyl phenyl)

Section 1.3. The chemistry of carbon-based localized singlet diradicals

Our laboratory also contributes to developing π single bond species by the 2,2-dialkoxy-cyclopentane-1,3-diyls, which is Type-1 singlet diradical tuned by introducing electron-deficient oxygen atoms at the C2 position.[17] Photo-denitrogenation reaction of azo alkane **AZ1a**, in which two radical carbons were connected by azo moiety, generates the singlet cyclopentane-1,3-diyls S-**DR1a** (Scheme 1.1 and Table 1.1). Detection of singlet diradicals S-**DR1a** was conducted by low-temperature matrix technics or transient absorption spectroscopy. The HOMO-LUMO absorption of S-**DR1a** corresponds to π-π* transition of the π single bond was observed at around 570 nm, significantly redshifted than π-π* transition of *trans*-stilbene, which is less than 340 nm.[37] The singlet diradical S-**DR1a** were transient species at room temperature and went to ring closure product **CP1a**.

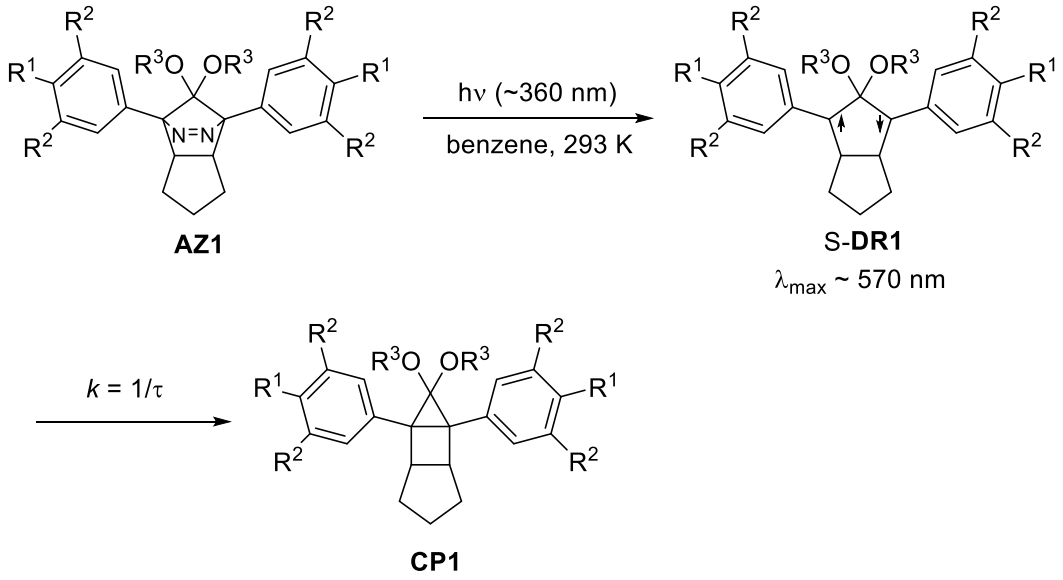

Scheme 1.1. The generation of singlet diradical S-**DR1** from **AZ1.**

Table 1.1. The effect of substitution R^{1-3} on the lifetime of S-**DR1.**

S-**DR1**	R^1	R^2	OR^3	τ_{293} / μs
S-**DR1a**	H	H	OCH_3	292
S-**DR1b**	CN	H	OCH_3	625
S-**DR1c**	OMe	H	OCH_3	1050
S-**DR1d**	H	H	$O^nC_3H_7$	1899
S-**DR1e**	H	H	$O^nC_6H_{13}$	2292
S-**DR1f**	H	H	$O^nC_{10}H_{21}$	2146
S-**DR1g**	H	OMe	OCH_3	580
S-**DR1h**	H	OMe	OCH_2Ar^*	5384

Ar*:3,5-dimethoxybenzene

Several challenges were conducted to get singlet diradical S-**DR1** with a longer lifetime in our laboratory. There are two types of methodology for stabilizing these highly labile molecules: thermodynamic stabilization and kinetic stabilization. Thermodynamic stabilization means that substituents electronically stabilize the reactive molecule selectively, and this causes the increase of the activation energy (Figure 1.7a). There are several examples of thermodynamic stabilization of unusual molecules such as carbodiphosphorane or dithieno[a,e]pentalene (Figure 1.7b).[38,39] Thermodynamic stabilization of 2,2-dialkoxy-cyclopentane-1,3-diyls was also conducted. Substituting the phenyl ring at the para position, such as S-**DR1b**,**c** in Table 1.1, or introducing nitrogen atoms at 4,5 position of cyclopentane-1,3-diyls, i.e. diradical **C** (in Figure 1.7b), extends the lifetime of diradical structure.[40,41]

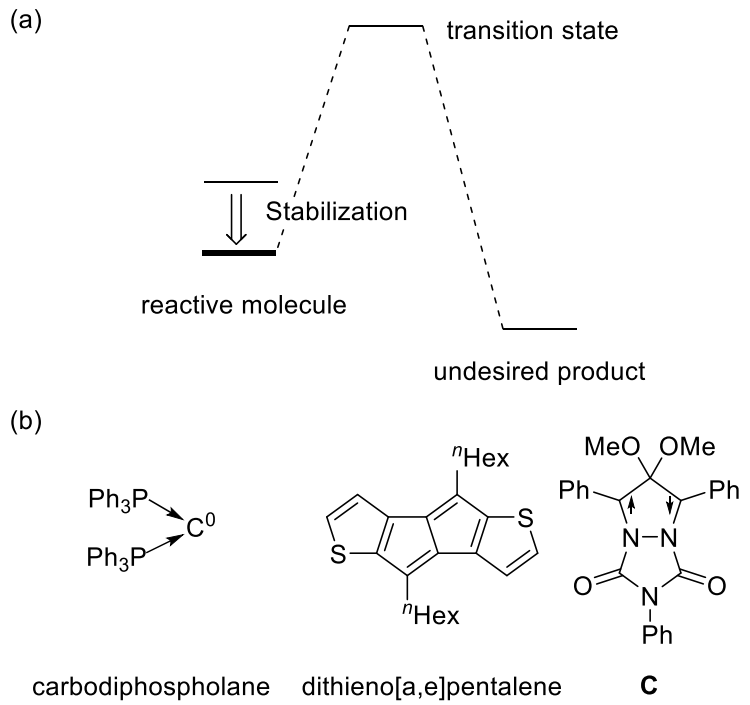

Figure 1.7. (a) The concept of thermodynamic stabilization. (b) the example of the thermodynamically stabilized reactive molecule.

On the other hand, the kinetic stabilization does not change the electronic configuration of the molecules. But it destabilizes the transition state and/or product using a steric hindrance (Figure 1.8a). As a result, the molecule was stabilized than the transition state or the product, relatively. The kinetic stabilization was an effective method for studying the unusual molecule because the molecule's reactivities or electronic features were maintained. So, the kinetic stabilization was developed to study low-valent main group element compounds and delocalized diradicals (Figure 1.8b).[42,43]

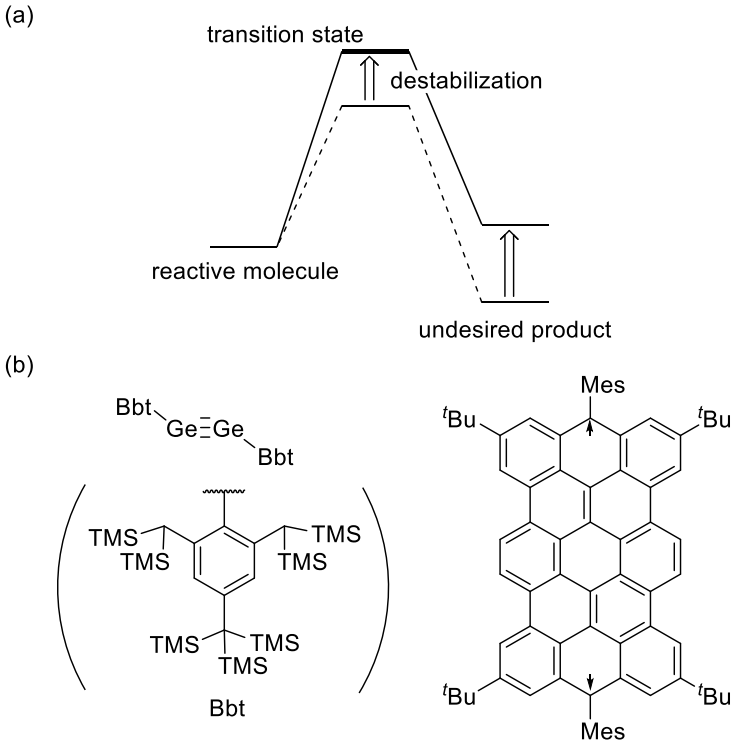

Figure 1.8. (a) The concept of the kinetic stabilization. (b) The selected example of the kinetically stabilized unusual molecule. (TMS: trimethylsilyl, Mes: 2,4,6-trimethyl-phenyl)

The kinetic stabilization of 2,2-dialkoxy-cyclopentane-1,3-diyls was also conducted by extending the alkoxy group (S-**DR1d**-**f**) or the replacement of the phenyl group at 1,3-position to 3,5-dimethoxy benzene (S-**DR1g**, **h**).[44,45] These studies suggest that the steric repulsion between the alkoxy group and the phenyl group determines the radical-radical coupling reaction's activation energy (Figure 1.9). The stretch effect is another example of the kinetic stabilization of cyclopentane-1,3-diyls (Figure 1.10). In recent years, singlet diradical **D**, **E**, which has ten or hundred microseconds timescale lifetime, appeared using benzene or naphthalene as the stretch unit.[46,47] Nevertheless, the lifetimes of singlet diradical were still microseconds order. To confirm the π single bonding character of singlet diradical S-**DR1** by nuclear magnetic resonance or X-ray diffraction analysis, the lifetime of singlet diradical in second-order is needed.

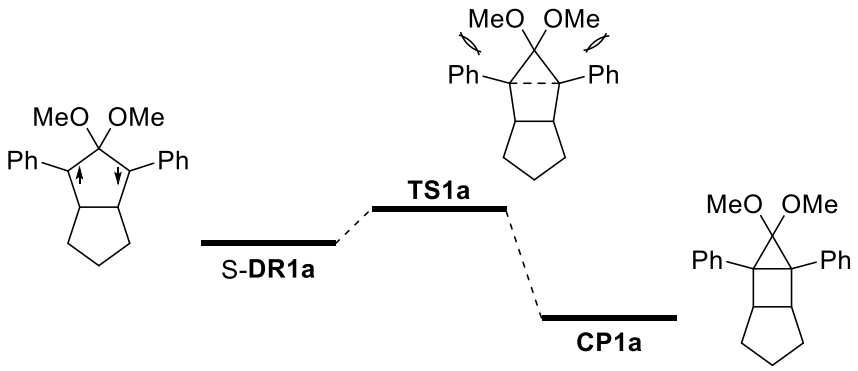

Figure 1.9. The plausible illustration for determining the lifetime of singlet diradical S-**DR1a** by the steric repulsion between methoxy groups and phenyl rings.

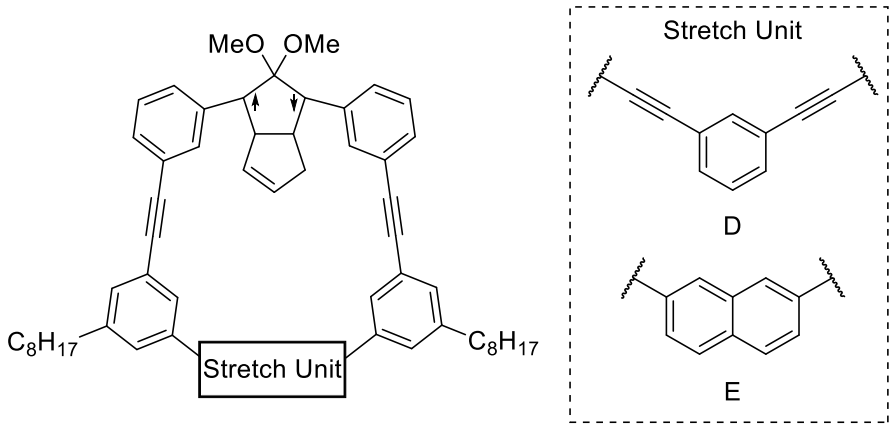

Figure 1.10. The example of singlet-cyclopentane-1,3-diyls stabilized by the stretch effect.

Section 1.4. The strategy of this thesis

In the previous study for expanding the alkoxy group, OR^3 group in singlet diradical S-**DR1**, there is the limitation for extending the lifetime of singlet diradical (S-**DR1g**, **f**). However, the influence of the bulkiness of the R^2 group, the meta position of the aryl group in S-**DR1**, on the lifetime of that was less studied. It was expected that the steric repulsion between not only the aryl group and alkoxy group but two bulky aryl groups in the transition state affect to determine the lifetime of singlet diradical. In other words, longer-lived singlet diradical should be generated by introducing the bulky substituents at the meta position of the aryl group in singlet diradicals. The theoretical and experimental studies in mainly benzene solution for bulky substituted singlet diradical were presented in chapter 2.[48] These studies concluded the bulky substituents in aryl groups succeeded in the kinetic stabilization of singlet diradical; however, it still goes bond forming between two radicals. In the later chapter, the solvent and pressure effect on the lifetime of singlet diradical having bulky substituents were investigated.[49] These results emphasize the importance of molecular motion and solvent motion in intramolecular reactions.

Reference

1 L. T. Scott, H. E. Bronstein, D. V. Preda, R. B. M. Ansems, M. S. Bratcher and S. Hagen, *Pure Appl. Chem.*, 1999, **71**, 209–219.

2 M. Yamada, T. Akasaka and S. Nagase, *Chem. Rev.*, 2013, 113, 7209–7264.

3 J. B. Briggs and G. P. Miller, *Comptes Rendus Chim.*, 2006, 9, 916–927.

4 C. L. Chochos, N. Tagmatarchis and V. G. Gregoriou, *RSC Adv.*, 2013, **3**, 7160.

5 D. M. Guldi, B. M. Illescas, C. M. Atienza, M. Wielopolski and N. Martín, *Chem. Soc. Rev.*, 2009, **38**, 1587.

6 F. Diederich and M. Gómez-López, *Chem. Soc. Rev.*, 1999, **28**, 263–277.

7 D. V. Konarev, S. S. Khasanov and R. N. Lyubovskaya, *Coord. Chem. Rev.*, 2014, 262, 16–36.

8 J. E. Anthony, *Angew. Chem. Int. Ed.*, 2008, **47**, 452–483.

9 P. Hu, J. Ye and H. Jiang, *J. Mater. Chem. C*, 2019, **7**, 5858–5873.

10 V. Brega, Y. Yan and S. W. Thomas, *Org. Biomol. Chem*, 2020, **18**, 9191.

11 N. C. Craig, P. Groner and D. C. McKean, *J. Phys. Chem. A*, 2006, **110**, 7461–7469.

12 M. Abe and R. Akisaka, *Chem. Lett.*, 2017, **46**, 1586–1592.

13 M. Abe, *Chem. Rev.*, 2013, **113**, 7011–7088.

14 R. Hoffmann, *Acc. Chem. Res.*, 1971, **4**, 1–9.

15 A. H. Goldberg and D. A. Dougherty, *J. Am. Chem. Soc.*, 1983, **105**, 284–290.

16 W. Thatcher Borden, *Effects of electron donation into C-F s* orbitals: explanations, predictions and experimental tests*, 1998.

17 M. Abe, J. Ye and M. Mishima, *Chem. Soc. Rev.*, 2012, **41**, 3808–3820.

18 W. W. Schoeller and E. Niecke, *Phys. Chem. Chem. Phys.*, 2012, **14**, 2015–2023.
19 W. W. Schoeller, *Eur. J. Inorg. Chem.*, 2019, **2019**, 1495–1506.
20 S. L. Buchwalter and G. L. Closs, *J. Am. Chem. Soc.*, 1975, **97**, 3857–3858.
21 R. Jain, M. B. Sponsler, F. D. Coms and D. A. Dougherty, *J. Am. Chem. Soc.*, 1988, **110**, 1356–1366.
22 E. Niecke, A. Fuchs, F. Baumeister, M. Nieger and W. W. Schoeller, *Angew. Chem. Int. Ed.*, 1995, **34**, 555–557.
23 H. Sugiyama, S. Ito and M. Yoshifuji, *Angew. Chem. Int. Ed.*, 2003, **42**, 3802–3804.
24 K. Takeuchi, M. Ichinohe and A. Sekiguchi, *J. Am. Chem. Soc.*, 2011, **133**, 12478–12481.
25 C. Cui, M. Brynda, M. M. Olmstead and P. P. Power, *J. Am. Chem. Soc.*, 2004, **126**, 6510–6511.
26 X. Wang, Y. Peng, M. M. Olmstead, J. C. Fettinger and P. P. Power, *J. Am. Chem. Soc.*, 2009, **131**, 14164–14165.
27 H. Cox, P. B. Hitchcock, M. F. Lappert and L. J. M. Pierssens, *Angew. Chem. Int. Ed.*, 2004, **43**, 4500–4504.
28 A. Hinz, R. Kuzora, U. Rosenthal, A. Schulz and A. Villinger, *Chem. Eur. J.*, 2014, **20**, 14659–14673.
29 A. Hinz, A. Schulz and A. Villinger, *Angew. Chem. Int. Ed.*, 2015, **54**, 2776–2779.
30 A. Hinz, A. Schulz and A. Villinger, *J. Am. Chem. Soc.*, 2015, **137**, 9953–9962.
31 D. Scheschkewitz, H. Amii, H. Gornitzka, W. W. Schoeller, D. Bourissou and G. Bertrand, *Science (80-.).*, 2002, **295**, 1880–1881.
32 P. Henke, T. Pankewitz, W. Klopper, F. Breher and H. Schnöckel, *Angew. Chem. Int. Ed.*, 2009, **48**, 8141–8145.
33 A. Doddi, C. Gemel, M. Winter, R. A. Fischer, C. Goedecke, H. S. Rzepa and G. Frenking, *Angew. Chem. Int. Ed.*, 2013, **52**,

450–454.
34 T. Nukazawa and T. Iwamoto, *J. Am. Chem. Soc.*, 2020, **142**, 9920–9924.
35 S. Kyushin, Y. Kurosaki, K. Otsuka, H. Imai, S. Ishida, T. Kyomen, M. Hanaya and H. Matsumoto, *Nat. Commun.*, 2020, **11**, 4009.
36 C. B. Yildiz, K. I. Leszczyńska, S. González-Gallardo, M. Zimmer, A. Azizoglu, T. Biskup, C. W. M. Kay, V. Huch, H. S. Rzepa and D. Scheschkewitz, *Angew. Chem. Int. Ed.*, 2020, **59**, 15087–15092.
37 M. Oelgemöller, B. Brem, R. Frank, S. Schneider, D. Lenoir, N. Hertkorn, Y. Origane, P. Lemmen, J. Lex and Y. Inoue, *J. Chem. Soc. Perkin Trans. 2*, 2002, **2**, 1760–1771.
38 F. Ramirez, N. B. Desai, B. Hansen and N. McKelvie, *J. Am. Chem. Soc.*, 1961, **83**, 3539–3540.
39 J. Usuba, M. Hayakawa, S. Yamaguchi and A. Fukazawa, *Chem. – A Eur. J.*, 2020, chem.202004244.
40 M. Abe, W. Adam, M. Hara, M. Hattori, T. Majima, M. Nojima, K. Tachibana and S. Tojo, *J. Am. Chem. Soc.*, 2002, **124**, 6540–6541.
41 S. Yoshidomi and M. Abe, *J. Am. Chem. Soc.*, 2019, **141**, 3920–3933.
42 Y. Sugiyama, T. Sasamori, Y. Hosoi, Y. Furukawa, N. Takagi, S. Nagase and N. Tokitoh, *J. Am. Chem. Soc.*, 2005, **128**, 1023–1031.
43 A. Konishi, Y. Hirao, M. Nakano, A. Shimizu, E. Botek, B. Champagne, D. Shiomi, K. Sato, T. Takui, K. Matsumoto, H. Kurata and T. Kubo, *J. Am. Chem. Soc.*, 2010, **132**, 11021–11023.
44 T. Nakagaki, T. Sakai, T. Mizuta, Y. Fujiwara and M. Abe, *Chem. Eur. J.*, 2013, **19**, 10395–10404.
45 J. Ye, Y. Fujiwara and M. Abe, *Beilstein J. Org. Chem.*, 2013, **9**,

925–933.
46 Y. Harada, Z. Wang, S. Kumashiro, S. Hatano and M. Abe, *Chem. Eur. J.*, 2018, **24**, 14808–14815.
47 Z. Wang, R. Akisaka, S. Yabumoto, T. Nakagawa, S. Hatano and M. Abe, *Chem. Sci.*, 2021. **12**, 613–625.
48 R. Akisaka and M. Abe, *Chem. – An Asian J.*, 2019, **14**, 4223–4228.
49 R. Akisaka, Y. Ohga and M. Abe, *Phys. Chem. Chem. Phys.*, 2020, **22**, 27949–27954.

Chapter 2.

Bulky substituents effect on the lifetime of the singlet cyclopentane-1,3-diyls

Section 2.1. Introduction to this chapter

First, the author summarizes the reactivity of parent singlet 2,2-dialkoxy-cyclopentane-1,3-diyls S-**DR1a**.[1] The S-**DR1a** has an extra cyclopentane ring, so there are two reaction paths and products for the radical bond formation process (Scheme 2.1). One is the *trans* configuration between the extra cyclopentane ring and cyclopropane rings, *trans*-**CP1a**. Another one is a *cis*-configured bond formation, *cis*-**CP1a**. Several studies are conducted to confirm the reaction path, such as the determination of activation parameters for the decay of S-**DR1a**, the difference between the effect of the alkoxy groups R^3 and $R^{3'}$ on the lifetimes of S-**DR1**, the product analysis of photoreaction of **AZ1** at room temperature and low temperature, and the theoretical calculations.[2,3] And these results suggest that the rapid radical bond formation generates *cis*-**CP1a** as the kinetic product. It is easily isomerized to *trans*-**CP1a** at room temperature via S-**DR1a**.

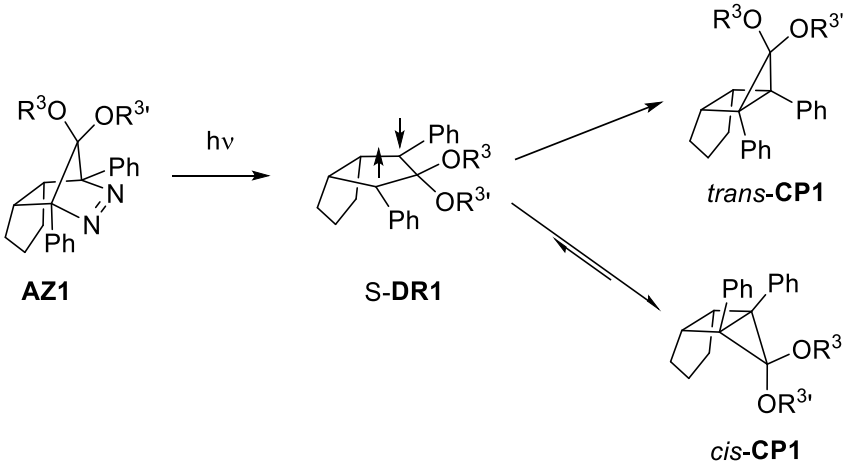

Scheme 2.1. The reactivity of S-**DR1**

To evaluate the effect of bulky substituents at the aryl groups' meta position on the reactivity of singlet diradicals, similar study was conducted for the corresponding diradicals S-**DR2-4** in this chapter (Figure 2.1).[4] In section 2.2, theoretical calculations were discussed to clarify the steric

effect on the singlet diradical S-**DR2**. The synthesis of the precursor **AZ3**,**4** was described in section 2.3. Section 2.4 mentioned the generation and the reactivity of S-**DR3**,**4** at room temperature, around 293 K. The isomerization of *cis*-**CP4e** to *trans*-**CP4e** was investigated in section 2.5.

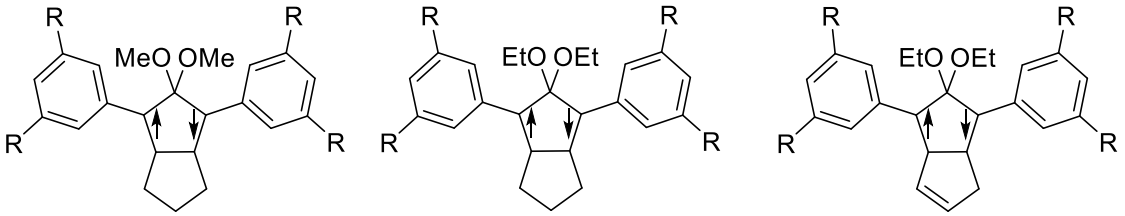

S-**DR2** S-**DR3** S-**DR4**

Figure 2.1. The chemical structure of S-**DR2**-**4**.

Section 2.2. Theoretical investigation for the effect of the bulky substituents at meta position on the stabilization of singlet diradicals

Theoretical calculations of S-**DR2** were conducted to elucidate the effect of the introduction of bulky substituents at the phenyl ring's meta-position for the singlet diradical's reactivities. In the previous study, the DFT calculation results at UB3LYP/6-31G(d) level with broken-symmetry methods were consistent with the experimental results.[2,3] So, the calculations were conducted at the same level. The structure optimizations were conducted for the diradicals with singlet or triplet state S/T-**DR2** and ring-closing isomers, **CP2**. Following section 2.1, the ring-closing isomers were called as *trans*-**CP2** and *cis*-**CP2**. The transition states from singlet diradicals to the ring-closing product were also optimized as *trans*-**TS2** and *cis*-**TS2**, respectively. The bromine (Br), methoxy (OMe), mesityl (Mes), and triisopropyl phenyl (Tip) groups were examined as the bulky substituents at the meta position of singlet diradicals S-**DR2**. The electronic energy differences from singlet diradical isomer with zero-point correlation were summarized in Table 2.1 (see next page).

In all cases, diradical structures were optimized as singlet ground state. These results were consistent with the electron-withdrawing atom effect at the C2 position. Although the most stable isomers were *trans*-**CP2**, the energies of *cis*-**TS2** were lower than that of *trans*-**TS2** in all cases. In the ring closure molecules, the extra cyclopentane ring and methoxy group's steric repulsion causes *cis*-**CP2** destabilization. For the transition state structures, the steric interaction between the aryl groups and the extra cyclopentane ring in *trans*-**TS2** is more significant than that in *cis*-**TS2**. These relative energy diagrams of the non-substituted case are agreed with the experimental results, discussed in section 2.1.

Table 2.1. Electronic energy difference ΔE including zero-point energy corrections between **CP2**/**TS2** and S-**DR2** at the (U)B3LYP/6-31G(d) level of theory.

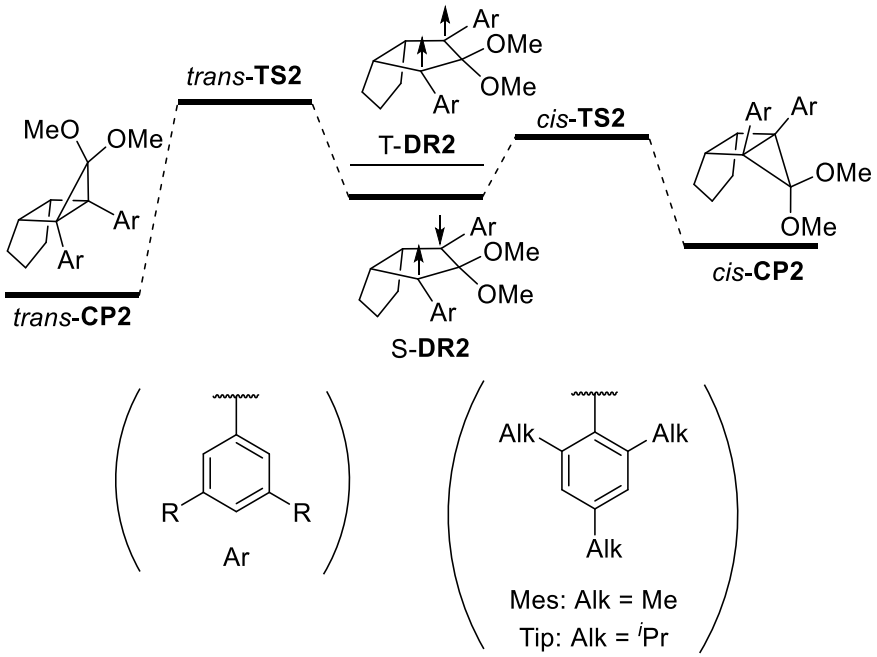

S-**DR**	R =	T-**DR2**	*trans*-**CP2**	*cis*-**CP2**	*trans*-**TS2**	*cis*-**TS2**
2a	H	9.03	-28.4	-12.8	66.6	46.4
2b	Br	7.71	-28.5	-13.0	69.2	46.0
2b	OMe	9.45	-38.0	-10.5	69.6	50.4
2d	Mes	8.28	-31.1	-5.96	66.2	47.9
2e	Tip	8.61	-22.3	1.73	69.6	51.1

When we pay attention to the difference of substituents R, the introduction of Tip groups increases both transition state *trans*-**TS2** and *cis*-**TS2**. Furthermore, one of the ring-closing products, *cis*-**CP2e**, was estimated almost same energy as singlet diradical, S-**DR2e**. This result encouraged Tip substituted diradical generation to observe the equilibrium between the S-**DR2e** and *cis*-**CP2e** and/or another radical bond formation path via *trans*-**TS2e** at room temperature.

In the last twenty years, several functionals were developed to solve a big problem for the reproducibility of energy by quantum calculation using B3LYP methods. There is stabilizing interaction between molecules

or substituents, which is increased by increasing the mass, and it was called the dispersion force.[5–9] Because the dispersion forces were not included in the B3LYP function, several researchers reported the steric repulsion calculated by this function was overestimated than the experiment. Mostly the reaction site has bulky substituents; this problem gets serious. To include the dispersion force to B3LYP function as empirical parameters, Grimme developed B3LYP-D3 and B3LYP-D3BJ functions. In the B3LYP-D3 function, the dispersion forces were inserted as stabilization energy proportional to R^{-6}, in which R is the distance between two atoms.[10] The B3LYP-D3BJ function is modifying the B3LYP-D3 function to make stabilize energy flat if the atoms' distance was less than the decided length.[11]

To reflect the dispersion force in the ring-closing reaction of S-**DR2a**,**d**,**e**, the energy calculations at B3LYP-D3 and B3LYP-D3BJ functional were conducted for optimized structures of S-**DR2a**,**d**,**e** and their isomers at B3LYP functional. Tables 2.2 presents the energy difference between S-**DR2** and isomers in B3LYP-D3 and B3LYP-D3BJ function after zero-point correction, which were obtained by the frequency calculation at the B3LYP function. The parent diradical, S-**DR2a**, shows almost no difference between these functionals. However, the energy differences between *cis*/*trans*-**CP2** and S-**DR2** for Mes or Tip substituted diradicals were highly affected by the dispersion correlation.

Table 2.2. The energy differences calculated at B3LYP-D3/6-31G(d) level and B3LYP-D3BJ/6-31G(d) level in parenthesis between S-**DR2a**,**d**,**e,** and their isomers including the zero point energy correlation obtained at B3LYP/6-31G(d) level.

S-**DR**	*trans*-**CP2**	*cis*-**CP2**	*trans*-**TS2**	*cis*-**TS2**
2a	-28.6 (-23.4)	-14.1 (-8.01)	67.1 (69.9)	46.8 (50.9)
2d	-50.8 (-45.1)	-21.9 (-15.7)	63.6 (66.5)	49.1 (53.5)
2e	-56.5 (-50.6)	-26.5 (-20.3)	64.7 (67.8)	48.6 (53.4)

To investigate the effect of ortho substitution of aryl groups for kinetic stabilization of diradical, the structure optimizations of **DR2d'** were also conducted for singlet and triplet state of diradical and ring-closing product, *trans*-**CP2d'** and *cis*-**CP2d'** at B3LYP/6-31G(d) theory (Figure 2.2). Compared to S-**DR2a**, the energy differences between diradical and *trans*- or *cis*-**CP2d'** were increased. This result was explained by the steric repulsion between the methyl group at the aryl group's ortho position and the methoxy group or extra cyclopentane ring (Figure 2.3). The dihedral angle between aryl group and cyclopentane-1,3-diyl moiety in the optimized structure of S-**DR2d'** were around 48°, but that of the non-substituted case, S-**DR2a**, was almost 0°. The mentioned dihedral angle should be 0° to stabilize the singlet diradical by the resonance effect of attached phenyl ring. From this result, the introduction of ortho-substituted aryl groups was not conducted in the synthesis.

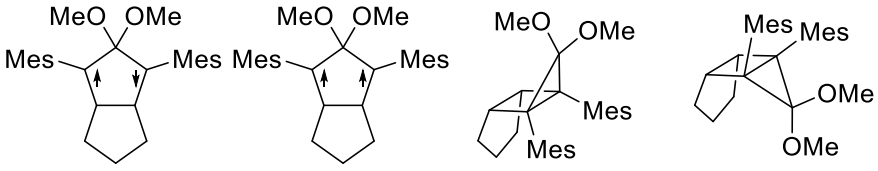

S-**DR2d'** (0.00) | T-**DR2d'** (19.0) | *trans*-**CP2d'** (-74.2) | *cis*-**CP2d'** (-63.3)

Figure 2.2. The structure of S-**DR2d'** and its isomers. The parentheses value presents the energy difference between the S-**DR2d'** and its isomers calculated at B3LYP/6-31G(d) level.

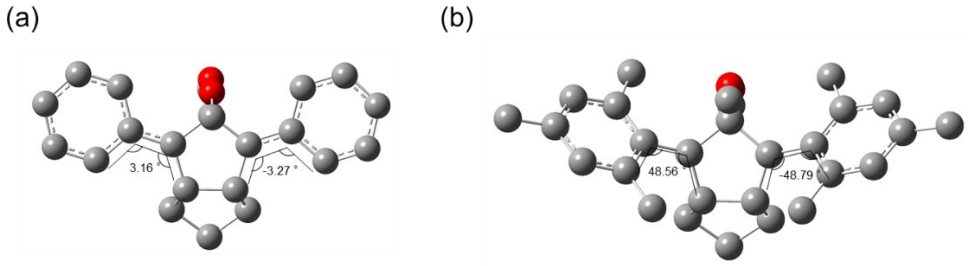

Figure 2.3. The optimized structure of (a) S-**DR2a** and (b) S-**DR2d'**.

Section 2.3. Synthesis of the azo precursor **AZ3**,**4**

From the theoretical calculations, the target diradical was determined to Tip substituted one. So, the synthesis of the azoalkane precursor **AZ2e** (R = Tip) was conducted. There are roughly two routes of the synthesis of bulky substituted azo compounds; one route is started from the synthesis of bulky substituted aryl group and then construct the azo moiety (route A in Scheme 2.2); another route is the last introduction of bulky groups by cross-coupling reaction after synthesis of tetra-halogenated azo compounds (route B). Because route A seems hard to change the R group, route B was adopted for Mes or Tip substituted azoalkanes.

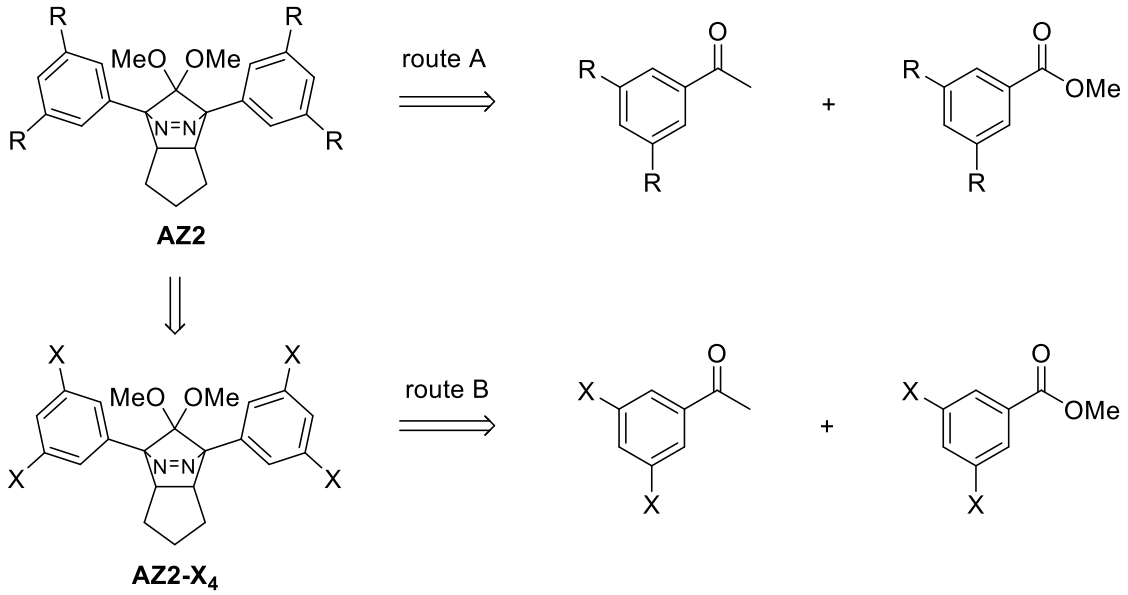

Scheme 2.2. Retro synthesis of target **AZ2** (R = bulky groups, X = halogen).

The brominated azo alkane **AZ2-Br$_4$** was chosen for the tetra halogenated azo compounds because the introduction of bromine is more comfortable than that of iodine and the reactivity of brominated arene is higher than that of the chlorinated arene. The 3,5-dibromo acetophenone and 3,5-dibromo benzoic acid methyl ester were obtained by the two steps

from corresponding aniline (Scheme 2.3). By the Claisen condensation reaction, the **DK-Br4** was synthesized in 67% yields. To construct the azo moiety, the following methoxy substitution of alpha carbon of 1,3-diketone **DK-Br4** was conducted. However, the desired reaction did not proceed well. The reason for it would be the low solubility of the **DK-Br4**.

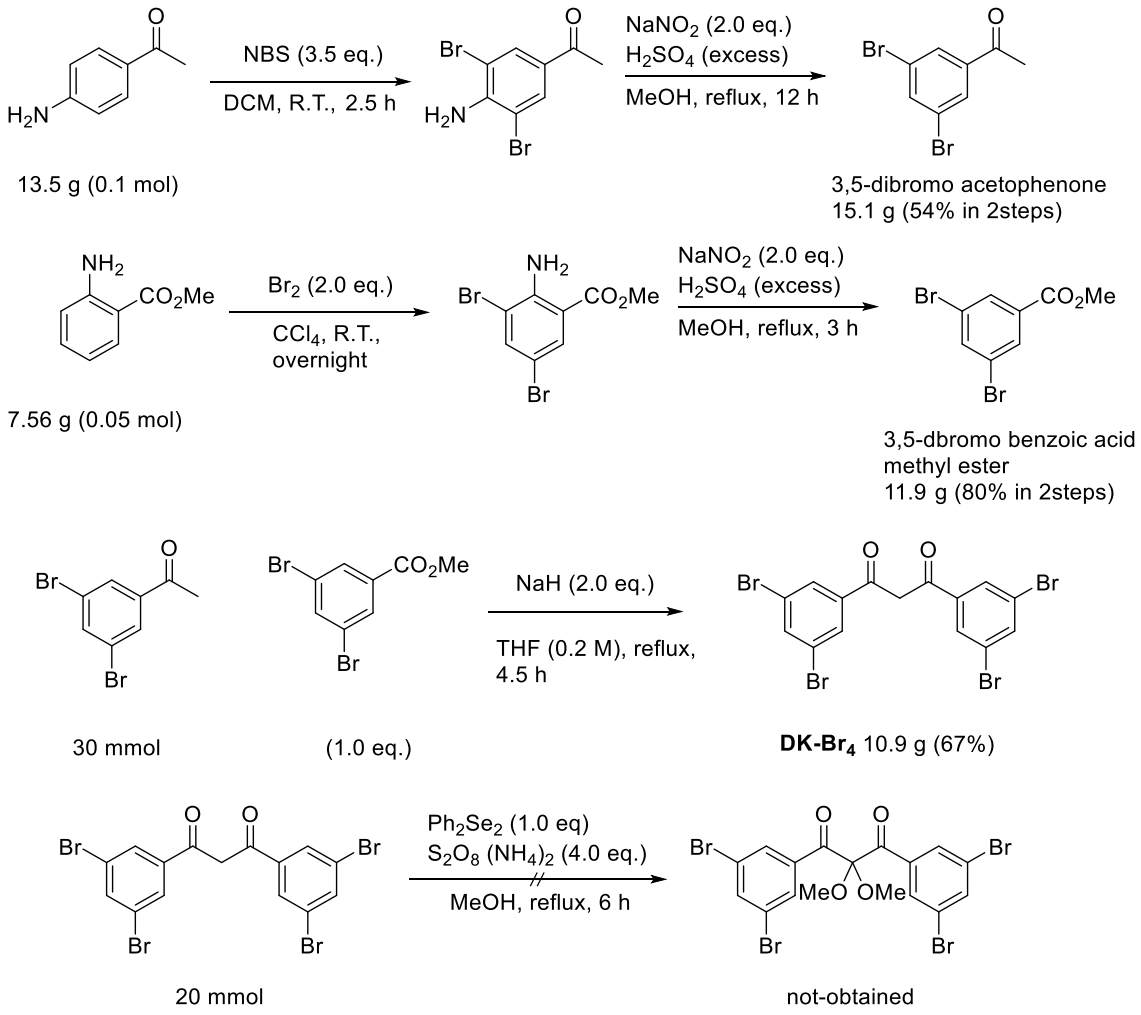

Scheme 2.3. The synthesis of **DK-Br4**.

The author tried to synthesize the azo moiety in another way via 2,3,5,6-tetrazine **TZ-R4**. Refer to the synthesis of dibromo-tetrazine,[12] the target tetrabromo-tetrazine **TZ-Br4** was synthesized from the 3,5-dibromo benzonitrile (Scheme 2.4). By the [1,4]-addition of diethoxy carbene generated from triethyl orthoformate, the synthesis of tetrabromo-pyrazole

PY-Br$_4$ was succeeded. The tetrabrominated azo compounds **AZ4b** were synthesized after the Diels-Alder reaction between **PY-Br$_4$** and cyclopentadiene. To synthesize **AZ3b**, the saturation of double bonding in the extra cyclopentane ring of **AZ4b** was performed using $Pd(OH)_2$ as catalysts.

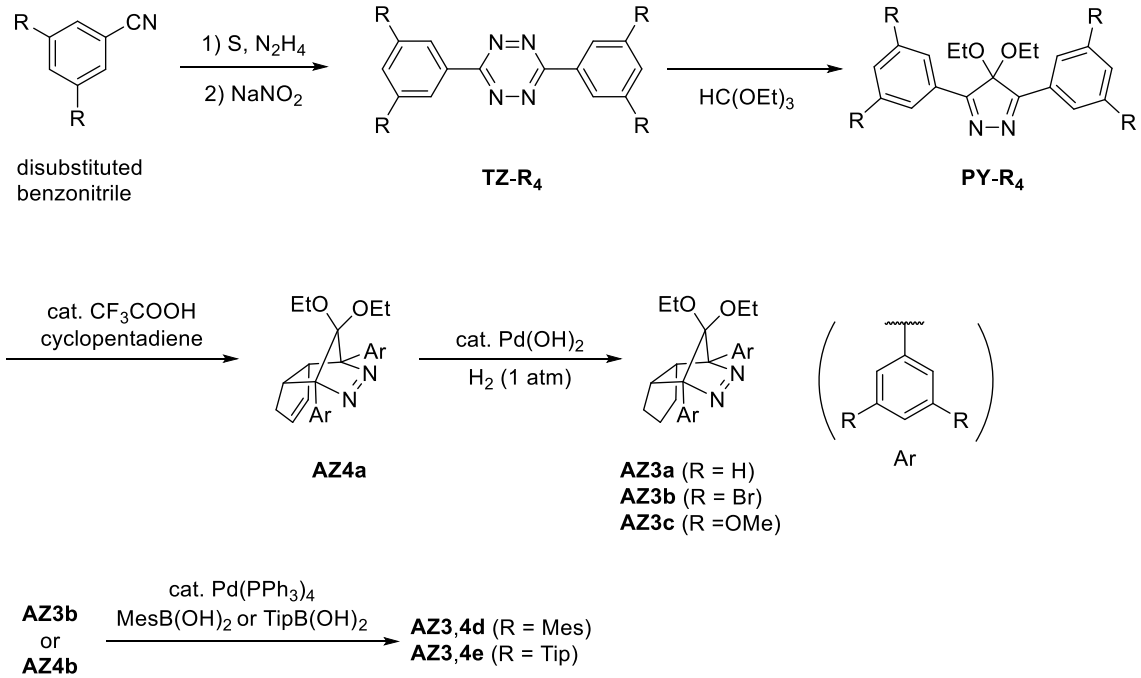

Scheme 2.4. Synthesis of **AZ3** and **AZ4**.

The synthesis of **AZ3a,c** and **AZ4a,c** were also conducted in the same way as **AZ3b** and **AZ4b**. The introduction of bulky substituents, Mes or Tip groups, were succeeded by the Suzuki-Miyaura cross-coupling reaction between **AZ3b** or **AZ4b** and corresponding boronic acid. The structures of newly synthesized compounds were fully characterized by ^{1}H, ^{13}C-NMR, 2D-NMR, and high-resolution mass spectra. The endo-configuration of all azoalkane was explained by the correlation between one methylene proton in the ethoxy group and methine proton, which corresponds to the C5 and C6 positions in azoalkane (for **AZ4e** in Figure 2.4a and other azo alkane **AZ3**,**4** in Figure 2.S1-S8). The n-π*

transitions of azo moiety were observed around 360 nm with the vibrational structure for all azo alkenes in benzene (for **AZ4e** in Figure 2.4b and other azo alkanes **AZ3**,**4** in Figure 2.S9, S10).

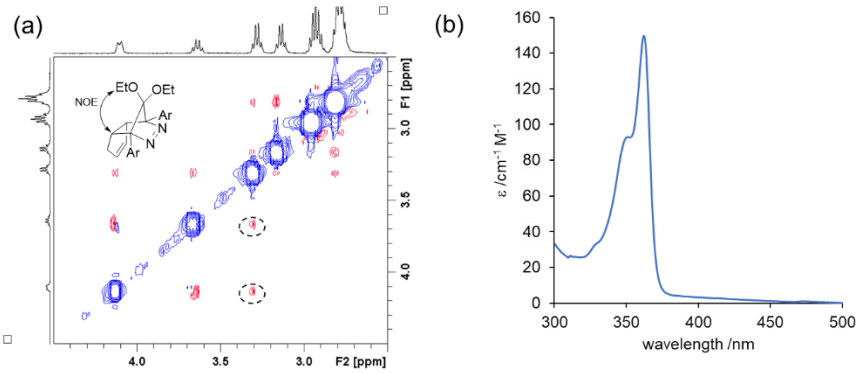

Figure 2.4. (a) NOESY spectra of **AZ4e** in $CDCl_3$. (b) UV-vis spectra of **AZ4e** in benzene.

Section 2.4. The generation and the reactivity of S-**DR3**,**4**

The photo-denitrogenation reactions of obtained azoalkane **AZ3**,**4** were conducted using the 365 nm LED lamp under nitrogen atmosphere in deuterated benzene (Scheme 2.5). Figure 2.4 shows the result of **AZ4e** as a representative of other azo alkanes. By photoirradiation, the degradation of signals such as 7.9 and 8.2 ppm correspond to **AZ4e** were observed with newly generated signals like 7.4 and 7.25 ppm. The structure of obtained molecule was confirmed as *trans*-**CP4e** by ^{1}H,^{13}C-NMR, 2D-NMR, and high-resolution mass spectra. The high field shift of protons H^{a}, which corresponds to ortho proton of attached phenyl ring, were understood as the disappearance of electron deficient azo moiety. And the release of ethoxy group from the shield region of aryl groups causes the low field shift of methyl proton of ethoxy group (H^{b}). Other azoalkanes are also converted to *trans* isomer of ring closed molecule *trans*-**CP3,4** by the photo-denitrogenation reaction (Figure 2.S11-S25).

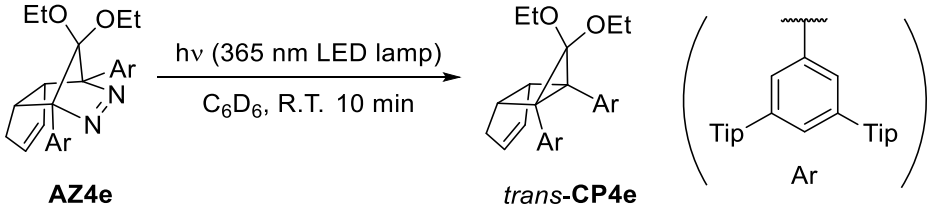

Scheme 2.5. Photo denitrogenation reaction of **AZ4e**.

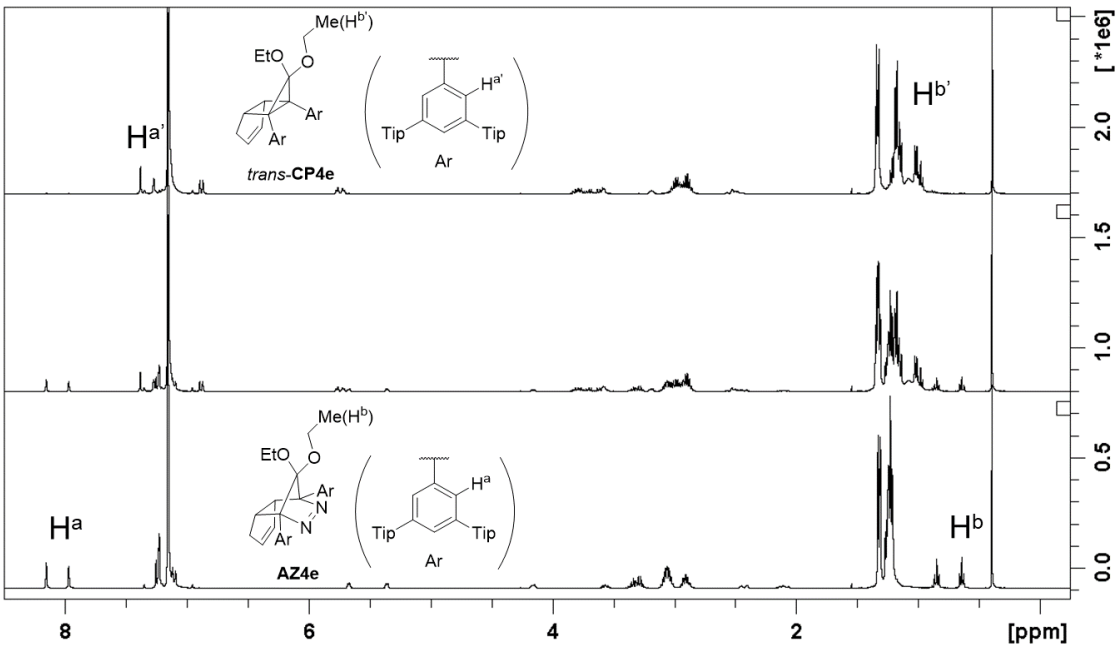

Figure 2.5. Photo denitrogenation of **AZ4e** in C_6D_6. (bottom: before irradiation, middle: after irradiation 2 min, top after 10 min irradiation.)

As mentioned in section 2.1, the singlet diradical S-**DR3**,**4** should be generated as intermediated between azoalkane **AZ3**,**4** and ring closure product *trans*-**CP3**,**4** after the photo-denitrogenation reaction. To slow down the radical-radical coupling reaction of singlet diradical, the photoreaction of **AZ4** was conducted by 360 nm Xenon lamp in 2-methyl tetrahydrofuran (M-THF) matrix at 115 K (Scheme 2.6). The generation of new species with a maximum absorption around 570-600 nm was observed by photoirradiation (Figure 2.6 and Table 2.3). They were assigned to S-**DR4** because 2,2-dialkoxy-cyclopentane-1,3-diyls S-**DR1** also has an absorption around 570 nm in the previous report.[1] The absorption maxima of S-**DR4** were slightly red-shifted by substituting the phenyl ring's meta-position at C1 and C3 positions. There were few differences between the absorption maximum of S-**DR4d** and that of S-**DR4e**. It implies that electronic structures were the same between them.

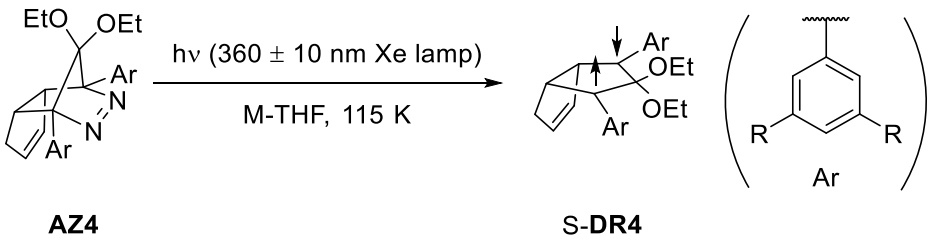

AZ4 **S-DR4**

Scheme 2.6. The photo-denitrogenation of **AZ4** at cryogenic conditions.

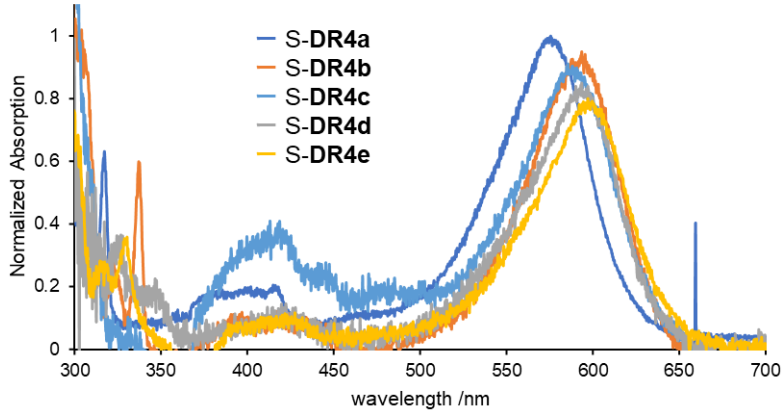

Figure 2.6. Electronic absorption spectra of singlet diradicals S-**DR4a-e** in MTHF glass at 115 K. To see the respective spectra clearly, the intensities of the signals were normalized: S-**DR4a** = 1.0, S-**DR4b** = 0.95, S-**DR4c** = 0.90, S-**DR4d** = 0.85, S-**DR4e** = 0.80.

Table 2.3. Aryl groups effect in S-**DR4** on the absorption maximum in M-THF at 115K

S-**DR**	**4a**	**4b**	**4c**	**4d**	**4e**
R =	H	Br	OMe	Mes	Tip
λ_{max} /nm	575	595	587	598	598

To detect the intermediate of photo denitrogenation reaction, singlet diradical S-**DR3**,**4**, at room temperature, the transient absorption spectroscopies of **AZ3**,**4** in benzene were carried out by 355 nm laser (Scheme 2.7). The transient spectra of **AZ4e** were shown in Figure 2.7a. Same as the low-temperature experiment, the transient species corresponds to absorption maximum around 570-600 nm were observed (see also Figure

2. S26a-S35a). The lifetimes of these species were not affected between air and nitrogen atmosphere (Figure 2.7b). So, the observed transient species were identified as singlet diradical S-**DR3**,**4**. The singlet diradical's lifetimes were highly dependent on the substituents R and double bond in extra cyclopentane ring (Figure 2.8 and 2.9). These observations were discussed later. The low-temperature NMR measurements (section 2.4) support that the lifetime of singlet diradical corresponded to the kinetics of ring-closing reaction to form *cis*-**CP3**,**4**.

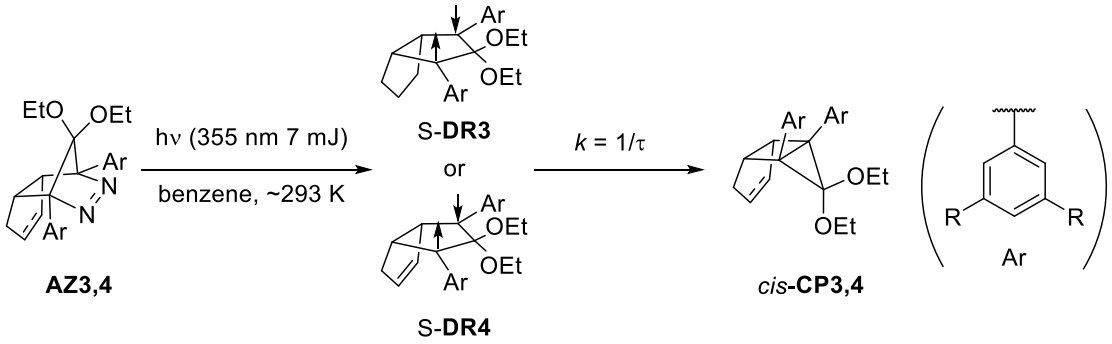

Scheme 2.7. Generation of S-**DR3**, **4** and bond formation between two radicals generate *cis*-**CP3**,**4**.

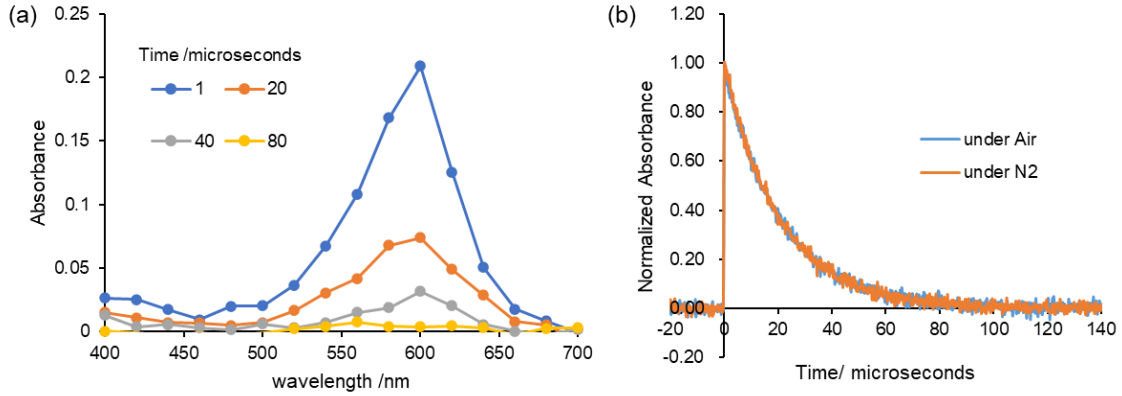

Figure 2.7. (a) Transient Absorption spectra of **AZ4e.** (1(blue), 20(orange), 40(gray), 80(yellow) microseconds after photolysis). (b) Time profile of S-**DR4e** (λ_{obs} = 600 nm) generated by the laser flash photolysis of **AZ4e** (λ_{exc} = 355 nm) in benzene at 295 K under nitrogen (orange) and air (blue).

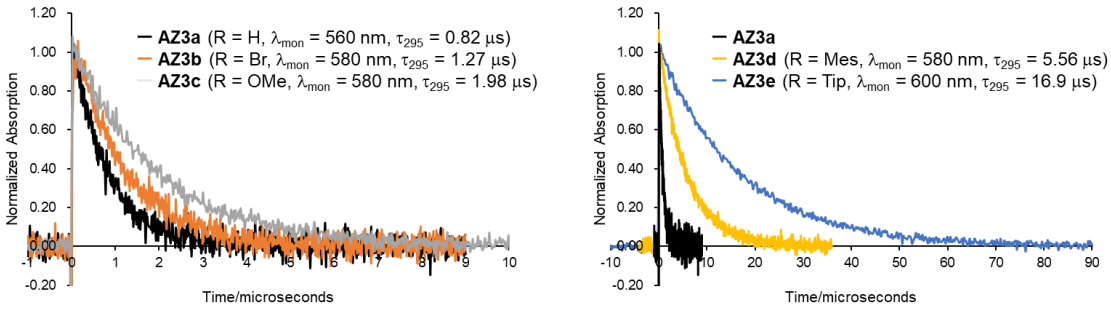

Figure 2.8. Time profile of S-**DR3** generated by laser flash photolysis of **AZ3** (λ_{exc}=355 nm) in benzene at 295 K.

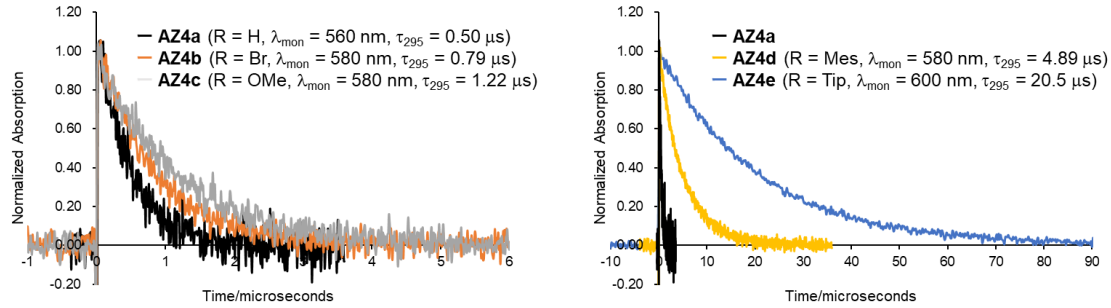

Figure 2.9. Time profile of S-**DR4** generated by laser flash photolysis of **AZ4** (λ_{exc}=355 nm) in benzene at 295 K.

The temperature dependencies on the lifetime of singlet diradical S-**DR3**,**4** were investigated to get the information for the ring-closing process. The lifetimes of S-**DR3**,**4** were measured at the five points between 283 K and 323 K (Figure 2.S26b-S35b). The Arrhenius plot and Eyring plot were obtained from the obtained temperature dependency of the lifetime. In all singlet diradical, the linear relationships were observed for both Arrhenius and Eyring plots (in Figure 2.10a,b for S-**DR4e**, in Figure 2. S.36-S39 for other S-**DR3,4**). The activation parameters (τ_{293}, E_a, log$A$, $\Delta H^{\ddagger}$, $\Delta S^{\ddagger}$) were estimated from these plots' linear approximations (Table 2.4). The lifetimes of singlet diradical S-**DR3**,**4** were extended by introducing bulkier groups at the meta position of phenyl rings. The activation energy E_a and activation enthalpy $\Delta H^{\ddagger}$ were significantly increased by substituting R position to Mes groups or Tip groups. This

observation support that the kinetic stabilization of singlet diradical was succeeded. When the obtained activation enthalpies were plotted against the activation entropies, which is called the enthalpy-entropy compensation plot (Figure 2.10c),[13,14] the linear relationship was roughly observed. This linear relationship gives support that the reaction mechanism was not changed in all singlet diradicals S-**DR3**,**4**.

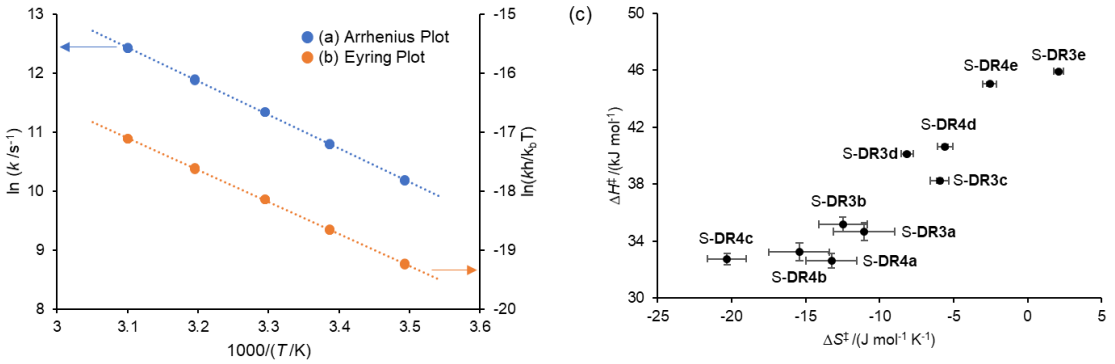

Figure 2.10. (a) Arrhenius plot and (b) Eyring plot for the decay process of S-**DR4e**. (c) Enthalpy-Entropy compensation plot for the decay process of S-**DR3**,**4**.

Table 2.4. Aryl groups effect on the lifetime (τ_{293}) of S-**DR3**,**4** in benzene at 293 K, and activation parameters (E_a, log$A$, $\Delta H^{\ddagger}$, and $\Delta S^{\ddagger}$) for the radical-coupling reaction.

S-**DR**	R =	τ_{293} /nm[a]	E_a /kJ mol^{-1}[b]	log(A s^{-1})[b]	$\Delta H^{\ddagger}$ /kJ mol^{-1}[c]	$\Delta S^{\ddagger}$ /J mol^{-1} T^{-1} [c]
3a/4a	H	0.94 ± 0.3	37.2 ± 0.6	12.7 ± 0.1	34.6 ± 0.6	-11.0 ± 2.0
		/0.53 ± 0.2	/35.1 ± 0.5	/12.4 ± 0.1	/32.6 ± 0.5	/-13.2 ± 1.7
3b/4b	Br	1.38 ± 0.4	37.7 ± 0.5	12.6 ± 0.1	35.1 ± 0.5	-12.5 ± 1.6
		/0.88 ± 0.3	/35.8 ± 0.6	/12.4 ± 0.1	/33.2 ± 0.6	/-15.4 ± 2.0
3c/4c	OMe	2.21 ± 0.2	40.8 ± 0.2	13.0 ± 0.1	38.2 ± 0.2	-5.9 ± 0.6
		/1.30 ± 0.3	/35.3 ± 0.2	/12.1 ± 0.1	/32.7 ± 0.4	/-20.3 ± 1.3
3d/4d	Mes	6.24 ± 0.4	42.6 ± 0.1	12.8 ± 0.1	40.1 ± 0.1	-8.2 ± 0.4
		/5.68 ± 0.4	/43.1 ± 0.2	/12.9 ± 0.1	/40.7 ± 0.2	/-5.7 ± 0.5
3e/4e	Tip	19.6 ± 0.8	48.5 ± 0.1	13.3 ± 0.1	45.9 ± 0.1	2.1 ± 0.3
		/23.8 ± 1.4	/47.5 ± 0.1	/13.1 ± 0.1	/45.0 ± 0.4	/-2.5 ± 0.5

[a] In benzene at 293 K; calculated from the Arrhenius parameter, E_a and log$A$. The error was obtained from the mean error of activation energy E_a. [b] Determined from the Arrhenius plot of the singlet diradicals' lifetimes at five temperatures between 285 and 333 K. The mean error obtained from regression analysis is shown as errors. [c] Determined from the Eyring plot of the singlet diradicals' lifetimes at five temperatures between 285 and 333 K. The mean error obtained from regression analysis is shown as errors.

Comparing the activation energy E_a and activation enthalpy $\Delta H^{\ddagger}$ for the singlet diradicals S-**DR3a**,**b** and S-**DR4a**,**b**, the extra cyclopentane ring's protons and protons in the ethoxy group inhibits the radical-radical coupling reaction (Figure 2.11a). The activation parameter differences between double bonding and single bonding in extra cyclopentane ring were decreased by introducing bulky substituents such as Mes and Tip groups. These results imply that the contribution of steric repulsion between the ethoxy group and extra cyclopentane ring for determining the kinetics of the ring-closing reaction was decreased (Figure 2.11a vs 2.11b). The introduced bulky groups increased steric repulsion between aryl groups and/or aryl groups and the ethoxy group.

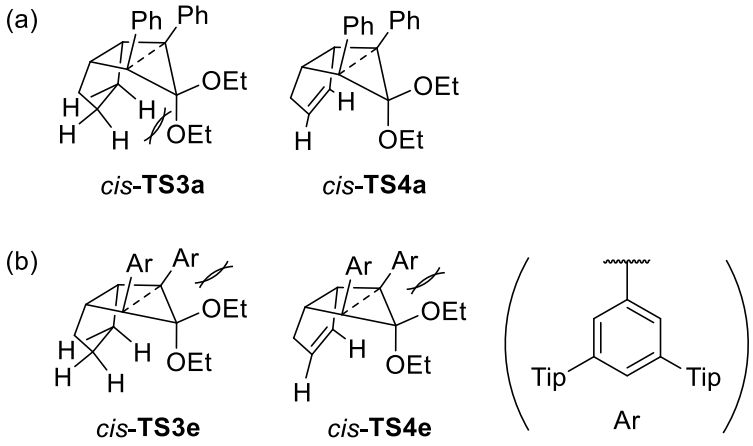

Figure 2.11. Illustration of the main component of determining the activation energy for the transition state (a) *cis*-**TS3**,**4a** and (b) *cis*-**TS3**,**4e**.

Section 2.5. The generation and the reactivity of *cis*-**CP4e**

The product analysis of the photo denitrogenation reaction under low-temperature was conducted to confirm the ring-closing reaction path. Following the previous study,[3] the ^{1}H NMR for the photolysis of **AZ4e** in deuterated toluene by 355 nm laser was measure at 200 K (Scheme 2.8 and Figure 2.12). Direct photo-irradiation generates two products (Figure 2.12b). Major product was characterized as *trans*-**CP4e**, same to the photolysis at room temperature (Figure 2.12b vs f). Another photoproduct was selectively produced by the benzophenone sensitized irradiation of **AZ4e** at the same temperature (Figure 2.12c). By the direct photo denitrogenation of **AZ4e**, there is a route for the formation of *trans*-**CP4e** without going through S-**DR4e**.[3,15,16] But in the presence of triplet sensitizer, benzophenone, the denitrogenation reaction of azoalkane **AZ4e** was selectively occurred via T-**DR4e** and S-**DR4e**. So, the triplet sensitized photo product should be coming from the S-**DR4e**. The thermolysis at the same temperature and raising the temperature to 234K converts the triplet sensitized product to *trans*-**CP4e** (Figure 2.12d,e). These observations suggest that the triplet sensitized product should be S-**DR4e** or *cis*-**CP4e**.

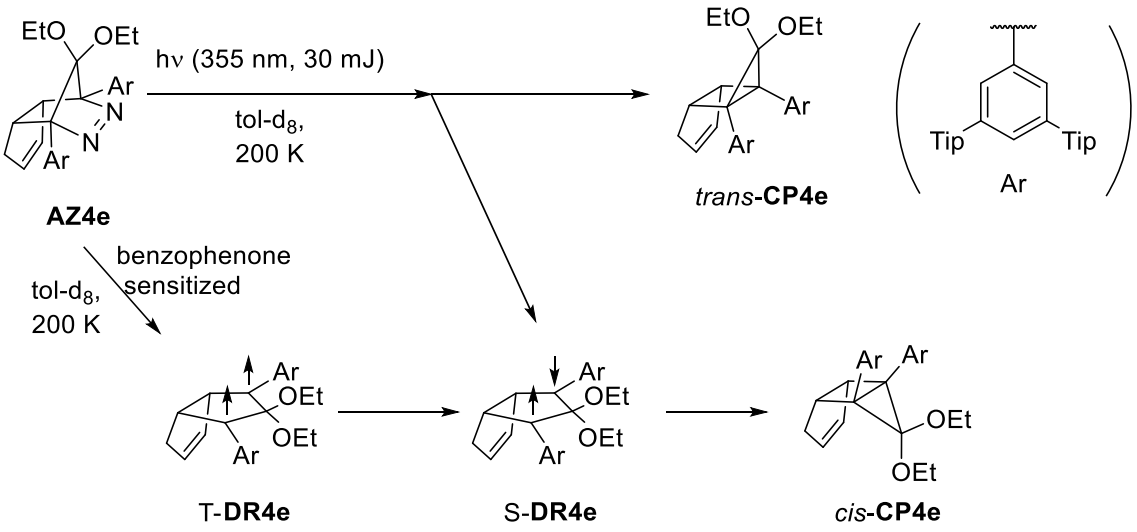

Scheme 2.8. The plausible mechanism of the denitrogenation reaction of **AZ4e** with and without benzophenone and the formation of *cis*-**CP4e**.

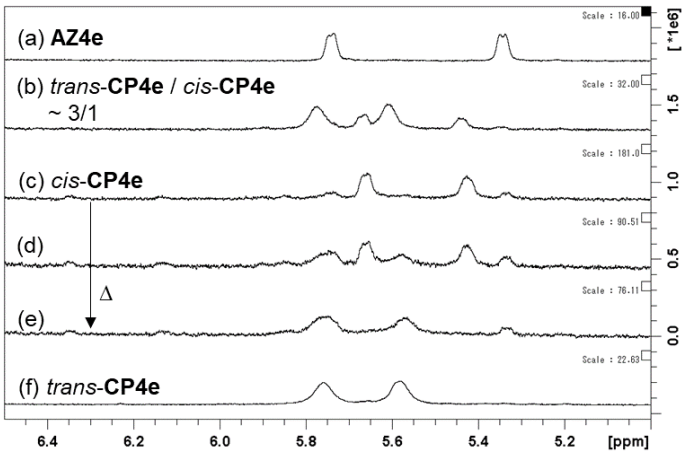

Figure 2.12. ^{1}H-NMR spectrum at 200 K (a)**AZ4e**, (b) after irradiation of **AZ4e**, (c) after irradiation of **AZ4e** with benzophenone, (d) after 440 min under the dark condition of (c), (e) after warming to 234 K then re-cooling to 200 K, (f) after irradiation of **AZ4e** at room temperature then cooling to 200 K.

The lifetime of singlet diradical S-**DR4e** was measured at a lower temperature, 122 K, in the M-THF matrix condition to disclose the observed species. At the dark condition, singlet diradical S-**DR4e** were almost disappeared after 1 hour at that temperature (Figure 2.13a). By the time trace of the absorption at 598 nm after photolysis of **AZ4e**, the lifetime of S-**DR4e** at 122 K was determined to about 24 min using a stretched exponential equation (Figure 2.13b).[17] Because the observed species at 200 K by NMR measurements were stable enough for 1 hour, they were judged to *cis*-**CP4e**, not S-**DR4e**.

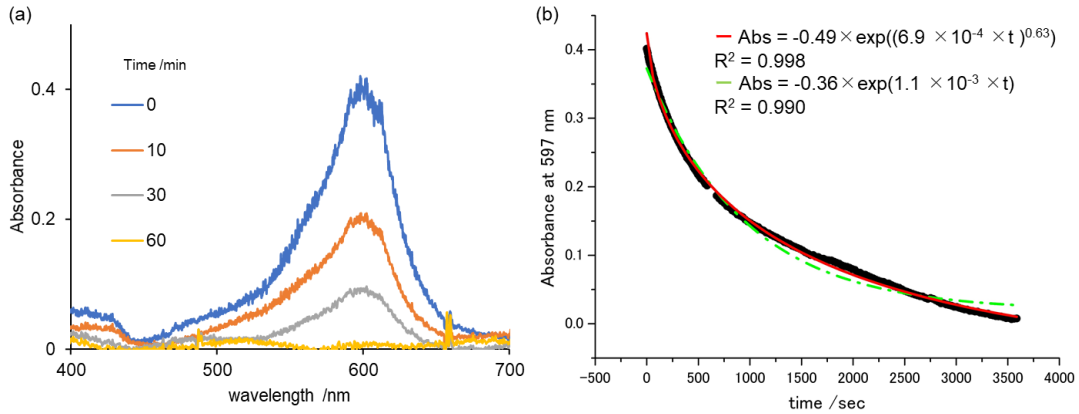

Figure 2.13. (a) Absorption spectra of S-**DR4e** at 122 K in M-THF. (blue: just after generation, orange: after 10 min, gray: after 30 min, yellow after 1 h), (b) black: the decay trace of S-**DR4e** at 597 nm under 122 K in M-THF. Red: fitting by a stretched exponential equation. Green: fitting by a single exponential equation.

The information for the thermal conversion from *cis*-**CP4e** to *trans*-**CP4e** was investigated by the temperature dependency of the lifetime of *cis*-**CP4e** between 205 K and 223 K (Scheme 2.9). For example, two-thirds of **AZ4e** in deuterated toluene were converted to *cis*-**CP4e** by the photolysis with benzophenone by 355 nm laser at 205 K (Figure 2.14a). After 11 hours, *cis*-**CP4e** was fully converted to *trans*-**CP4e** (Figure 2.14c). The integration ratio between *cis*-**CP4e** or *trans*-**CP4e** and **AZ4e** were recorded as the function of time under dark condition (Figure 2.14e). From the time trace of the amount of *cis*-**CP4e**, the lifetime of *cis*-**CP4e** was determined to 1.5×10^4 sec = 4.2 hours. The almost same reaction rates between the decay of *cis*-**CP4e** and the generation of *trans*-**CP4e** inform the quantitative isomerization have occurred.

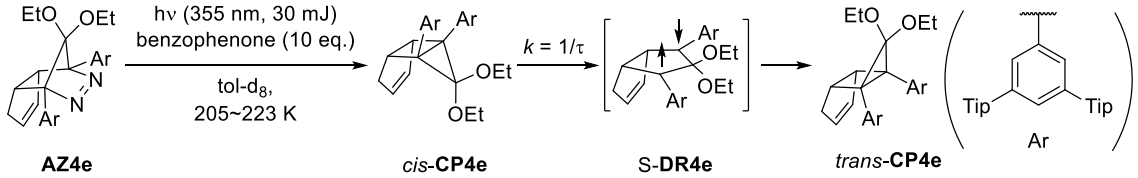

Scheme 2.9. Generation of *cis*-**CP4e** with benzophenone and isomerization from *cis*-**CP4e** to *trans*-**CP4e**.

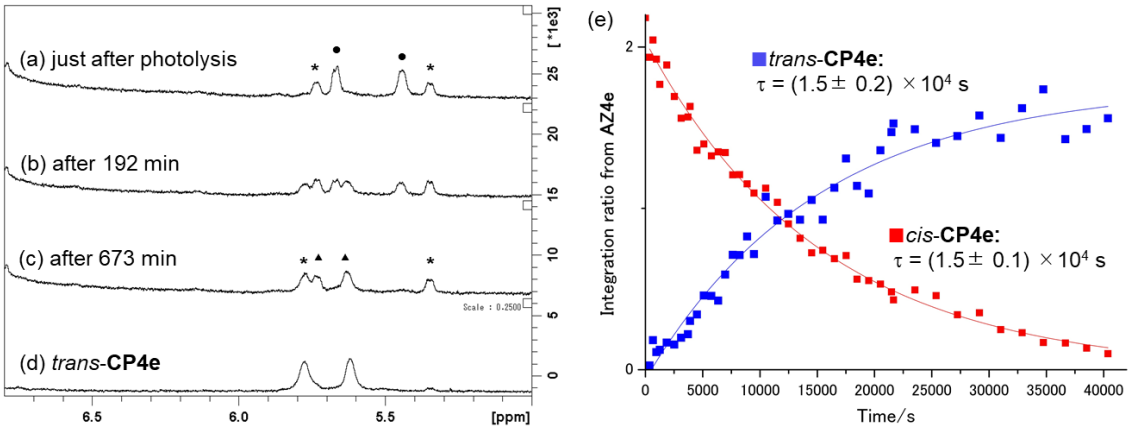

Figure 2.14. ^{1}H-NMR spectra at 205 K in toluene-d_8:(a) after irradiation of **AZ4e** in the presence of benzophenone (*marks corresponded to **AZ4e** and ● marks were corresponded to *cis*-**CP4e**), (b) after 192 min under dark conditions,(c) after 673 min under dark conditions(*marks corresponded to **AZ4e** and ▲ marks were corresponded to *trans*-**CP4e**), (d) *trans*-**CP4e**;(e) Time profiles of integration ratio of NMR signals between *cis*-**CP4e** (red, 5.45 ppm) or *trans*-**CP4e** (blue, 5.78 ppm) and **AZ4e**(5.35ppm) at 205 K.

The lifetimes of *cis*-**CP4e** at 211, 217, 223 K were calculated by the same procedure (Figure 2.S40). They were plotted against the inverse of temperature to make the Arrhenius plot and the Eyring plot (Figure 2.15). The activation parameters of the isomerization process of *cis*-**CP4e** to *trans*-**CP4e** were estimated from linear approximation of these plots to E_a = 63.8 ± 0.9 kJ/mol, log(A /s) = 12.0 ± 0.2, $\Delta H^{\ddagger}$ = 62.0 ± 0.9 kJ/mol and $\Delta S^{\ddagger}$ = -20.3 ± 4.4 J/(mol·K). Comparing between the obtained activation parameter for isomerization of *cis*-**CP4e** and that of *cis*-**CP1a** (E_a = 60.4 ± 0.9 kJ/mol and log(A /s) = 12.0 ± 0.1), the activation energy increase by the introduction of Tip groups were slightly observed. Nevertheless, the pre-exponential factor was the same between the isomerization of *cis*-**CP1a** and that of *cis*-**CP4e**. On the other hand, the introduction of Tip groups changes both the activation energy and pre-exponential factors in the formation process of *cis*-**CP4e** from S-**DR4e**, mentioned in section 2.4.

Because of this, the observed activation energy in low-temperature NMR experiments might be assigned the ring-closing process from S-**DR4e** to *trans*-**CP4e**.

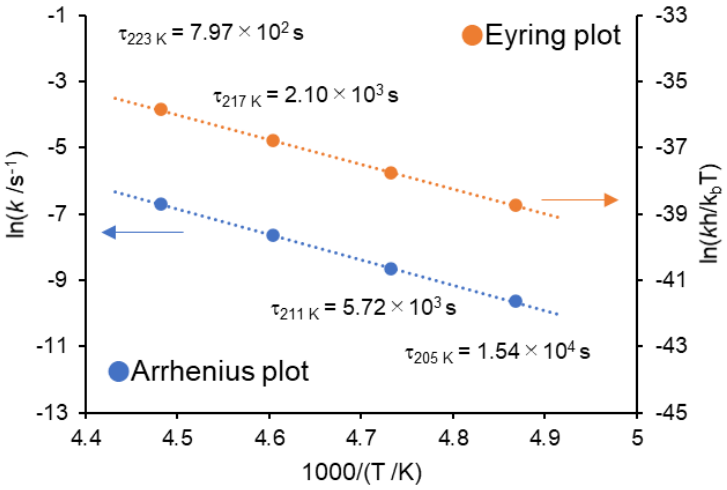

Figure 2.15. Arrhenius plot (blue) and Eyring plot (orange) of thermal isomerization process from *cis*-**CP4e** to *trans*-**CP4e**.

Section 2.6. Summary of this chapter

The steric effects on the reactivity of the cyclopentane-1,3-diyls were investigated theoretically and experimentally. Theoretical calculation informs the introduction of bulky groups at the meta position of the phenyl ring is better to stabilize the singlet diradical S-**DR2** than the ortho position of that. The synthesis of **AZ3**,**4b** was succeeded via [4+1] cycloaddition reaction. The Suzuki-Miyaura cross-coupling reaction also plays a crucial role in the synthesis of **AZ3**,**4d** and **AZ3**,**4e**. The efficient denitrogenation of **AZ3**,**4** and generation of S-**DR3**,**4** were observed by the low temperature and ambient temperature photoreaction. No difference of electronic structure of S-**DR4d**,**e** was confirmed by the absorption spectra at cryogenic conditions. Moreover, the introduction of bulky substituents at the aryl groups' meta-position in singlet cyclopentane-1,3-diyls extends the lifetime of singlet diradicals S-**DR3**,**4**. The increase of activation energy and activation enthalpy by increasing the bulkiness of aryl groups supports the kinetic stabilization of S-**DR3**,**4**. Although the double bonding at the extra cyclopentane ring makes the lifetime of S-**DR4a** as much as half of that of S-**DR3a**, the lifetime of S-**DR4d** and S-**DR4e** were almost the same as S-**DR3d** and S-**DR3e**, respectively. These results imply the introduction of bulky substituents can change the contribution for determining the activation energy from the steric repulsion include the extra cyclopentane ring to the steric repulsion include the aryl groups. The activation enthalpy and entropy compensation were observed for the ring-closing process by introducing bulky substituents. It concludes the decay process is same between them. By the low-temperature experiments for the photolysis of **AZ4e**, the decay processes of S-**DR4e** were confirmed to *cis*-**CP4e**. And the thermal *cis*-*trans* isomerization of **CP4e** via singlet diradical S-**DR4e** was investigated. The detail analysis of this process contributes to the insight for another radical-radical bond formation process, *trans*-**TS4e**.

Section 2.7. Experimental section

Section 2.7.1. General Information

Benzene (Spectro grade) and starting materials for the synthesis were purchased from commercial suppliers. 3,5-dibromo-benzonitrile were synthesized according to the literature procedure.[18] **AZ3**,**4a** were synthesized according to the literature procedure.[19] ^{1}H NMR spectra were obtained at 400 MHz, chemical shifts are reported in ppm, and referenced to the $CHCl_3$ and C_6H_6 singlet at 7.26 and 7.16 ppm, respectively. ^{13}C NMR spectra were obtained at 100 MHz and referenced to the center peak of the $CDCl_3$ and C_6D_6 triplet at 77.06 and 128.06 ppm, respectively. The abbreviations s, d, t, sept, and m stand for the resonance multiplicities singlet, doublet, triplet, septet and multiplet, respectively. Mass-spectrometric data were measured with a mass spectrometric Thermo Fisher Scientific LTQ Orbitrap XL.

The theoretical calculations have been done by Gaussian 09 Revision D.01. The Gauss View 5.0 were used as visualization software.

Laser Flash Photolysis Measurements The concentration of samples was adjusted to an optical density of ca. 0.5 at the excited wavelength (355 nm). The excitation source for the LFP system was an Nd:YAG laser (λ_{exc}=355 nm, 5 ns pulse, 7 mJ). The monitoring system consisted of a 150 W xenon lamp as light source, Unisoku-MD200 monochromator and a photomultiplier. The temperature was controlled with a CoolSpek USP-203-B (Unisoku).

Section 2.7.2. Synthesis

Synthesis of **PZ-Br$_4$**

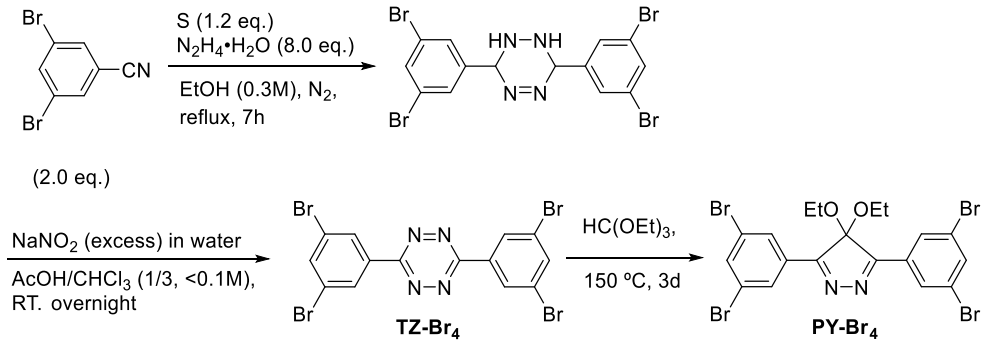

To a suspension of 3,5-dibromo benzonitrile (1.56 g, 6 mmol, 2.0 eq,) in ethanol (20 ml, 0.3 M) under nitrogen were added monohydrate hydrazine (2.6 ml, 8.0 eq) and sulfur (230 mg, 1.2 eq). The mixture was refluxed for 7 h. All volatile substances were removed by concentration under reduced pressure to give a yellow solid used without further purification. in the next step.

The yellow solid (1 eq) was dissolved in chloroform (30 ml, 0.1 M). After Acetic acid 10 ml add, a solution of sodium nitrite (excess) in water (0.3 M) was added. The mixture was stirred at room temperature for 12 h. All volatile substances were removed by concentration under reduced pressure to give a red solid **TZ-Br$_4$**. It was used without further purification in the next step.

The crude mixture of previous reaction was suspended to triethyl orthoformate 25 ml. The suspension was stirred at 150 ºC until the color of the reaction mixture becomes brown. All volatile substances were removed by concentration under reduced pressure to give crude product. The crude residue was purified by flash chromatography on silica gel using hexane/ethyl acetate as eluent to afford the desired product **Py-Br$_4$** (530 mg, 28% in 3steps). ^{1}H NMR (400 MHz, $CDCl_3$) δ 8.39 (d, *J* = 1.64 Hz, 4H), 7.89 (t, *J* = 1.64 Hz, 2H), 3.16 (q, *J* = 6.95 Hz, 4H), 1.16 (t, *J* = 6.95 Hz, 6H). ^{13}C NMR (100 MHz, $CDCl_3$) δ 166.3, 137.9, 130.5, 129.2, 123.8, 115.3, 60.5, 14.9. HRMS (ESI+): m/z Calcd for $C_{19}H_{17}O_2N_2Br_4$ $[M+H]^+$: 620.80267, Found 620.80180.

Synthesis of **Py-OMe4**

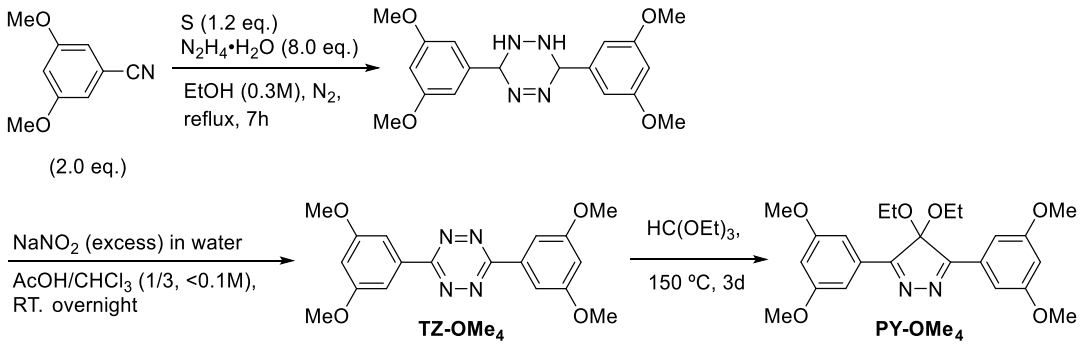

Compounds **TZ-OMe4** were synthesized with same procedure as **TZ-Br4**. Compounds **Py-OMe4** were synthesized with same procedure as **Py-Br4** and the yields were calculated to be 22 % in 3 steps. ^{1}H NMR (400 MHz, $CDCl_3$) δ 8.39 (d, *J* = 1.64 Hz, 4H), 7.89 (t, *J* = 1.64 Hz, 2H), 3.87 (s, 12H), 3.18 (q, *J* = 6.96 Hz, 4H), 1.11 (t, *J* = 6.96 Hz, 6H). ^{13}C NMR (100 MHz, $CDCl_3$) δ 167.7, 161.0, 129.6, 115.5, 105.4, 105.3, 60.0, 55.6, 15.0. HRMS (ESI+): m/z Calcd for C_{23} H_{29} O_6 N_2 $[M+H]^+$: 429.20201, Found 429.20200.

Synthesis of **AZ4b**

To a mixture of **Py-Br4** (930 mg, 1.5 mmol) in dichloromethane (15 ml, 0.1 M) under nitrogen were added cyclopentadiene (2.5 ml, 20 eq.). The mixture was cooled to 0 ºC, trifluoroacetic acid (22 ml, 20 mol%) was added. The mixture was mixed for 2 h at 0 ºC. The reaction mixture was quenched by sat. $NaHCO_3$ aq. then extracted by dichloromethane. The organic layer was dried over Na_2SO_4, filtered and concentrated. Recrystallization from dichloromethane gave **AZ3e** (650 mg, 63 %). ^{1}H NMR (400 MHz, $CDCl_3$) δ 8.08(d, *J* = 1.76 Hz, 2H), 7.97 (d, *J* = 1.76 Hz, 2H), 7.74 (d, *J* = 1.64 Hz, 4H), 7.73 (t, *J* = 1.74 Hz, 1H), 7.71 (t, *J* = 1.76 Hz, 1H), 5.58-5.62(m, 1H), 5.45-5.60 (m, 1H), 4.40-4.10 (m, 1H), 3.55-3.65 (m, 1H), 3.17 (q, J = 7.06 Hz, 2H), 2.82-2.99 (m, 2H), 2.36 (ddq, *J* = 17.5 Hz, *J* = 10.7 Hz, *J* = 2.19 Hz, 1H), 2.18 (dsep, *J* = 17.7 Hz, *J* = 2.10 Hz, 1H) 1.15 (t, *J* = 7.04 Hz, 3H), 0.89 (t, *J* = 7.02 Hz, 3H). ^{13}CNMR (100 MHz, $CDCl_3$) δ 140.1, 139.9, 134.8, 133.9, 133.7, 130.4, 129.6, 125.8,

123.2, 123.1, 118.2, 93.8, 91.9, 60.5, 60.1, 57.7, 42.6, 32.1, 15.4, 14.8. HRMS (ESI+): m/z Calcd for C_{24} H_{22} O_2 N_2 Br_4 Na $[M+Na]^+$: 708.83070, Found 708.83105.

Synthesis of **AZ4c**

Compounds **AZ4c** were synthesized with same procedure as **AZ4b** and the yields were calculated to be 52 %. ^{1}H NMR (400 MHz, C_6D_6) δ 7.59(d, *J* = 2.12 Hz, 2H), 7.44 (d, *J* = 2.12, 2H), 6.65 (t, *J* = 2.12, 2H),5.56-5.64 (m, 1H), 5.34-5.42(m, 1H), 4.54-4.10 (m, 1H), 3.46-3.54 (m, 1H), 3.436 (s, 6H), 3.427 (s, 6H), 3.07-3.27 (m, 4H), 2.36-2.48 (m, 1H), 2.08-2.16 (m, 1H), 0.84 (t, *J* = 7.04 Hz, 3H), 0.68 (t, *J* = 7.04 Hz, 3H). ^{13} CNMR (100 MHz, C_6D_6) δ 161.2, 161.1, 139.7, 139.3, 133.9, 127.0, 118.4, 107.2, 106.3, 100.2, 100.1, 94.4, 92.6, 59.6, 57.9, 54.6, 42.6, 32.4, 15.0, 14.8. HRMS (ESI+): m/z Calcd for C28 H35 O6 N2 [M+H]+: 495.24896, Found 495.24811.

Synthesis of **AZ3b**

The **AZ4b** (963 mg) was dissolved in ethyl acetate (7.5 ml) and $Pd(OH)_2$ on charcoal (280 mg) was added. The mixture was stirred under hydrogen gas atmosphere for 2 hours, the palladium catalyst was removed by filtration over celite and the ethyl acetate was evaporated under reduced pressure. **AZ3b** was purified by column chromatography. Yields was 34 % (330 mg). ^{1}H NMR (400 MHz, C_6D_6) δ 8.17(d, *J* = 1.8 Hz, 4H), 7.51 (t, *J* = 1.8, 2H), 2.92-3.01 (m, 2H), 2.75 (q, *J* = 7.04 Hz, 2H), 2.64 (q, *J* = 7.04 Hz, 2H), 1.29-1.40 (m, 3H), 1.13-1.24 (m, 2H), 1.00-1.09 (m, 1H), 0.68 (t, *J* = 7.04 Hz, 3H), 0.44 (t, *J* = 7.04 Hz, 3H). ^{13}CNMR (100 MHz, C_6D_6) δ 141.0 133.5, 130.2, 123.2, 118.9, 93.3, 60.1, 59.4, 49.0, 27.7, 25.1, 14.8, 14.2. HRMS (ESI+): m/z Calcd for C24 H25 O2 N2 Br4 $[M+H]^+$: 688.86440, Found 688.86560.

Synthesis of **AZ3c**

Compounds **AZ3c** were synthesized with same procedure as **AZ3b** and the yields were calculated to be 54 %. ^{1}H NMR (400 MHz, $CDCl_3$) δ 7.14(d, *J* = 2.3 Hz, 4H), 6.49 (t, *J* = 2.3, 2H), 3.84(s, 12H), 3.43-3.53(m, 2H), 3.18(q, *J* = 7.1 Hz, 2H), 2.96(q, *J* = 7Hz, 2H), 1.32-1.70(m, 4H), 1.08(t, *J* = 7.1 Hz, 3H), 0.84(t, *J* = 7.0Hz, 3H). ^{13}CNMR (100 MHz, $CDCl_3$) δ 160.6, 139.2, 119.1, 106.5, 100.0, 94.5, 59.4, 59.2, 55.4, 49.2, 27.8, 25.9, 15.5, 15.1. HRMS (ESI+): m/z Calcd for C26 H38 O6 N2 Na $[M+Na]^+$: 497.26221, Found 497.26312.

Synthesis of **AZ4d**

To a mixture **AZ4b** (69.8 mg, 0.1mmol), 2,4,6-Trimethyl-phenylboronic Acid (131.2 mg, 8 eq.), Na_2CO_3 (160 mg, 16 eq.), palladium acetate (2.7 mg, 12 mol%) and triphenylphosphine (12.6 mg, 48 mol%) was added THF (4 ml) and water (1 ml) under nitrogen. Then the mixture was heated at 70 ºC for 16 h. The reaction mixture was quenched with 1 M HCl aq and extracted with $CHCl_3$. The obtained organic layer was dried by Na_2SO_4 and evaporated under reduced pressure. Flash chromatography on silica gel using hexane/CH_2Cl_2 afforded desired product **AZ4d** (23 mg, 27%). ^{1}H NMR (400 MHz, $CDCl_3$) δ 7.73(d, *J* = 1.56 Hz, 1H), 7.68 (d, *J* = 1.48 Hz, 1H), 6.96 (t, *J* = 1.54 Hz, 1H), 6.95 (t, *J* =1.5 Hz,1H), 6.94 (m, 1H), 5.56(dd, *J* = 5.8 Hz, 1.8 HZ, 1H), 5.82 (dd, *J* = 5.8 HZ, *J* = 1.86 Hz,1H), 4.11-4.19 (m, 1H), 3.68 (q, *J* = 7.75 Hz, 1H), 3.20-3.30(m, 2H), 3.02-3.12(m,2H),2.68-2.75(m, 1H) 2.32(s, 12H), 2.26-3.34 (m, 2H), 2.073 (s, 6H), 2.067(s, 6H), 2.058(s, 12H), 1.09 (t, *J* = 7.1 Hz, 3H), 0.80 (t, *J* = 7.1 Hz, 3H). ^{13}CNMR (100 MHz, $CDCl_3$) δ 141.2, 141.1, 139.1, 136.8, 136.6, 136.51. 136.49, 135.79, 135.76, 134.2, 130.0, 129.9, 128.11, 128.09, 127.96, 127.3, 126.7, 118.3, 94.6, 93.1, 60.0, 59.6, 56.9, 42.7, 32.1, 21.0, 20.7, 15.6, 15.2. HRMS (ESI+): m/z Calcd for C_{60} H_{67} O_2 N_2 $[M+H]^+$ 847.51971:, Found 847.52057.

Synthesis of **AZ3d**

Compounds **AZ3d** were synthesized with same procedure as **AZ4d** using **AZ3b** instead of **AZ4b** and the yields were calculated to be 40 %. ^{1}H NMR (400 MHz, $CDCl_3$) δ 7.69(d, *J* = 1.5 Hz, 4H), 6.94 (s, 10H), 3.48-3.60 (m, 2H), 3.21 (q, *J* = 7.1 Hz, 2H), 3.06 (q, *J* = 7.1 Hz, 2H), 2.32(s, 12H), 2.07(s, 12H), 2.06(s, 12H), 1.55-1.67(m, 4H), 1.30-1.55(m, 2H), 0.99 (t, *J* = 7.1 Hz, 3H), 0.79 (t, *J* = 7.1 Hz, 3H). ^{13}CNMR (100 MHz, $CDCl_3$) δ 141.1, 139.2, 137.2, 136.6, 135.95, 135.92, 129.8, 128.21, 128.19, 127.8, 119.2, 94.8, 59.9, 59.5, 49.0, 28.0, 25.8, 21.2, 20.9, 15.7, 15.3. HRMS (ESI+): m/z Calcd for C_{60} H_{69} O_2 N_2 $[M+H]^+$ 849.53536:, Found 849.53565.

Synthesis of **AZ4e**

To a mixture **AZ4b** (69.8 mg, 0.1mmol), 2,4,6-Triisopropyl-phenylboronic Acid (200 mg, 8 eq.), $Ba(OH)_2 \cdot 8H_2O$ (252 mg, 8 eq.), and palladium acetate (4.5 mg, 20 mol%) and triphenylphosphine (21 mg, 80 mol%) was added 1,4-dioxane (4 ml) and water (1 ml). After that, the mixture was Freeze-Pump-Thaw (FPT) cycled 3 times. Then the mixture was heated at 100 ºC for 4 days under nitrogen atmosphere. The reaction mixture was quenched with 1 M HCl aq and extracted with $CHCl_3$. The obtained organic layer was dried by Na_2SO_4 and evaporated under reduced pressure. Flash chromatography on silica gel using hexane/CH_2Cl_2 afforded desired product **AZ4e** (65 mg, 56%). ^{1}H NMR (400 MHz, $CDCl_3$) δ 7.78 (d, *J* =1.2 Hz, 2H), 7.76 (d, *J* = 0.64 Hz, 2H), 7.04 (s, 10H), 5.56 (dd, *J* = 5.6, 1.7 Hz, 1H), 5.49 (dd, *J* = 5.6, 1.7 Hz, 1H), 4.06-4.16 (m, 1H), 3.58-3.70 (m, 1H), 3.28 (q, *J* = 7.0 Hz, 2H), 3.14 (q, *J* = 6.9 Hz, 2H), 2.93 (sept, *J* = 6.9 Hz, 4H), 2.79 (sept, *J* = 6.8 Hz, 8H), 2.22-2.30 (m, 2H), 1.29 (d, *J* = 6.9Hz, 24H), 1.00-1.17(m, 48), 1.01 (t, *J* = 7.1 Hz, 3H), 0.79 (t, *J* = 7.1 Hz, 3H). ^{13}CNMR (100 MHz, $CDCl_3$) δ147.8, 146.35, 146.31, 140.45, 140.41, 137.08, 137.06, 136.1, 135.9, 134.3, 131.0, 128.2, 126.7, 120.41, 120.35, 118.4, 94.3, 93.0, 60.1, 59.7, 56.9, 43.1, 34.3, 32.0, 30.5, 24.14, 24.12,

24.08, 23.99, 15.7, 15.3. HRMS (ESI+): m/z Calcd for C_{84} H_{115} O_2 N_2 $[M+H]^+$ 1183.89531:, Found 1183.89624.

Synthesis of **AZ3e**

Compounds **AZ3e** were synthesized with same procedure as **AZ4e** using **AZ3b** instead of **AZ4b** and the yields were calculated to be 20 %. ^{1}H NMR (400 MHz, $CDCl_3$) δ 7.75(d, J = 1.3 Hz, 4H), 7.03 (s, 8H), 7.02 (d, *J* = 1.3 Hz, 2H), 3.43-3.55 (m, 2H), 3.24 (q, 7.0 Hz, 2H), 3.11 (q, *J* = 7.0 Hz, 2H), 2.93(sept, *J* = 6.9 Hz, 4H), 2.79 (sept, *J* = 6.1 Hz, 8H), 1.50-1.62 (m, 2H), 1.40-1.50 (m, 2H), 1.20-1.40(m, 2H), 1.29(d, *J* = 6.8Hz, 2H), 1.13(d, *J* = 6.8 Hz, 12H), 1.11(d, *J* = 7.0 Hz, 12H), 1.058(d, *J* = 6.8 Hz, 12H), 1.053(d, *J* = 6.8Hz, 12H), 0.99(t, *J* = 7.1 Hz, 3H), 0.78(t, *J* = 7.1 Hz, 3H). ^{13}CNMR (100 MHz, $CDCl_3$) δ 147.7, 146.4, 146.3, 140.3, 137.2, 136.3, 130.7, 128.1, 120.37, 120.32, 119.3, 94.3, 59.9, 59.5, 49.2, 34.3, 30.47, 30.43, 27.9, 25.5, 24.13, 24.08, 24.04, 24.02, 15.7, 15.3. HRMS (ESI+): m/z Calcd for C_{84} H_{117} O_2 N_2 $[M+H]^+$ 1185.91096:, Found 1185.91248.

Section 2.7.3. Photoreaction and product analysis of azoalkane **AZ3b-e**,**4b-e** at NMR tube scale

The solution of **AZ3,4** (5 μmol) in C_6D_6 (0.5 ml, 10 mM) was bubbled with nitrogen for 15 minutes. Before light irradiation NMR was measured, and then LED light (365 nm) was applied for 30 minutes. NMR was measured after light irradiation, and the compound *trans*-**CP3**,**4** was identified.

AZ3b → *trans*-**CP3b**

AZ3b (3.4 mg, 5 μmol) were used and after photo irradiation *trans*-**CP3b** were obtained quantitatively.

trans-**CP3b**:^{1}H NMR (400 MHz, C_6D_6) δ 7.34(s, 6H), 3.46(q, *J* = 7.0 Hz, 2H), 2.95 (q, *J* = 7.1 Hz, 2H), 2.59(d, *J* = 6.6 Hz, 2H), 1.12-1.51(m, 6H) ,1.09 (t, *J* = 7.0 Hz, 3H), 0.64 (t, *J* = 7.1 Hz, 3H). ^{13}CNMR (100 MHz, C_6D_6) δ 138.5, 132.1, 131.4 122.5, 96.9, 62.2, 61.0, 46.8, 41.1, 27.5, 24.7, 14.7, 14.4. HRMS (APCI+): m/z Calcd for C_{22} H_{19} O Br_4 $[M\text{-}OEt]^+$ 614.81639:, Found 614.81818.

AZ3c → *trans*-**CP3c**

AZ3c (3.4 mg, 5 μmol) were used and after photo irradiation *trans*-**CP3c** were obtained quantitatively.

trans-**CP3c**: ^{1}H NMR (400 MHz, C_6D_6) δ 6.81 (d, *J* = 2.3 Hz, 4H), 6.49(t, *J* = 2.3 Hz, 2H), 3.86 (q, *J* = 7.1 Hz, 2H), 3.37 (s, 12 H), 3.35(q, *J* = 7.1 Hz, 2H), 2.98(d, *J* = 6.4 Hz, 2H), 1.92-2.07(m, 3H), 1.52-1.62(m, 1H), 1.38-1.52(m, 2H), 1.25(t, *J* = 7.1 Hz, 3H), 0.78(t, *J* = 7.1 H, 3H). ^{13}CNMR (100 MHz, C_6D_6) δ 160.6, 137.5, 108.6, 98.5, 97.5, 62.0, 60.6, 54.4, 47.8, 41.5, 28.1, 25.2, 15.10, 15.01. HRMS (ESI+): m/z Calcd for C_{28} H_{36} O_6 Na $[M+Na]^+$ 491.24041:, Found 491.24002.

AZ3d → *trans*-**CP3d**

AZ3d (4.2 mg, 5 μmol) were used and after photo irradiation

trans-**CP3d** were obtained quantitatively. The obtained solution wase evaporated and dissolved to $CDCl_3$. ^1H,^{13}C-NMR were collected.
trans-**CP3d**: ^1H NMR (400 MHz, $CDCl_3$) δ 6.97 (d, *J* = 1.5 Hz, 4H), 6.86 (d, *J* = 1.6 Hz, 8H), 6.68(t, *J* = 1.5 Hz, 2H), 3.83 (q, *J* = 7.0 Hz, 2H), 3.30(q, *J* = 7.0 Hz, 2H), 2.83 (d, *J* = 6.2 Hz, 2H), 2.33 (s, 12 H), 1.88(s, 12H), 1.83 (s, 12H), 1.32(t, *J* = 7.1 Hz, 3H), 0.77 (t, *J* = 7.0 Hz, 3H). ^{13} CNMR (100 MHz, $CDCl_3$) δ 140.3, 139.3, 136.2, 136.0, 135.9, 135.6, 129.3, 128.1, 128.0, 127.8, 97.4, 62.6, 59.9, 47.6, 41.5, 28.4, 24.8, 21.2, 20.7, 20.6, 15.3, 15.2. HRMS (APCI+): m/z Calcd for C_{60} H_{68} O_2 Na $[M+Na]^+$ 843.51115:, Found 843.51053.

AZ3e → *trans*-**CP3e**

AZ3e (5.7 mg, 5 μmol) were used and after photo irradiation *trans*-**CP3e** were obtained quantitatively. The obtained solution wase evaporated and dissolved to $CDCl_3$. ^1H,^{13}C-NMR were collected.
trans-**CP3e**: ^1H NMR (400 MHz, $CDCl_3$) δ 7.09 (d, *J* = 1.5 Hz, 4H), 6.92 (s, 8H), 6.77(t, *J* = 1.5 Hz, 2H), 3.72 (q, *J* = 7.1 Hz, 2H), 3.49(q, *J* = 7.1 Hz, 2H), 2.90(sept, *J* = 6.9 Hz, 4H), 2.82 (d, *J* = 5.7 Hz, 2 H), 2.70(sept, *J* = 6.9 Hz, 4H), 2.64(sept, *J* = 6.8 Hz, 4H),1.61- 1.80(m, 3H), 1.50-1.60(m, 1H), 1.35-1.50(m, 2H), 1.30(d, *J* = 6.9 Hz, 24H), 1.24(t, *J* = 7.1 Hz, 3H), 0.99(d, *J* = 6.2 Hz, 12H), 0.97(d, *J* = 6.1 Hz, 12H), 0.88 (brs, 24H), 0.76(t, *J* = 7.0 Hz, 3H). ^{13}CNMR (100 MHz, $CDCl_3$) δ 147.4, 146.4, 146.2, 139.6, 137.1, 125.8, 129.1, 128.7, 120.2, 96.6, 61.7, 60.5, 49.8, 41.2, 34.4, 30.31, 30.26, 28.2, 24.17, 24.11, 24.08, 23.9, 23.7, 15.2, 14.9. HRMS (APCI+): m/z Calcd for C_{84} H_{116} O_2 Na $[M+Na]^+$ 1179.88675:, Found 1179.88623.

AZ4b → *trans*-**CP4b**

AZ4b (4.2 mg, 5 μmol) were used and after photo irradiation *trans*-**CP4b** were obtained quantitatively.
trans-**CP4b**: ^1H NMR (400 MHz, C_6D_6) δ 7.36(t, *J* = 1.58 Hz, 1H), 7.33 (t, *J* = 1.56, 1H), 7.23 (d, *J* = 1.52, 2H), 7.17 (d, *J* = 1.24 Hz, 1H), 5.41-5.46 (m, 1H), 5.27-5.33(m, 1H), 3.35-3.50(m, 2H), 3.20-3.25(m, 1H),

2.89-3.04(m, 2H), 2.68-2.75(m, 1H), 2.13(ddd, *J* = 17.9 Hz, 8.9, 1.8 Hz, 1H), 2.05 (dt, *J* = 17.6, 2.5 Hz, 1H), 1.09 (t, *J* = 7.0 Hz, 3H), 0.67 (t, *J* = 7.0 Hz, 3H). ^{13}CNMR (100 MHz, C_6D_6) δ 138.5, 137.4, 132.9, 132.3, 132.0, 131.8, 131.1, 129.1, 122.4, 122.3, 98.1, 62.3, 61.2, 52.6, 48.9, 37.7, 14.7, 14.4. HRMS (APCI+): m/z Calcd for C_{22} H_{17} O_2 N_2 Br_4 $[M\text{-}OEt]^+$ 612.80074:, Found 612.80249.

AZ4c → *trans*-**CP4c**

AZ4c (3.2 mg, 5 μmol) were used and after photo irradiation *trans*-**CP4c** were obtained quantitatively.

trans-**CP4c**: ^{1}H NMR (400 MHz, C_6D_6) δ 6.70(d, *J* = 2.2 Hz, 2H), 6.66 (d, *J* = 2.3 Hz, 2H), 6.51(t, *J* = 2.2 Hz, 1H), 6.49 (t, *J* = 2.3 Hz, 1H), 5.78-5.84(m,1H), 5.68-5.74(m, 1H), 3.74-3.92(m, 2H), 3.62-3.68(m, 1H), 3.24-3.46(m, 2H), 3.344(s, 6H), 3,339(s, 6H), 3.04-3.12(m, 1H), 2.58-2.69(m, 1H), 2.36-2.48(m, 1H), 1.24(t, *J* = 7.0 Hz, 3H), 0.81(t, *J* = 7.1 Hz, 3H), ^{13}CNMR (100 MHz, C_6D_6) δ 160.6, 160.4, 137.8, 136.2, 132.0, 130.9, 109.0, 108.1, 98.8,98.7, 98.6, 62.0, 60.8, 54.44, 54.42, 53.4, 49.1, 38.3, 34.2, 15.1, 15.0. HRMS (ESI+): m/z Calcd for C_{28} H_{35} O_6 $[M+H]^+$ 467.24282:, Found 467.24203.

AZ4d → *trans*-**CP4d**

AZ4d (4.2 mg, 5 μmol) were used and after photo irradiation *trans*-**CP4d** were obtained quantitatively. The obtained solution wase evaporated and dissolved to $CDCl_3$. ^{1}H,^{13}C-NMR were collected.

trans-**CP4d**: ^{1}H NMR (400 MHz, $CDCl_3$) δ 6.80-6.98 (m, 12H), 6.70(t, *J* = 1.6HZ, 1H), 6.65 (t, *J* = 1.6 Hz, 1H), 5.78-5.84(m, 1H), 5,56-5.62(m, 1H), 3.88(qd, *J* = 7.1 Hz, 2.5 Hz, 2H), 3.46(brs, 1H), 3.30 (qd, *J* = 7.0Hz, 2.9 Hz, 2H). 2.98-3.05(m, 1H), 2.40-2.57(m, 2H), 2.32(s, 12H), 1.92(s, 6H), 1.88(s, 6H), 1.84(s, 12H) 1.35(t, *J* = 7.1Hz, 3H), 0.84(t, *J* = 7.1Hz, 3H). ^{13}CNMR (100 MHz, $CDCl_3$) δ 140.2, 140.0, 139.2, 139.0, 136.09, 136.06, 136.00, 135.9, 135.76, 135.72, 135.6, 134.8, 132.5, 130.5, 129.3, 128.8, 128.1 127.93, 127.87, 127.82, 98.4, 62.7, 59.9, 53.2, 49.9, 49.3, 38.2, 34.3, 21.0,

20.67, 20.64, 20.53, 20.47, 15.2, 15.0. HRMS (ESI+): m/z Calcd for C_{60} H_{66} O_2 Na $[M+Na]^+$ 841.49550:, Found 841.49567.

AZ4e → *trans*-**CP4e**

AZ4e (5.7 mg, 5 μmol) were used and after photo irradiation *trans*-**CP4e** were obtained quantitatively. The obtained solution wase evaporated and dissolved to $CDCl_3$. ^1H,^{13}C-NMR were collected.

trans-**CP4e**: ^1H NMR (400 MHz, $CDCl_3$) δ 7.12(d, *J* = 1.4Hz, 2H), 7.05(brs, 3H), 6.95(s, 7H), 6.79(t, *J* = 1.56Hz, 1H), 6.78(t, *J* = 1.3Hz, 1H), 5.75-5.80(m, 1H), 5.48-5.54(m, 1H), 3.71-3.89(m, 2H), 3.40-3.60(m, 3H), 3.03-3.11(m, 1H), 2.92(sept, *J* = 6.8Hz, 4H), 2.60-2.82(m, 8H), 2.44-2.54(m, 1H), 2.29-2.39(m, 1H), 1.31(d, *J* = 6.9Hz, 24H), 1.29(t, *J* = 7Hz, 3H), 0.82(t, *J* = 7.0Hz, 3H). 0.60-1.22 (m, 48H). ^{13}CNMR (100 MHz, $CDCl_3$) δ 147.3, 146.49, 146.28, 146.15, 139.4, 137.1, 137.0, 135.9, 135.8, 132.2, 130.5, 129.1, 129.0, 120.2, 97.6, 62.1, 60.5, 55.6, 52.4, 49.6, 38.7, 34.3, 30.3, 30.2, 24.12, 23.06, 24.01, 23.9, 23.7, 15.1, 15.0. HRMS (ESI+): m/z Calcd for C_{84} H_{114} O_2 Na $[M+Na]^+$ 1177.87231:, Found 1177.87110.

Section 2.7.4. NOESY spectrum of **AZ3b-e**, **AZ4b-e**

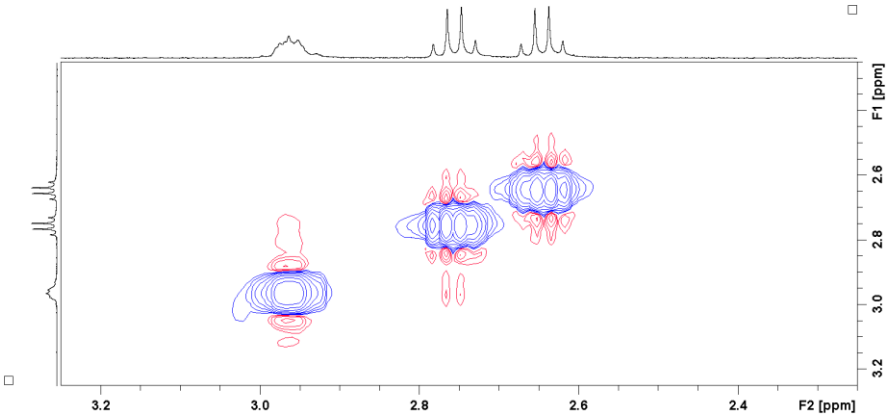

Figure 2.S1. NOESY spectrum of **AZ3b** in C_6D_6.

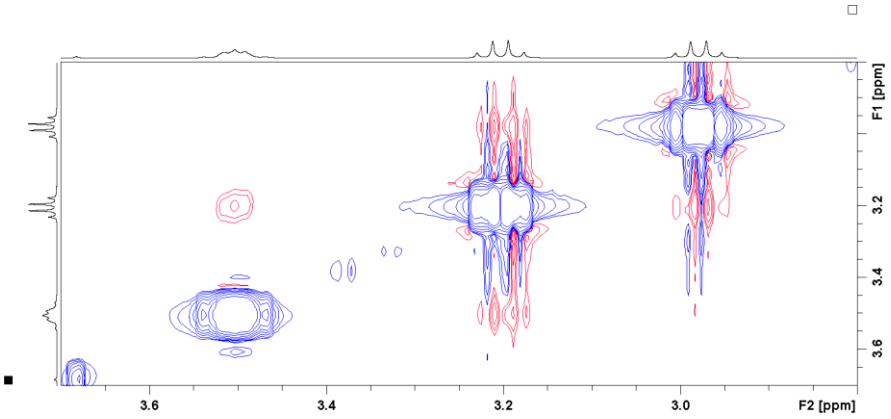

Figure 2.S2. NOESY spectrum of **AZ3c** in $CDCl_3$.

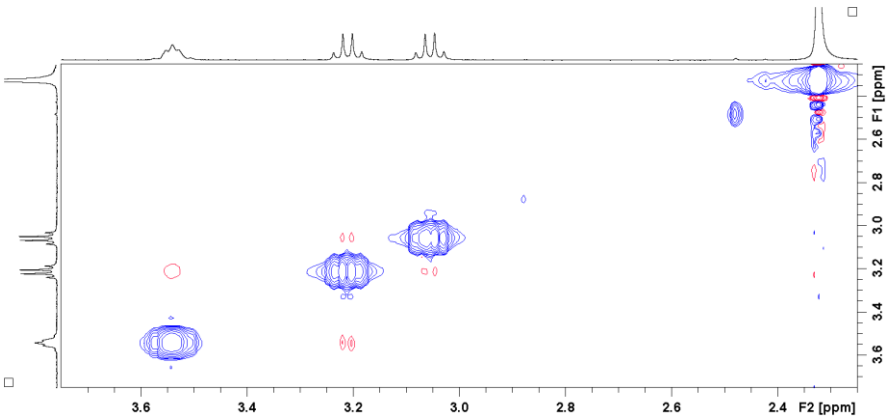

Figure 2.S3. NOESY spectrum of **AZ3d** in $CDCl_3$.

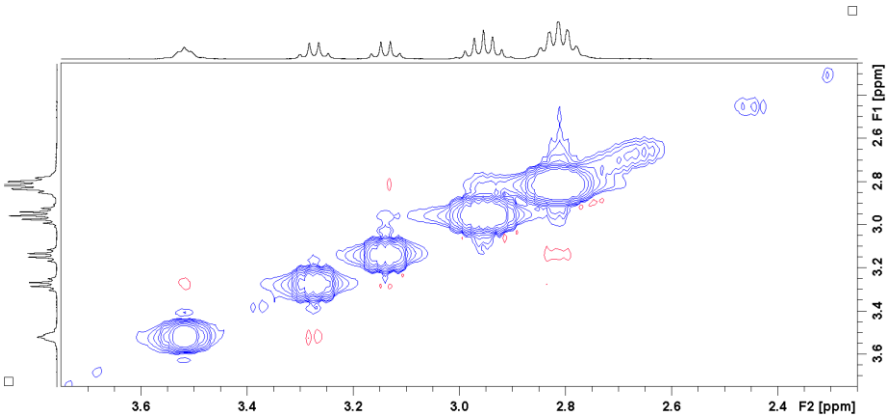

Figure 2.S4. NOESY spectrum of **AZ3e** in $CDCl_3$.

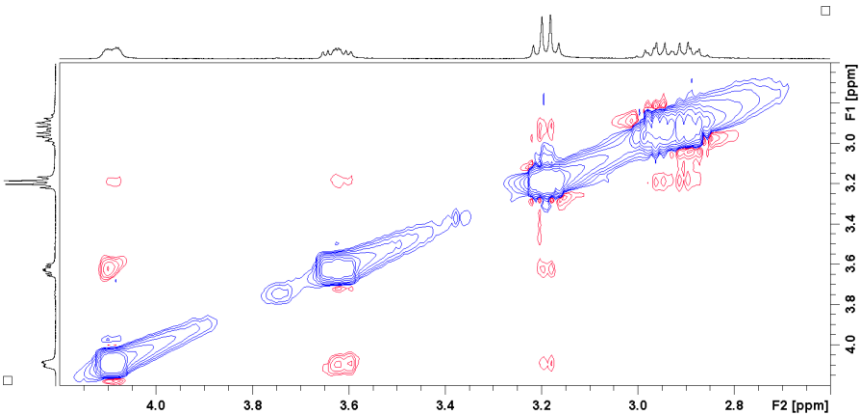

Figure 2.S5. NOESY spectrum of **AZ4b** in $CDCl_3$.

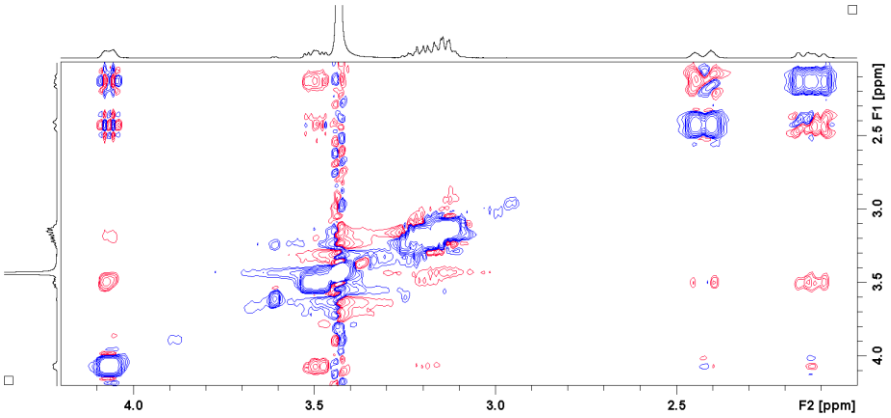

Figure 2.S6. NOESY spectrum of **AZ4c** in C_6D_6.

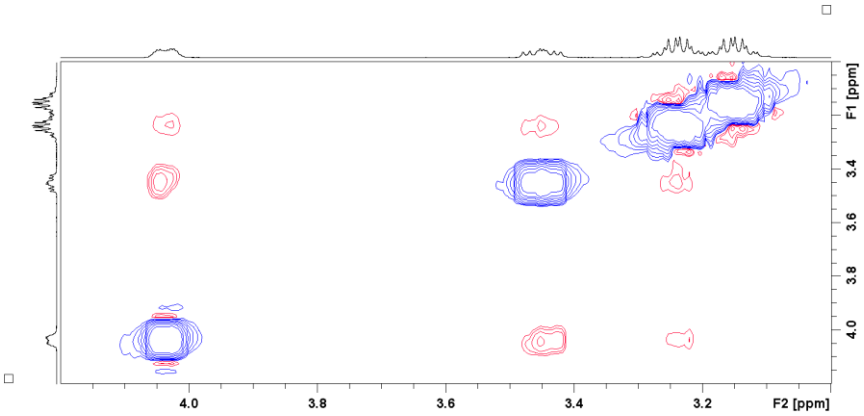

Figure 2.S7. NOESY spectrum of **AZ4d** in C_6D_6.

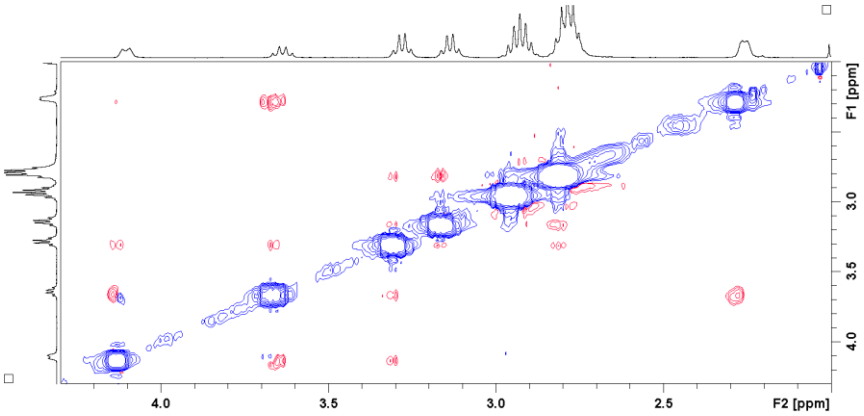

Figure 2.S8. NOESY spectrum of **AZ4e** in $CDCl_3$.

Section 2.7.5. UV-vis spectra of **AZ3**, **AZ4**

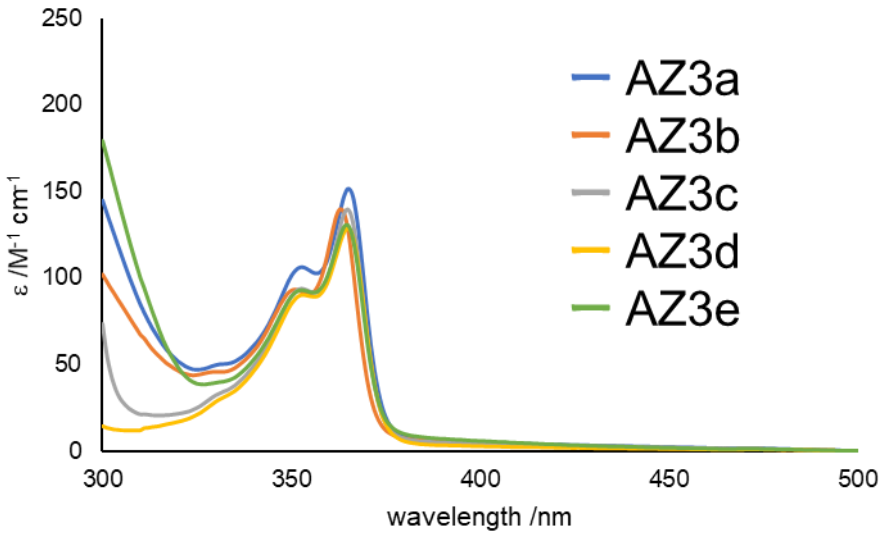

Figure 2.S9. UV-vis spectra of **AZ3a-e**. (Blue: **AZ3a**, orange: **AZ3b**, gray: **AZ3c**, yellow: **AZ3d**, green: **AZ3e**.)

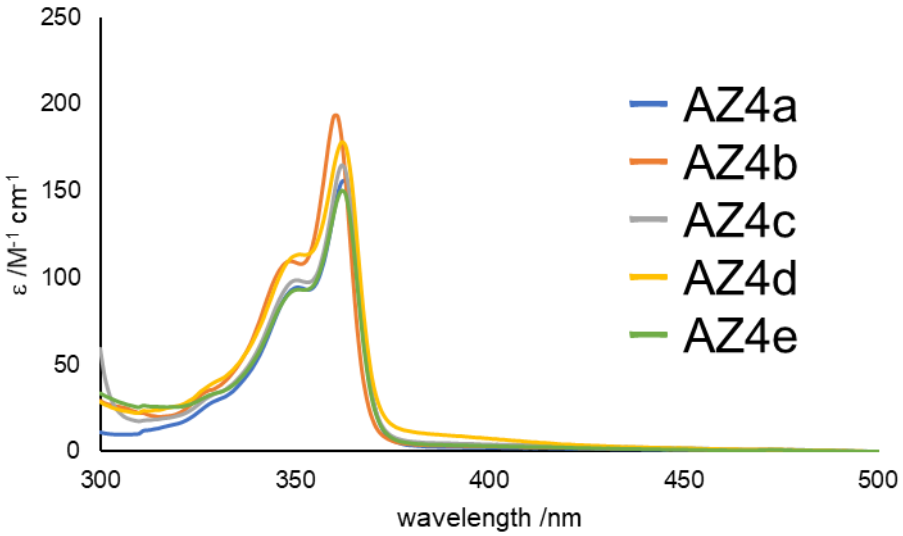

Figure 2.S10. UV-vis spectra of **AZ4a-e**. (Blue: **AZ4a**, orange: **AZ4b**, gray: **AZ4c**, yellow: **AZ4d**, green: **AZ4e**.)

Section 2.7.6. The ^{1}H NMR result of photoreaction of **AZ3b-e** and **AZ4b-d**

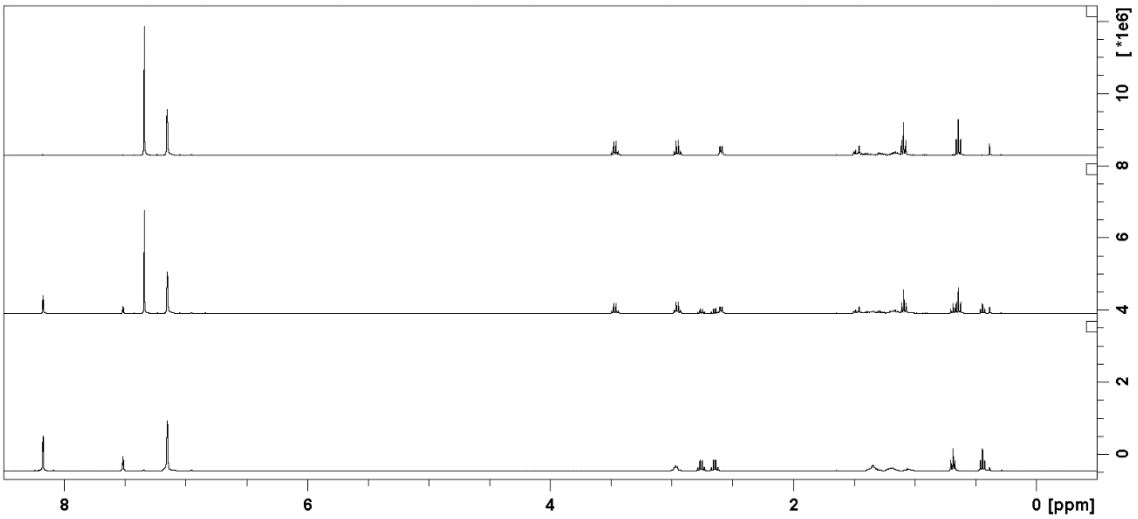

Figure 2.S11. ^{1}H NMR spectrum (C_6D_6, 400 MHz) bottom: before photochemical irradiation of **AZ3b**. middle: 30 sec irradiations, up: 2 min irradiation using 365 nm LED under nitrogen.

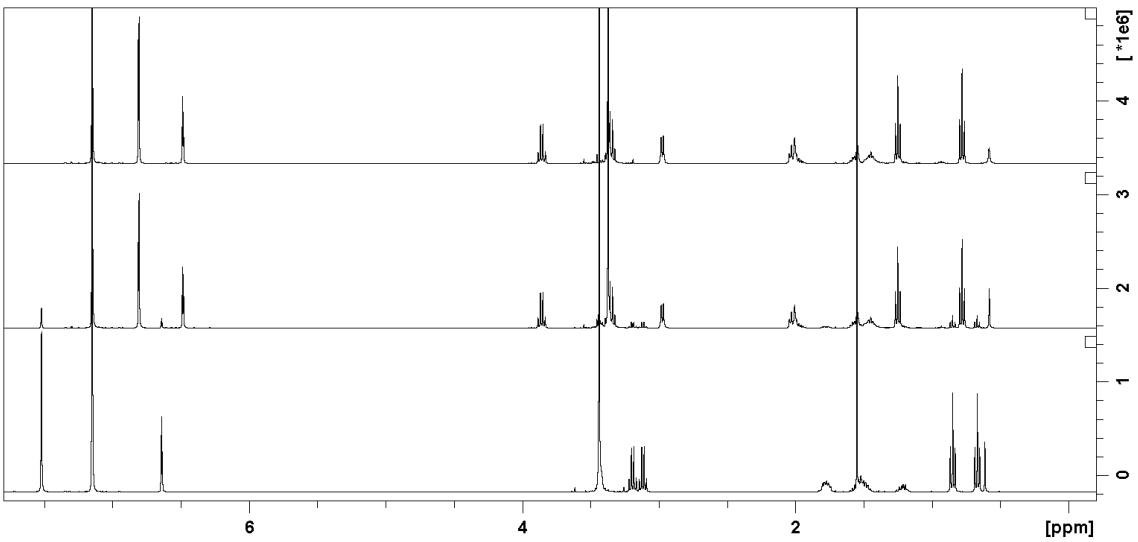

Figure 2.S12. ^{1}H NMR spectrum (C_6D_6, 400 MHz) bottom: before photochemical irradiation of **AZ3c**. middle: 60 sec irradiations, up: 3 min irradiation using 365 nm LED under nitrogen.

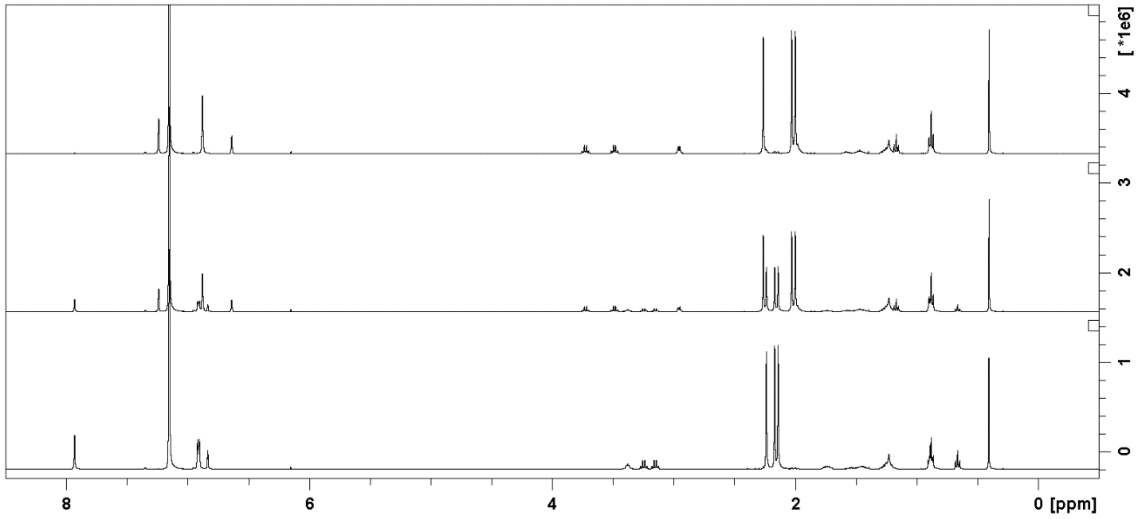

Figure 2.S13. ^{1}H NMR spectrum (C_6D_6, 400 MHz) bottom: before photochemical irradiation of **AZ3d**. middle: 1 min irradiation, up: 3 min irradiation using 365 nm LED under nitrogen.

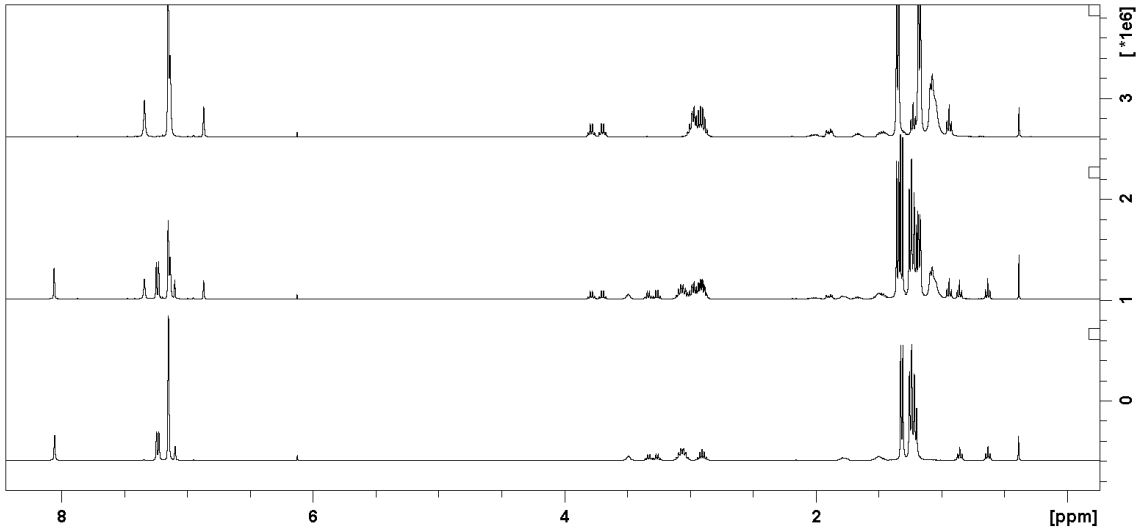

Figure 2.S14. ^{1}H NMR spectrum (C_6D_6, 400 MHz) bottom: before photochemical irradiation of **AZ3e**. middle: 90 sec irradiations, up: 20 min irradiation using 365 nm LED under nitrogen.

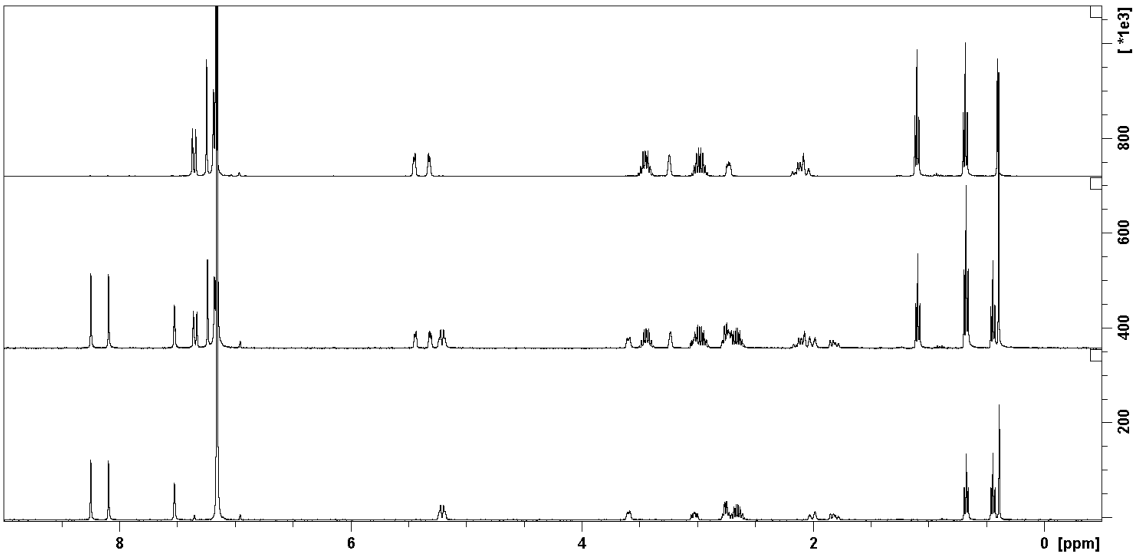

Figure 2.S15. ^{1}H NMR spectrum (C_6D_6, 400 MHz) bottom: before photochemical irradiation of **AZ4b**. middle: 210 sec irradiations, up: 30 min irradiation using 365 nm LED under nitrogen.

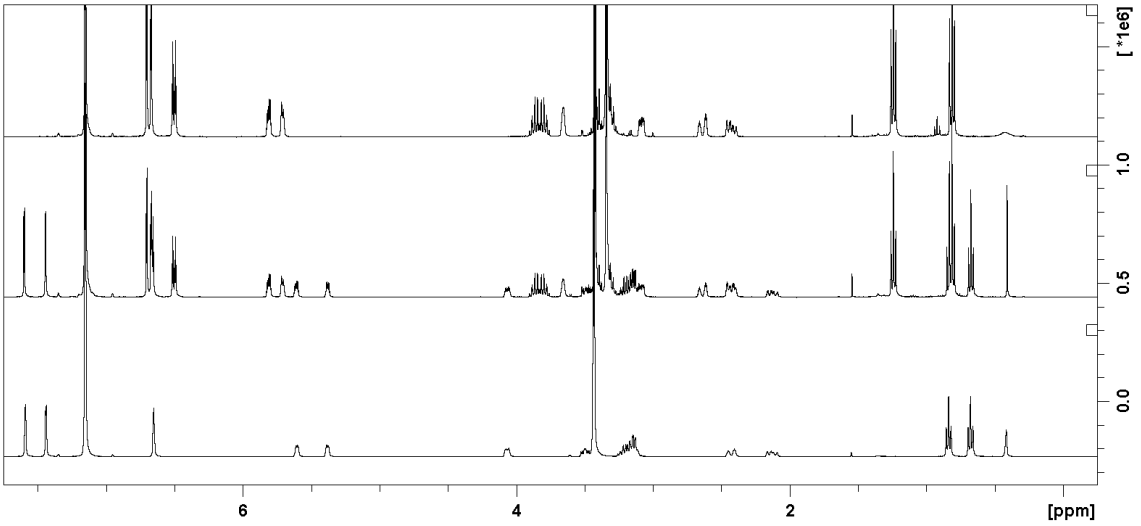

Figure 2.S16. ^{1}H NMR spectrum (C_6D_6, 400 MHz) bottom: before photochemical irradiation of **AZ4c**. middle: 40 sec irradiations, up: 35 min irradiation using 365 LED under nitrogen.

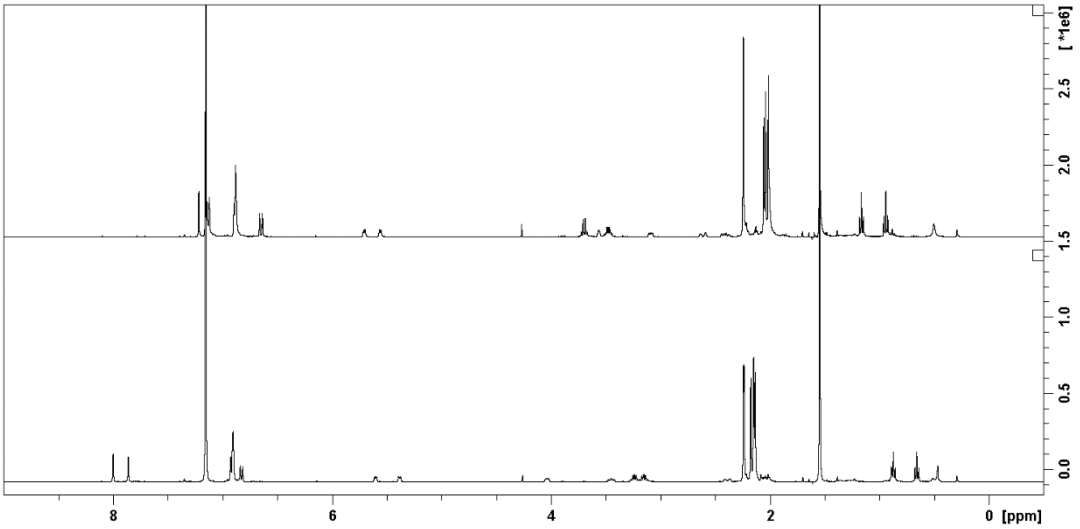

Figure 2.S17. ^{1}H NMR spectrum (C_6D_6, 400 MHz) bottom: before photochemical irradiation of **AZ4d**. up: 10 min irradiation using 365 LED under nitrogen.

Section 2.7.7. NOESY spectrum of photo product of **AZ3b-e** and **AZ4b-e**

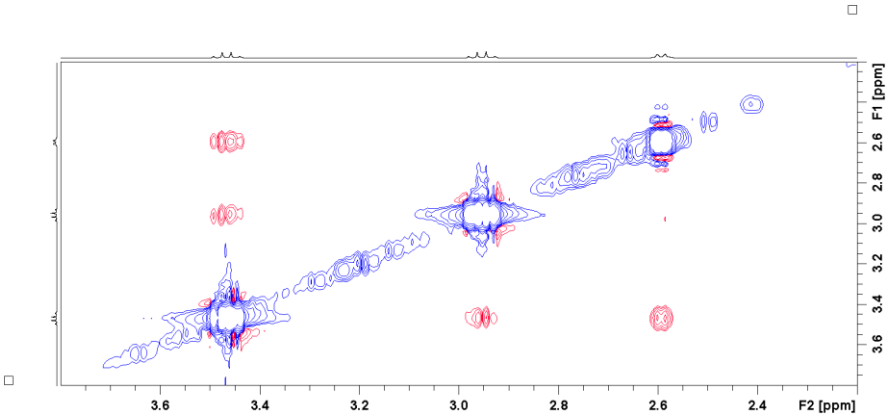

Figure 2.S18. NOESY spectrum of *trans*-**CP3b** in C_6D_6.

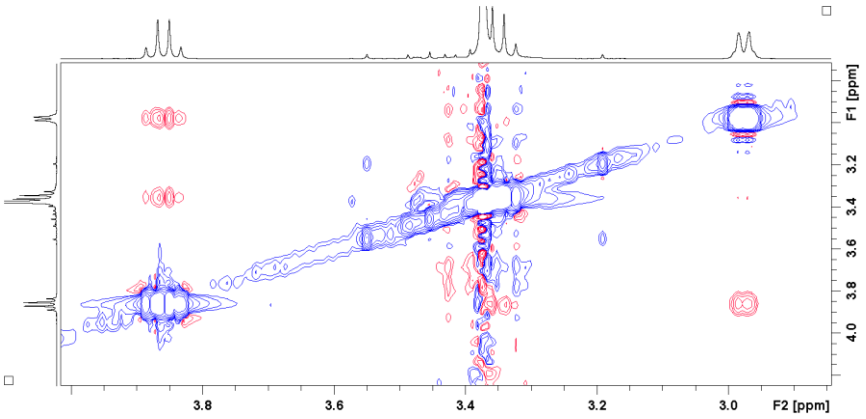

Figure 2.S19. NOESY spectrum of *trans*-**CP3c** in C_6D_6.

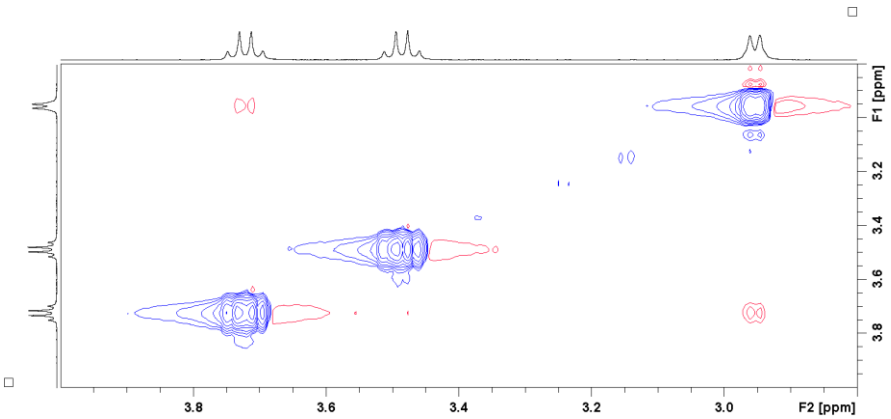

Figure 2.S20. NOESY spectrum of *trans*-**CP3d** in C_6D_6.

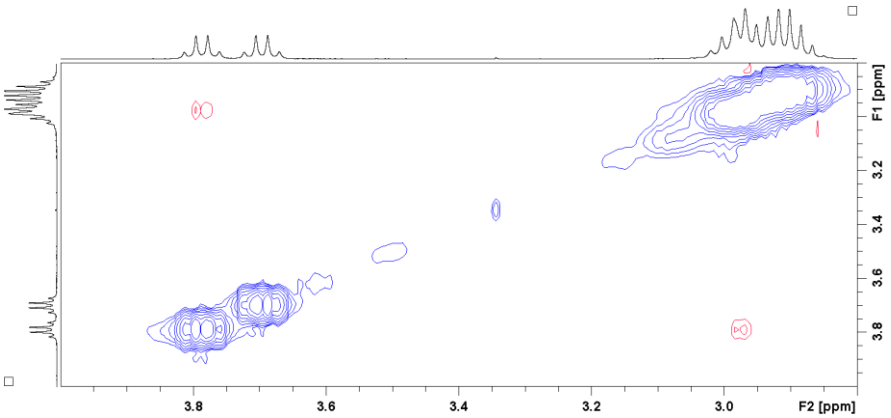

Figure 2.S21. NOESY spectrum of *trans*-**CP3e** in C_6D_6.

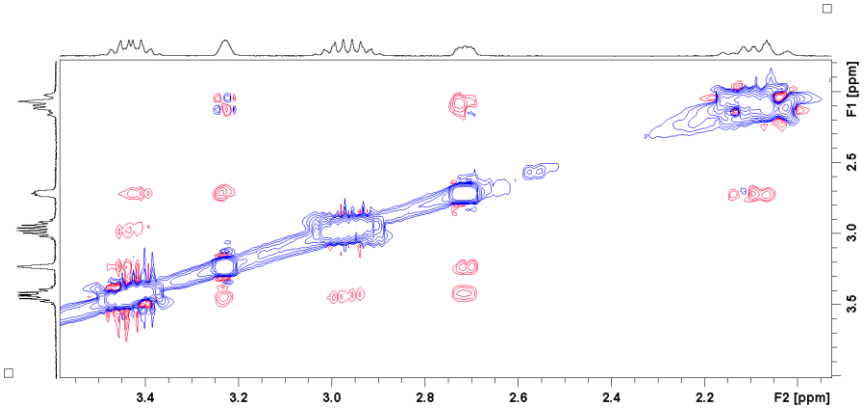

Figure 2.S22. NOESY spectrum of *trans*-**CP4b** in C_6D_6.

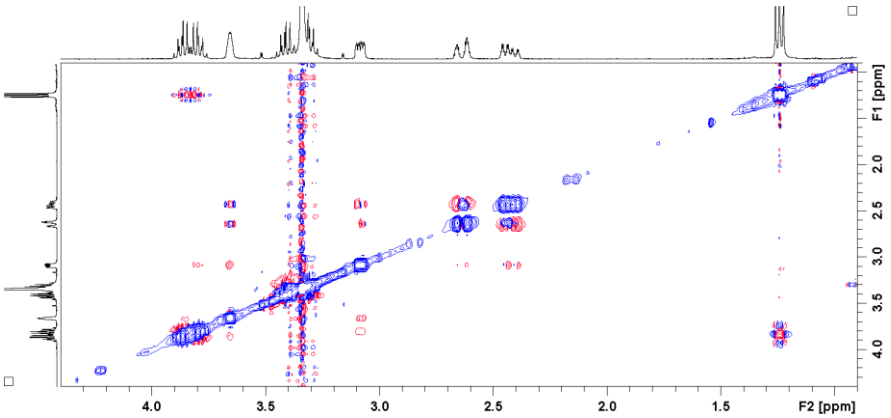

Figure 2.S23. NOESY spectrum of *trans*-**CP4c** in C_6D_6.

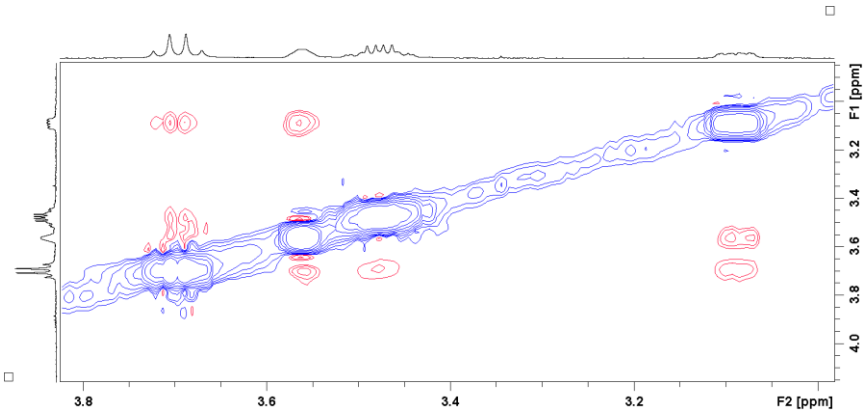

Figure 2.S24. NOESY spectrum of *trans*-**CP4d** in C_6D_6.

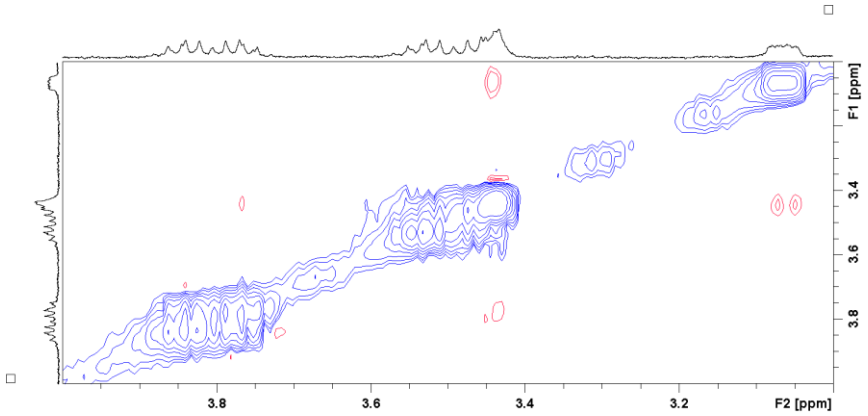

Figure 2.S25. NOESY spectrum of *trans*-**CP4e** in $CDCl_3$.

Section 2.7.8. Transient absorption spectra and temperature dependency of the decay trace of S-**DR3**,**4**

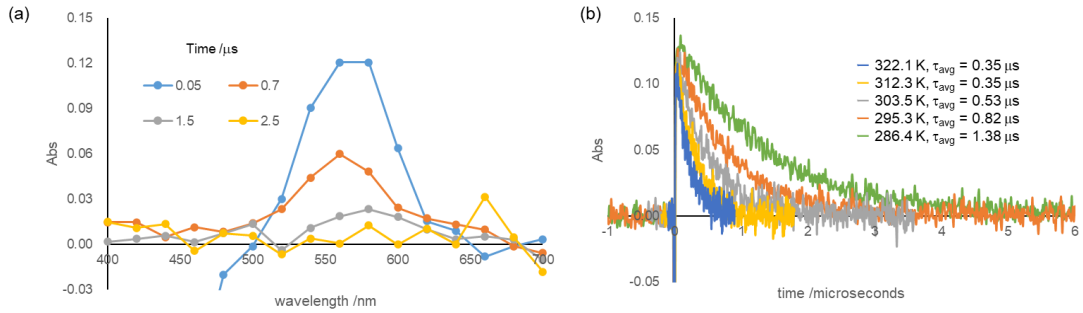

Figure 2.S26. (a) Transient absorption spectra of **AZ3a** and (b) temperature dependency of the decay trace of S-**DR3a** in benzene.

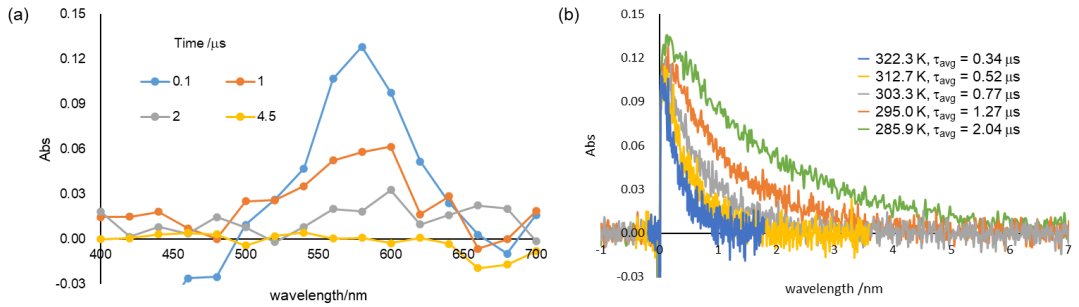

Figure 2.S27. (a) Transient absorption spectra of **AZ3b** and (b) temperature dependency of the decay trace of S-**DR3b** in benzene.

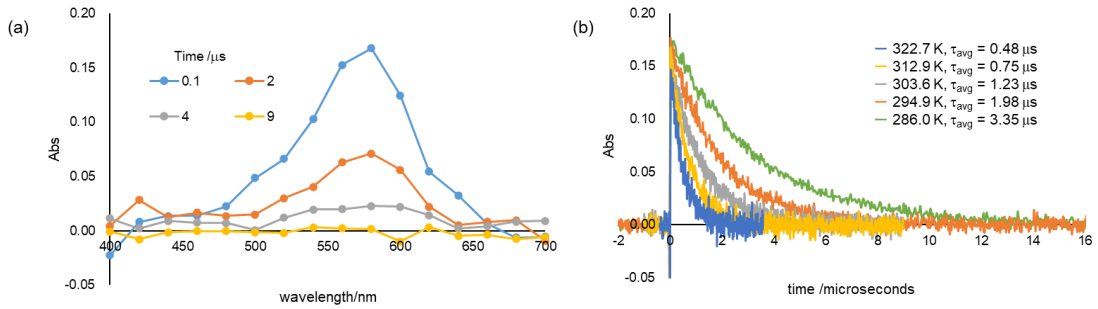

Figure 2.S28. (a) Transient absorption spectra of **AZ3c** and (b) temperature dependency of the decay trace of S-**DR3c** in benzene.

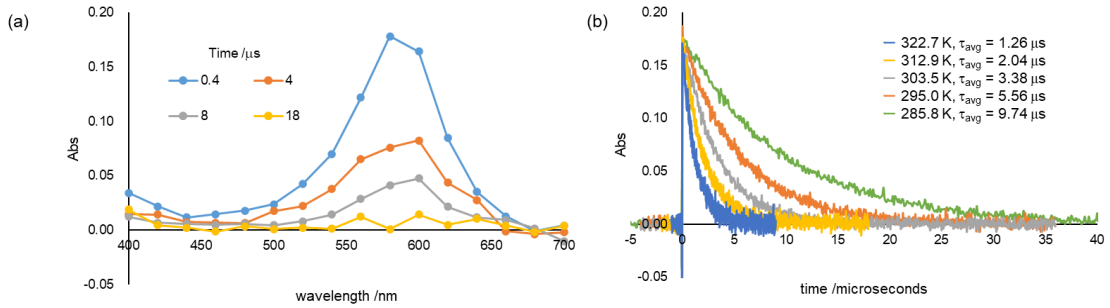

Figure 2.S29. (a) Transient absorption spectra of **AZ3d** and (b) temperature dependency of the decay trace of S-**DR3d** in benzene.

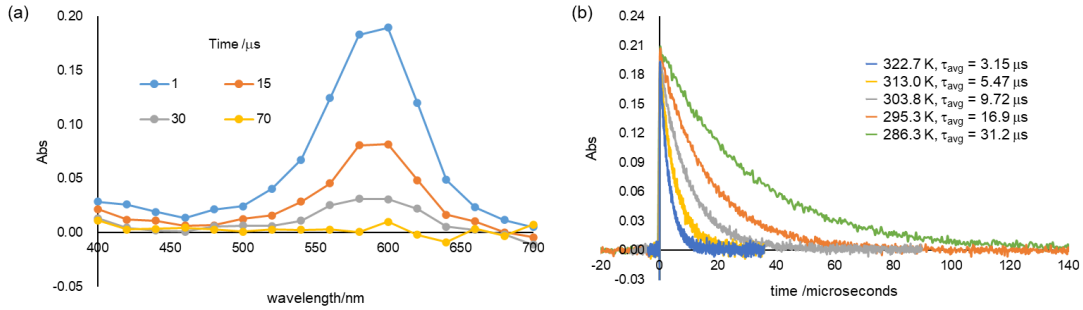

Figure 2.S30. (a) Transient absorption spectra of **AZ3e** and (b) temperature dependency of the decay trace of S-**DR3e** in benzene.

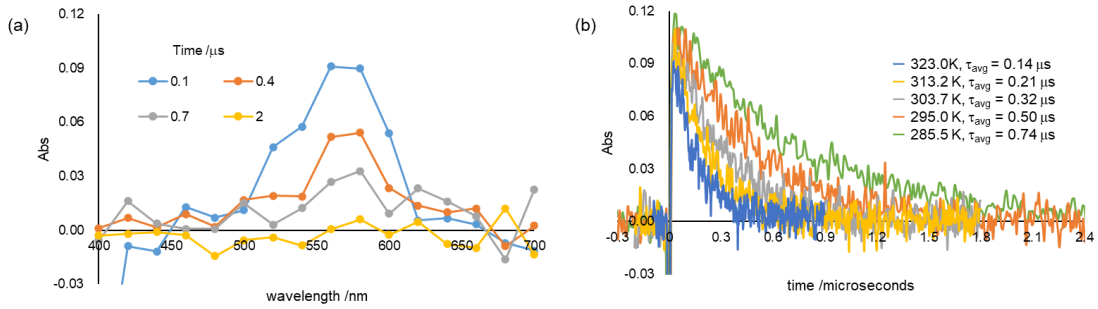

Figure 2.S31. (a) Transient absorption spectra of **AZ4a** and (b) temperature dependency of the decay trace of S-**DR4a** in benzene.

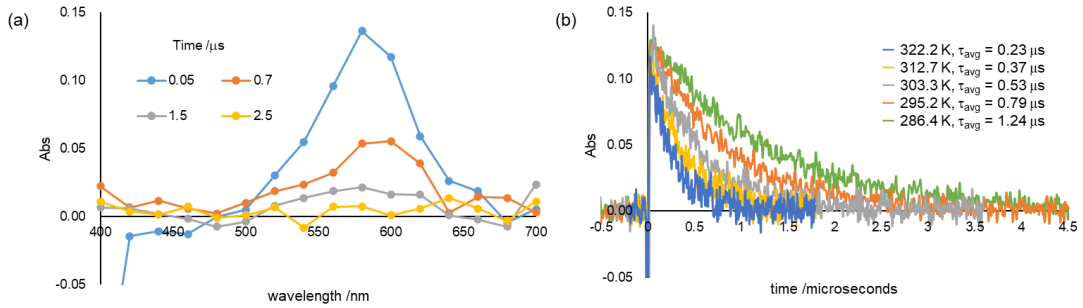

Figure 2.S32. (a) Transient absorption spectra of **AZ4b** and (b) temperature dependency of the decay trace of S-**DR4b** in benzene.

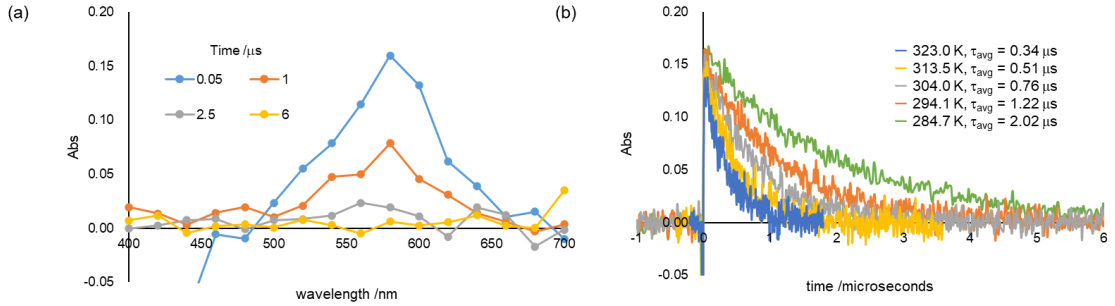

Figure 2.S33. (a) Transient absorption spectra of **AZ4c** and (b) temperature dependency of the decay trace of S-**DR4c** in benzene.

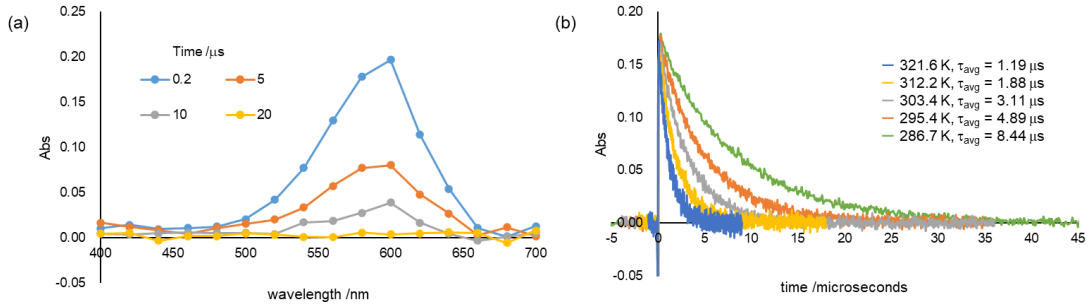

Figure 2.S34. (a) Transient absorption spectra of **AZ4d** and (b) temperature dependency of the decay trace of S-**DR4d** in benzene.

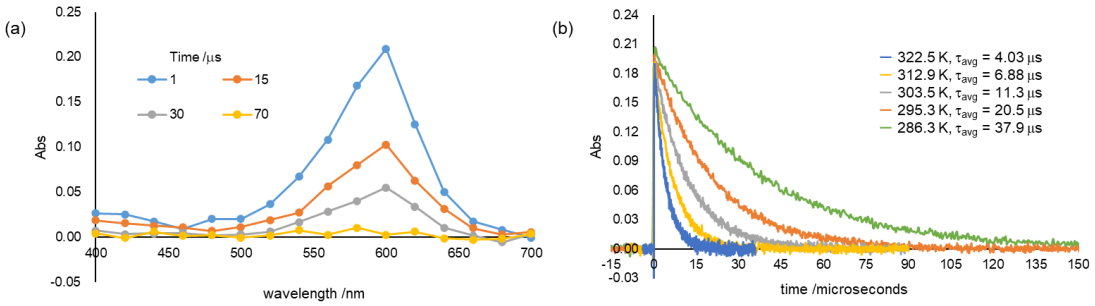

Figure 2.S35. (a) Transient absorption spectra of **AZ4e** and (b) temperature dependency of the decay trace of S-**DR4e** in benzene.

Section 2.7.8. Arrhenius plot and Eyring plot for LFP measurements

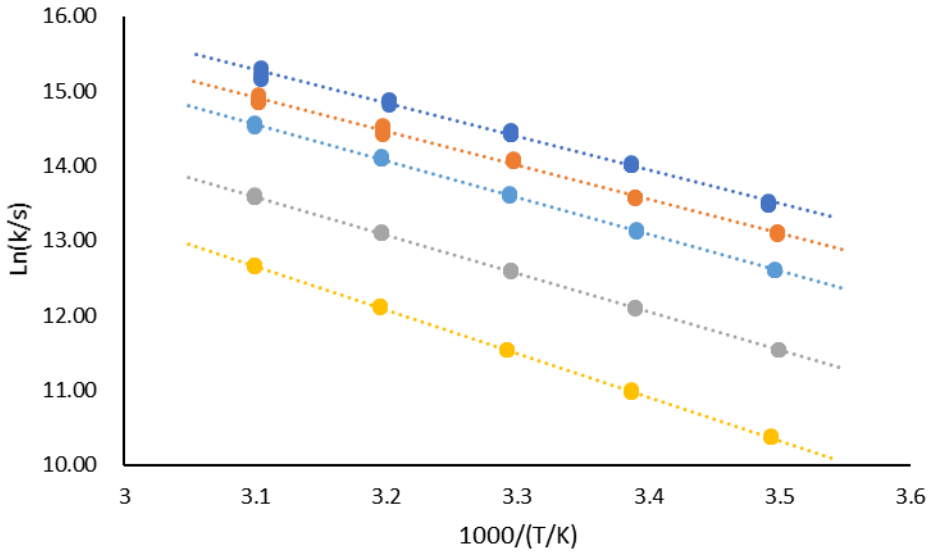

Figure 2.S36. Arrhenius plot of S-**DR3a** (blue), S-**DR3b**(orange), S-**DR3c** (light blue), S-**DR3d** (gray), S-**DR3e** (yellow).

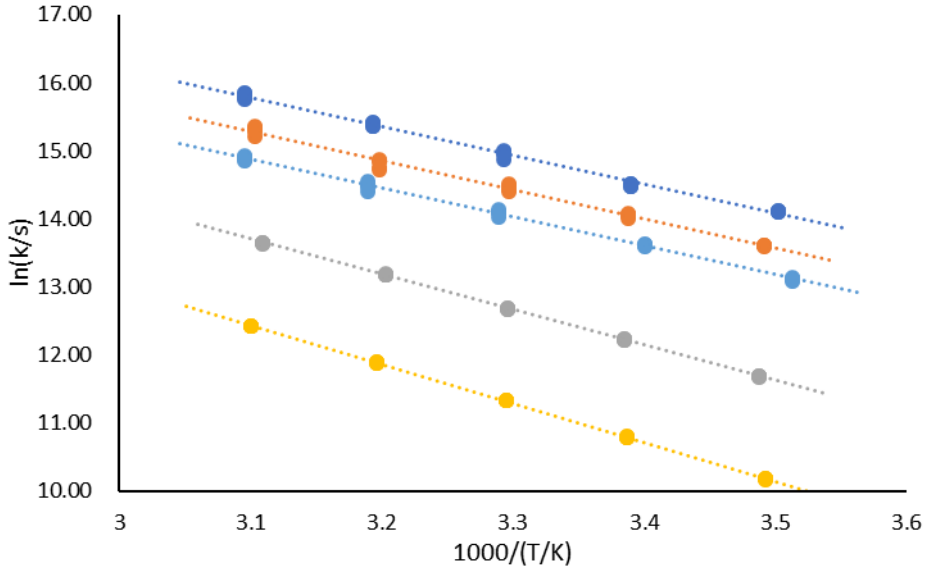

Figure 2.S37. Arrhenius plot of S-**DR4a** (blue), S-**DR4b**(orange), S-**DR4c** (light blue), S-**DR4d** (gray) and S-**DR4e** (yellow).

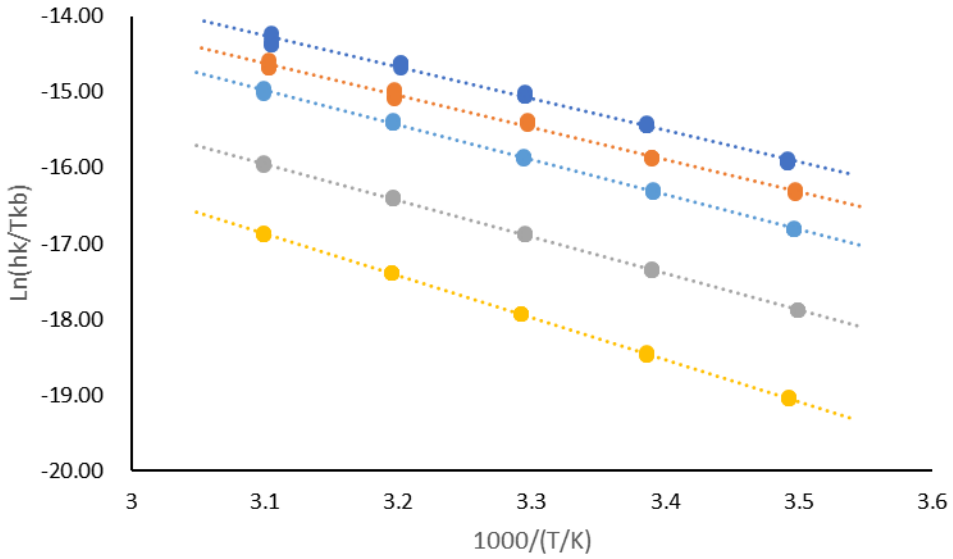

Figure 2.S38. Eyring plot of S-**DR3a** (blue), S-**DR3b**(orange), S-**DR3c** (light blue), S-**DR3d** (gray) and S-**DR3e** (yellow).

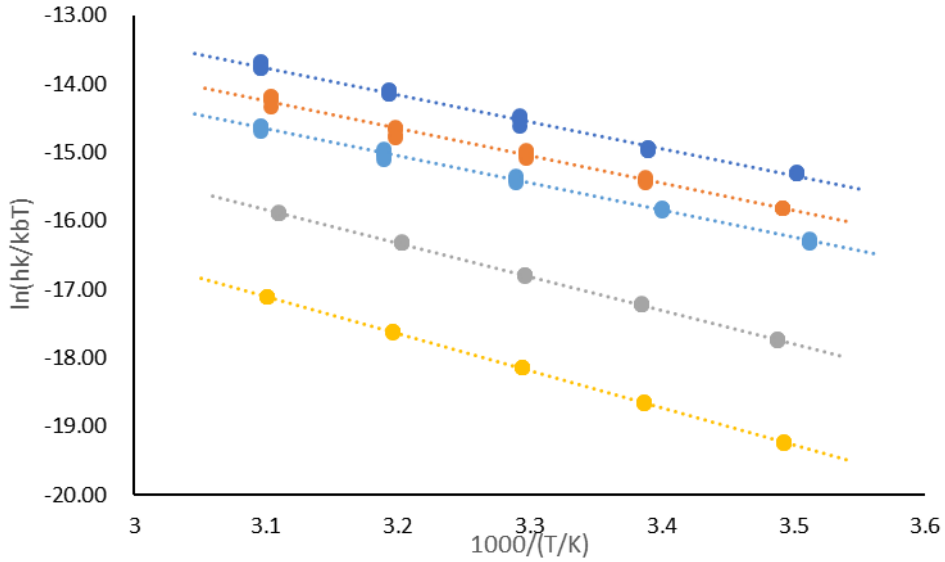

Figure 2.S39. Eyring plot of S-**DR4a** (blue), S-**DR4b**(orange), S-**DR4c** (light blue), S-**DR4d** (gray) and S-**DR4e** (yellow).

Section 2.7.9. Time profiles of integration ratio of NMR signals between *cis*-**CP4e** and **AZ4e** at low temperature

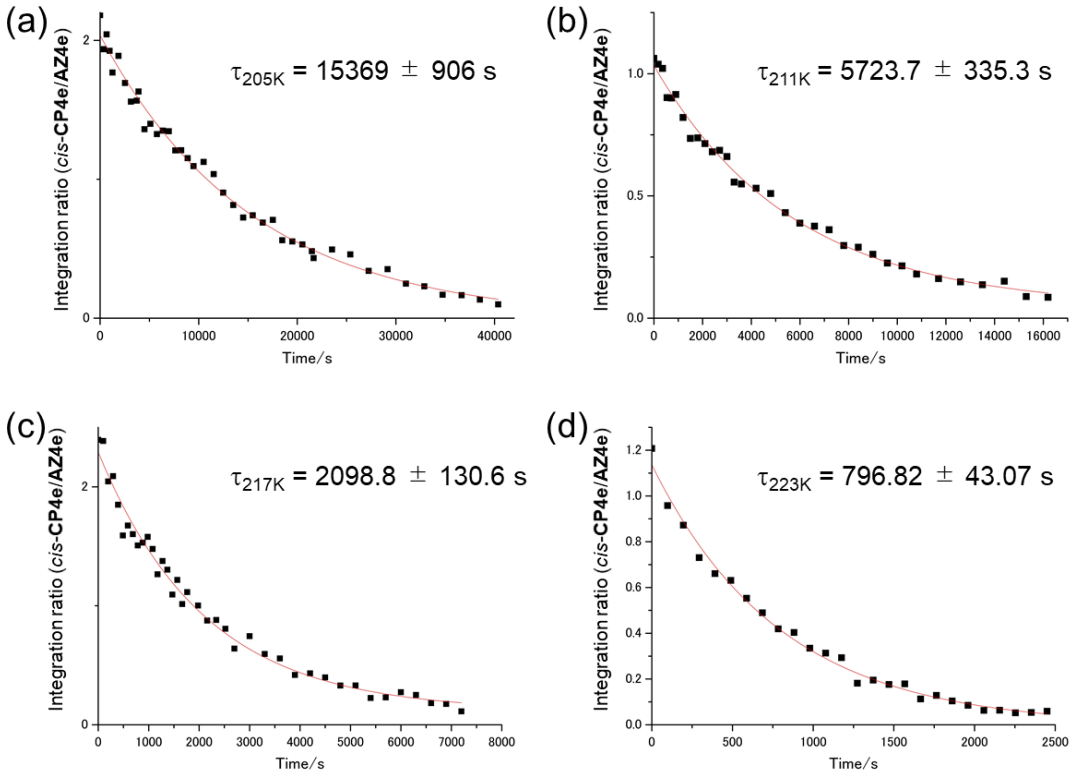

Figure 2.S40. Time profiles of integration ratio of NMR signals between *cis*-**CP4e** and **AZ4e** at (a) 205 K, (b) 211 K, (c) 217 K, (d) 223 K.

Section 2.7.10 NMR chart

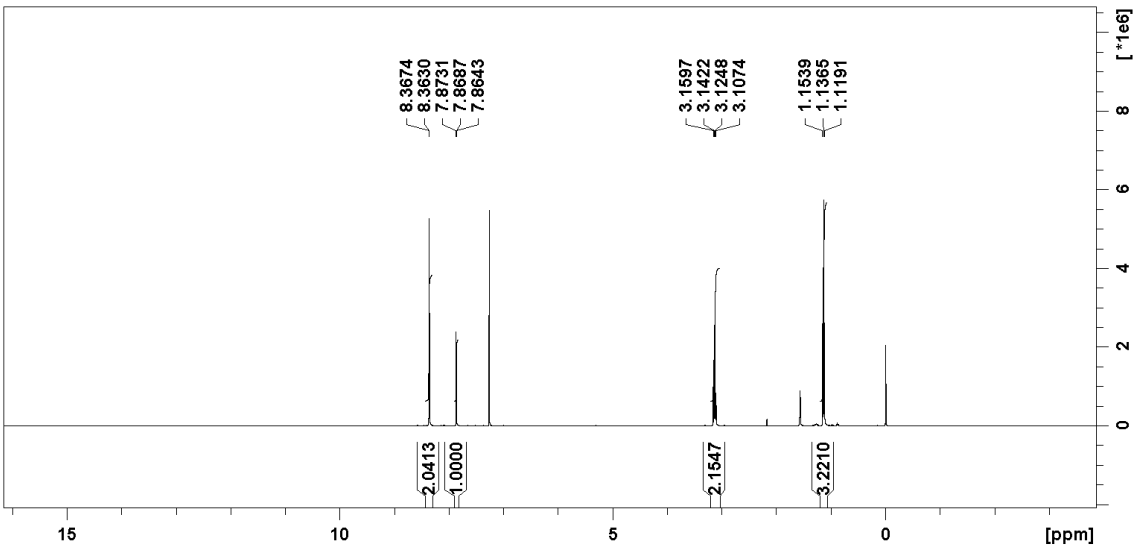

Figure 2.S41. ^{1}H NMR of Compound **PZ-Br$_4$** in $CDCl_3$ (400 MHz).

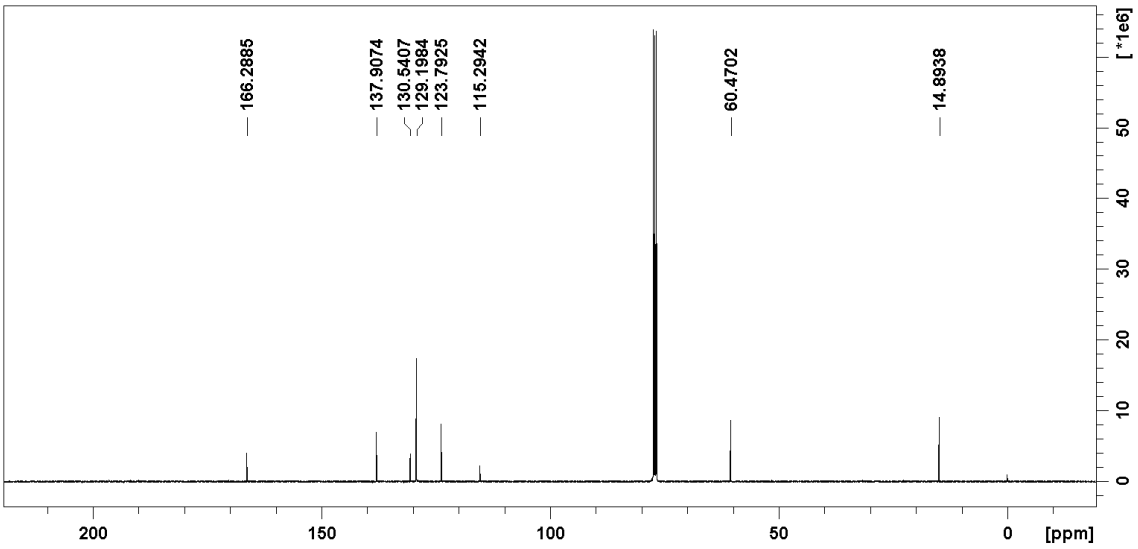

Figure 2.S42. ^{13}C NMR of compound **PZ-Br$_4$** in $CDCl_3$ (100 MHz).

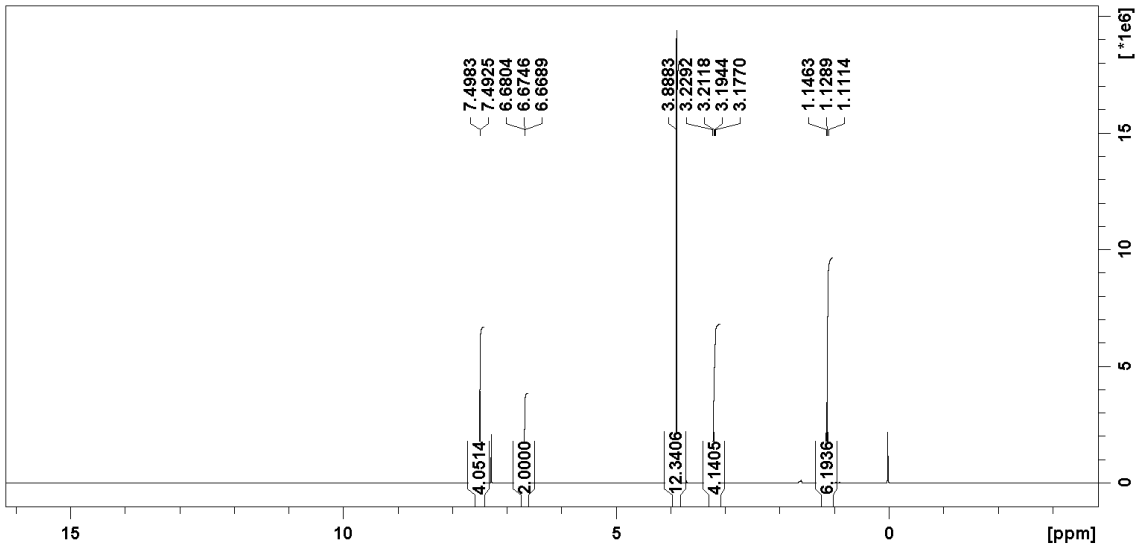

Figure 2.S43. ^{1}H NMR of compound **PZ-OMe$_4$** in $CDCl_3$ (400 MHz).

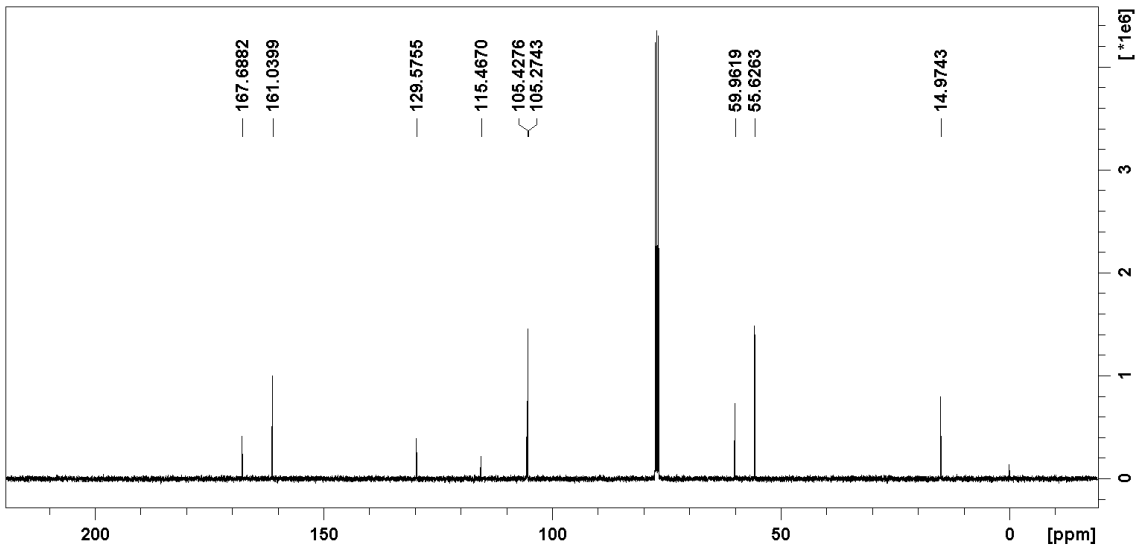

Figure 2.S44. ^{13}C NMR of Compound **PZ-OMe$_4$** in $CDCl_3$ (100 MHz).

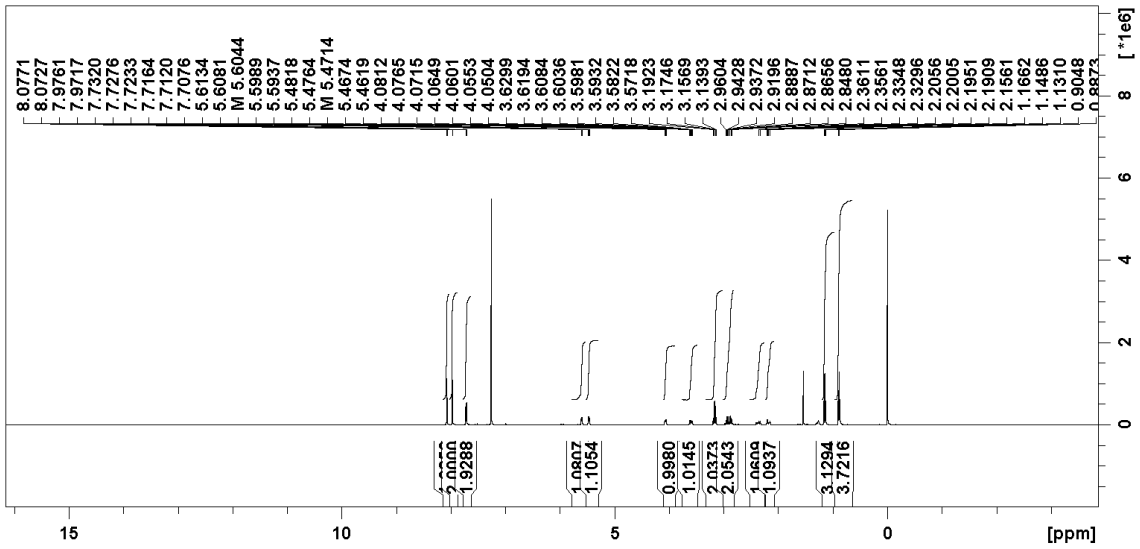

Figure 2.S45. ^{1}H NMR of **AZ4b** in $CDCl_3$ (400 MHz).

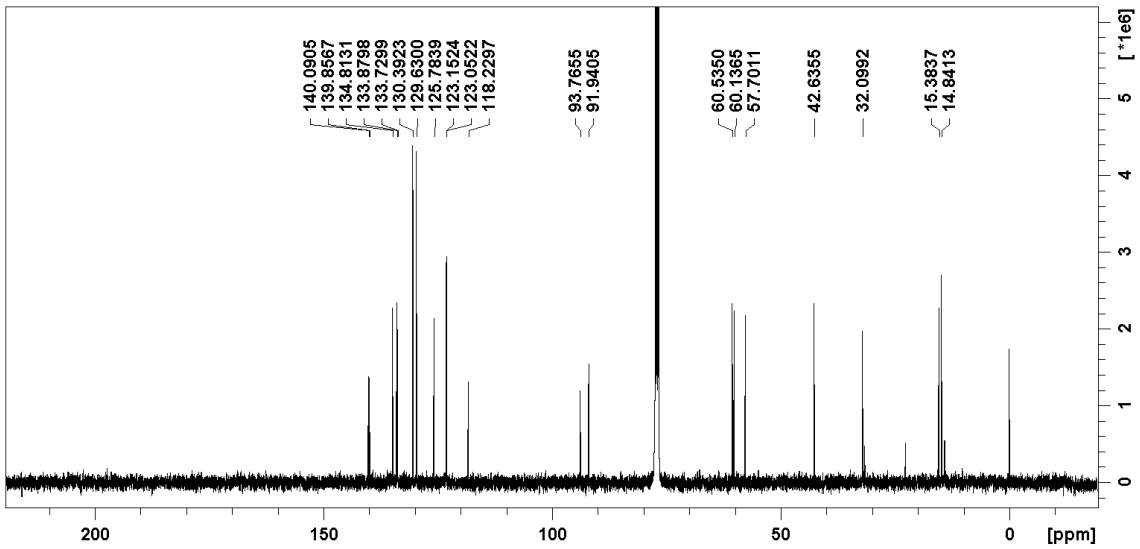

Figure 2.S46. ^{13}C NMR of **AZ4b** in $CDCl_3$ (100 MHz).

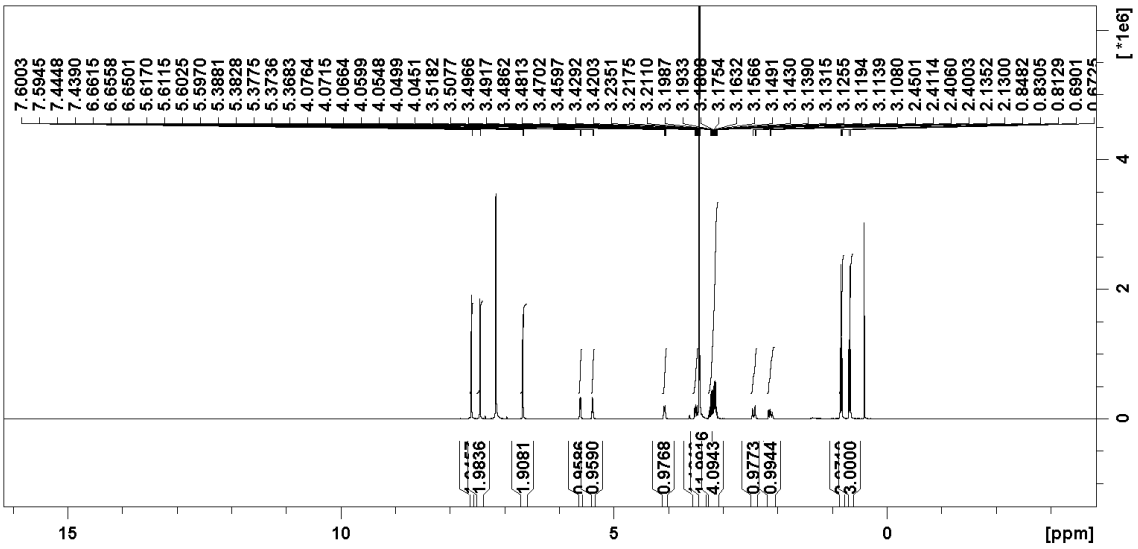

Figure 2.S47. ^{1}H NMR of **AZ4c** in C_6D_6 (400 MHz).

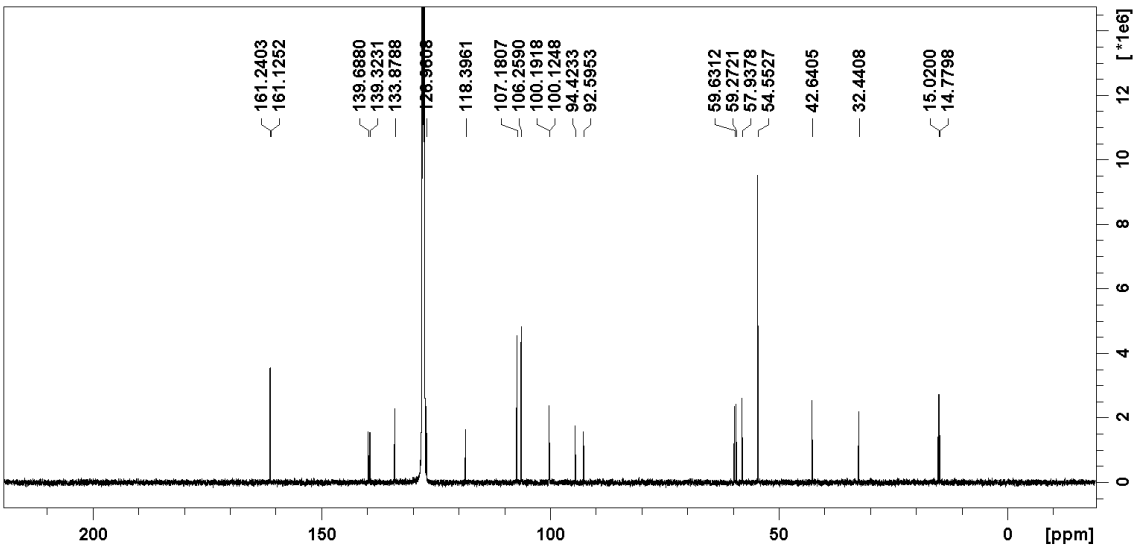

Figure 2.S48. ^{13}C NMR of **AZ4c** in C_6D_6 (100 MHz).

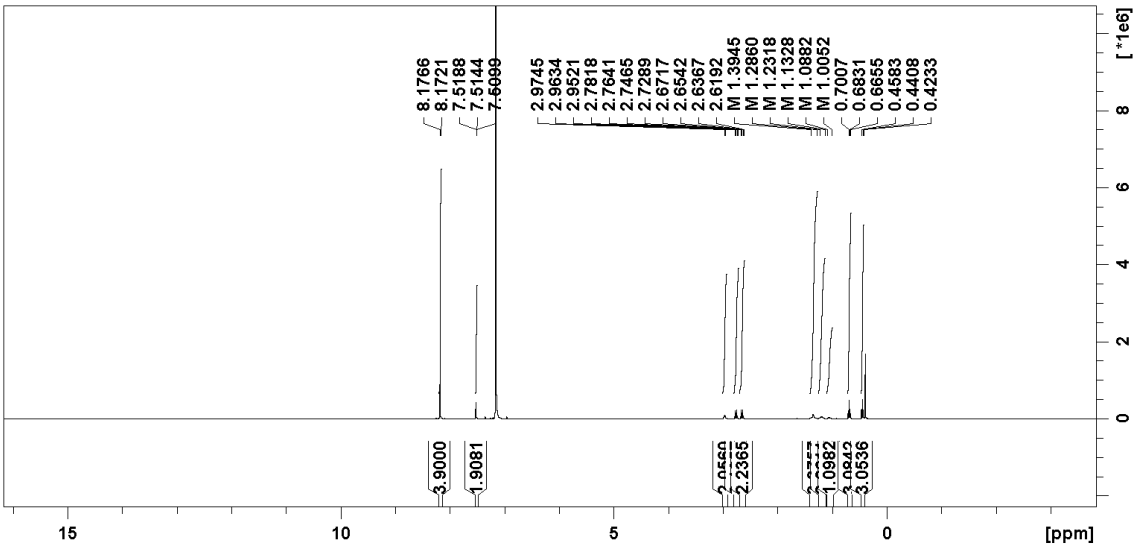

Figure 2.S49. ^{1}H NMR of **AZ3b** in C_6D_6 (400 MHz).

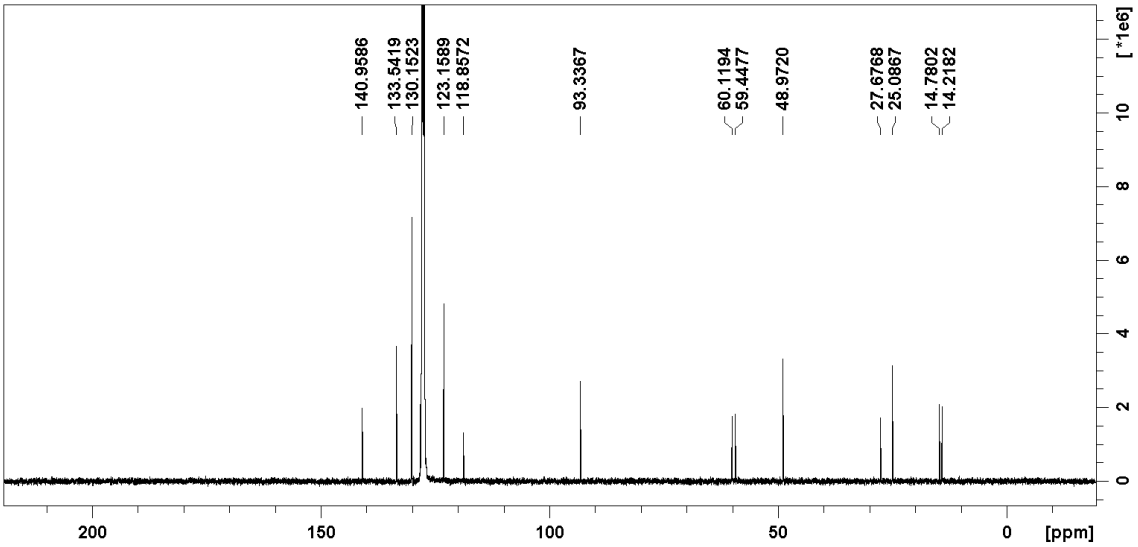

Figure 2.S50. ^{13}C NMR of **AZ3b** in C_6D_6 (100 MHz).

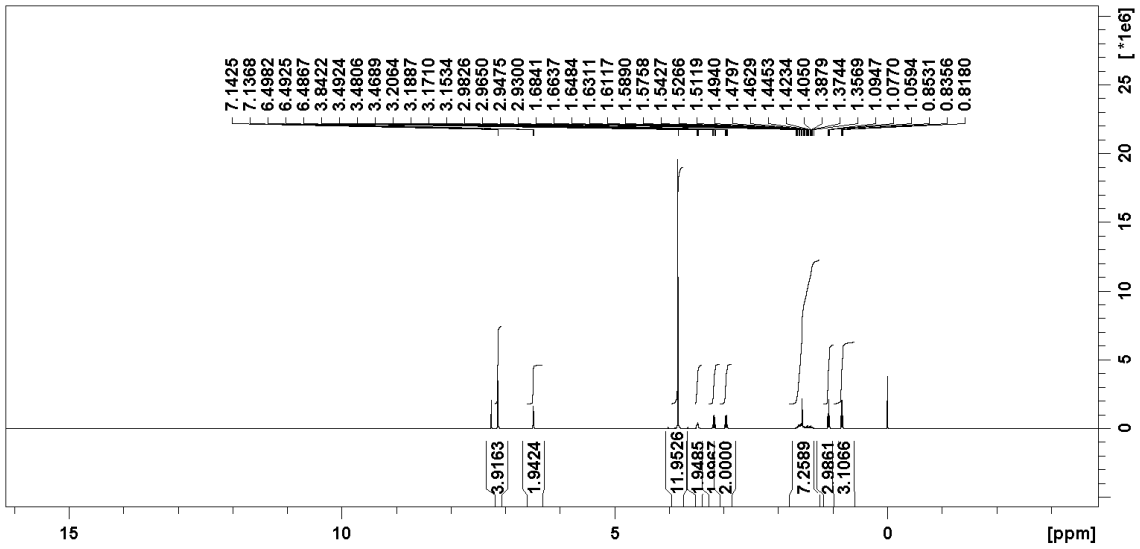

Figure 2.S51. ^{1}H NMR of **AZ3c** in $CDCl_3$ (400 MHz).

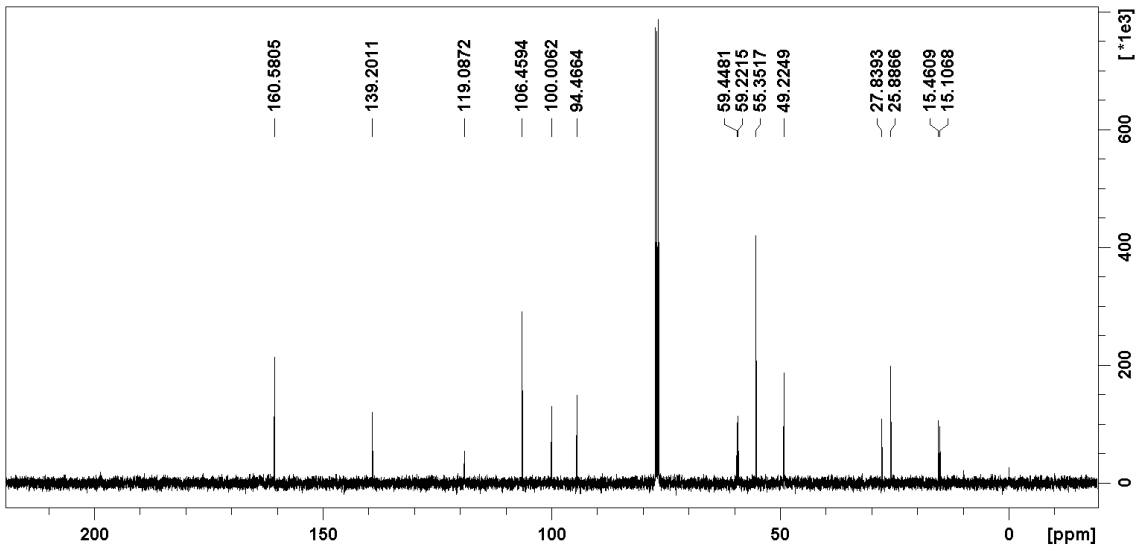

Figure 2.S52. ^{13}C NMR of **AZ3c** in $CDCl_3$ (100 MHz).

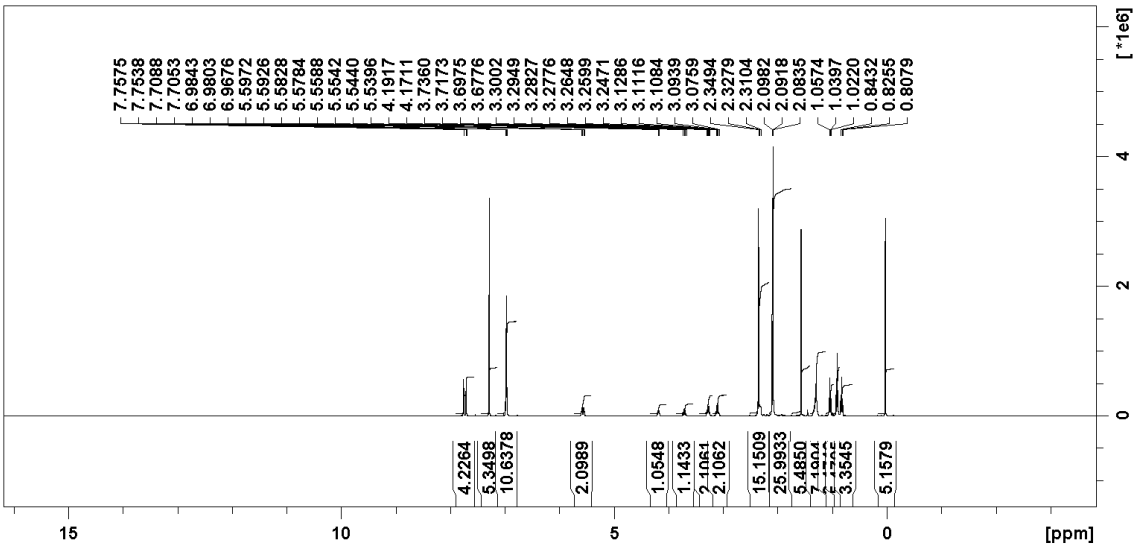

Figure 2.S53. ^{1}H NMR of **AZ4d** in $CDCl_3$ (400 MHz).

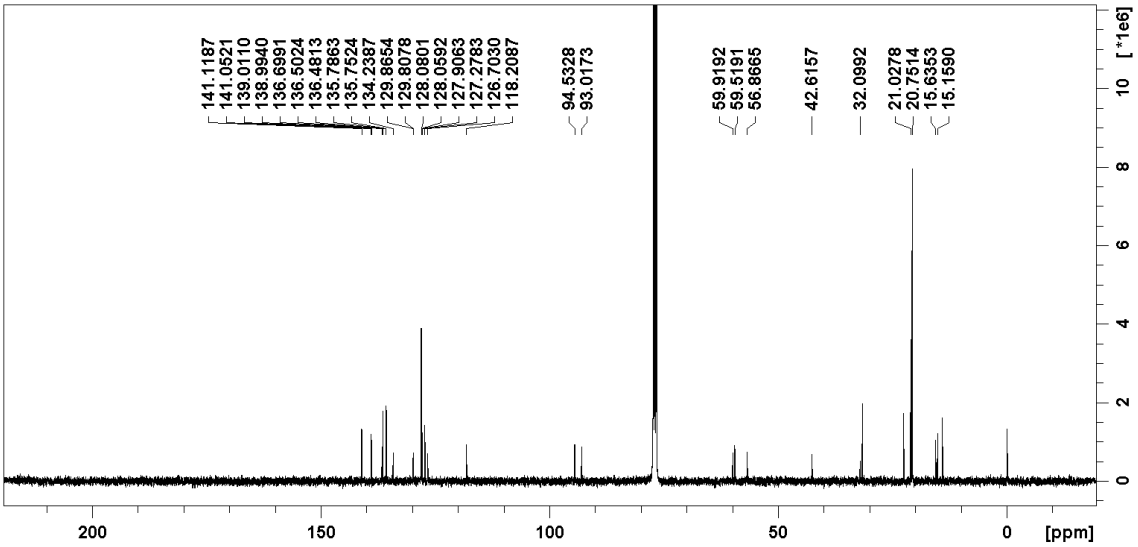

Figure 2.S54. ^{13}C NMR of **AZ4d** in $CDCl_3$ (100 MHz).

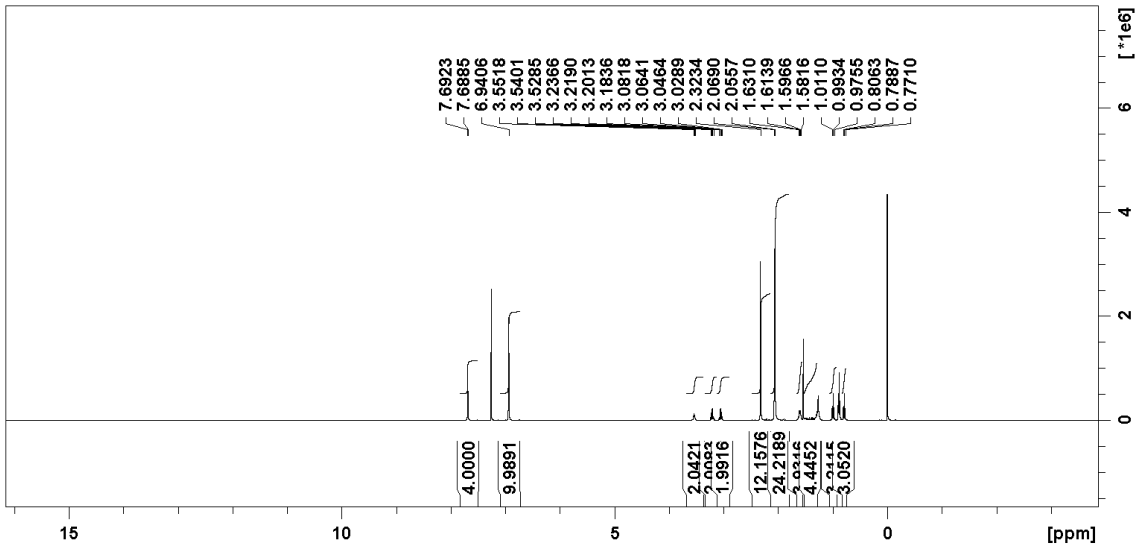

Figure 2.S55. ^{1}H NMR of **AZ3d** in $CDCl_3$ (400 MHz).

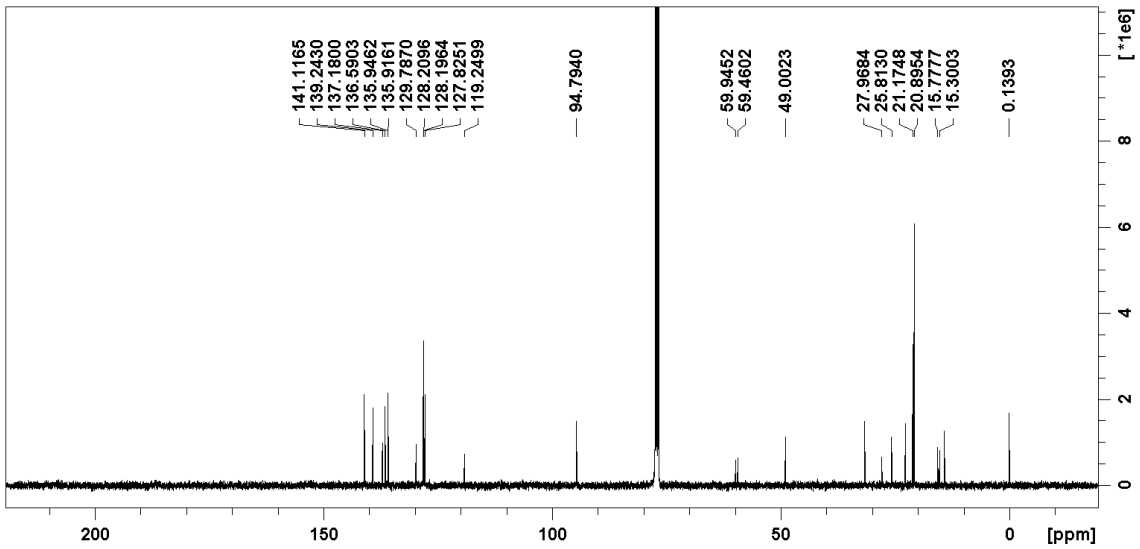

Figure 2.S56. ^{13}C NMR of **AZ3d** in $CDCl_3$ (100 MHz).

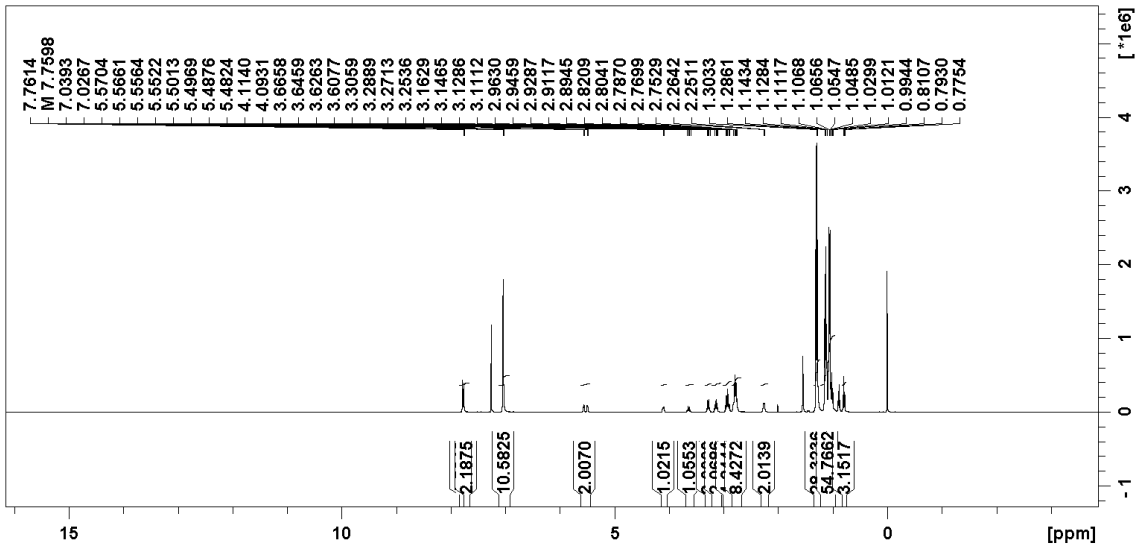

Figure 2.S57. ^{1}H NMR of **AZ4e** in $CDCl_3$ (400 MHz).

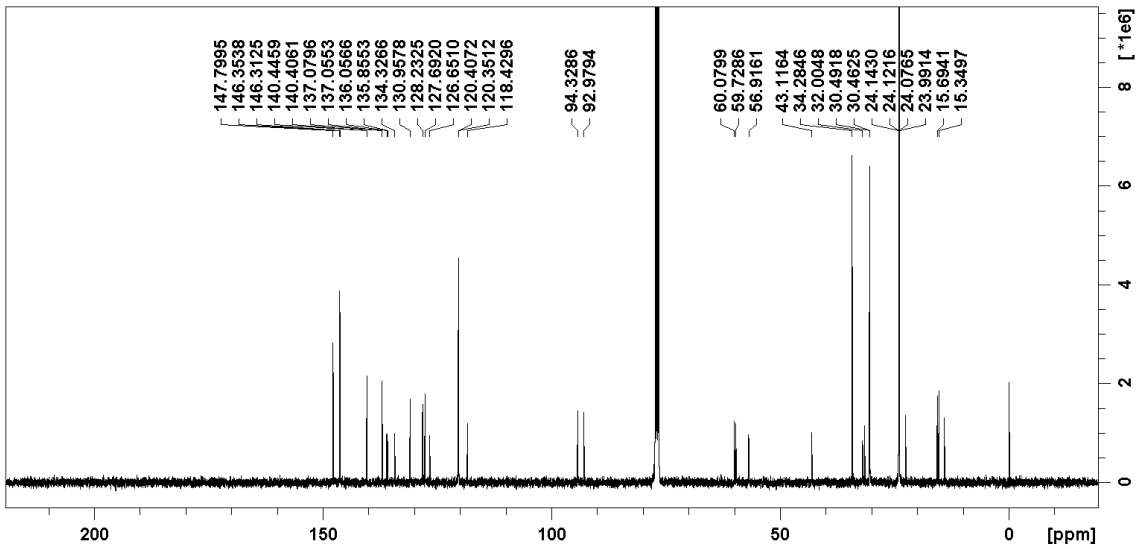

Figure 2.S58. ^{13}C NMR of **AZ4e** in $CDCl_3$ (100 MHz).

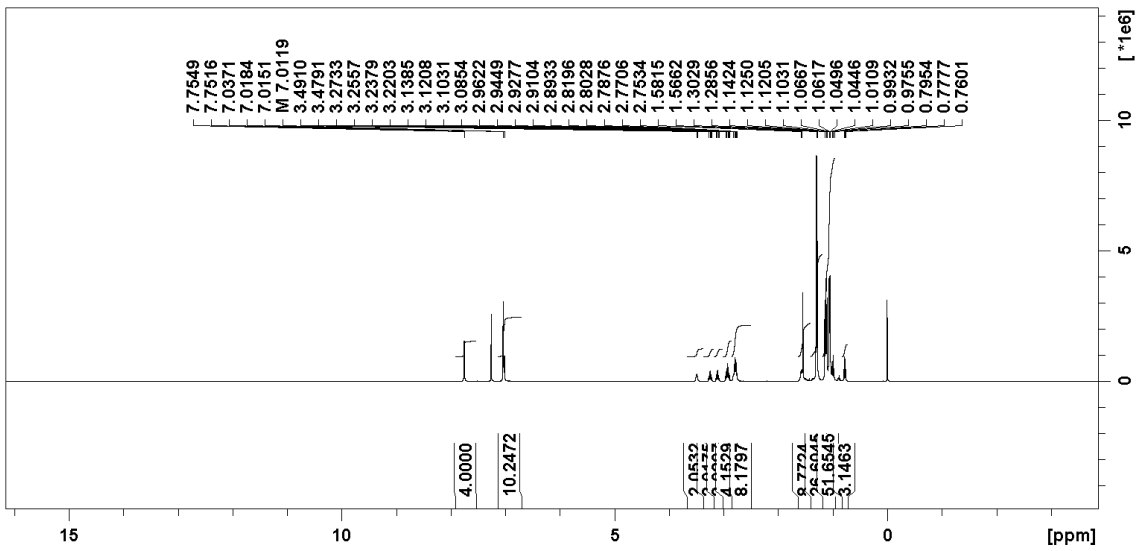

Figure 2.S59. ^{1}H NMR of **AZ3e** in $CDCl_3$ (400 MHz).

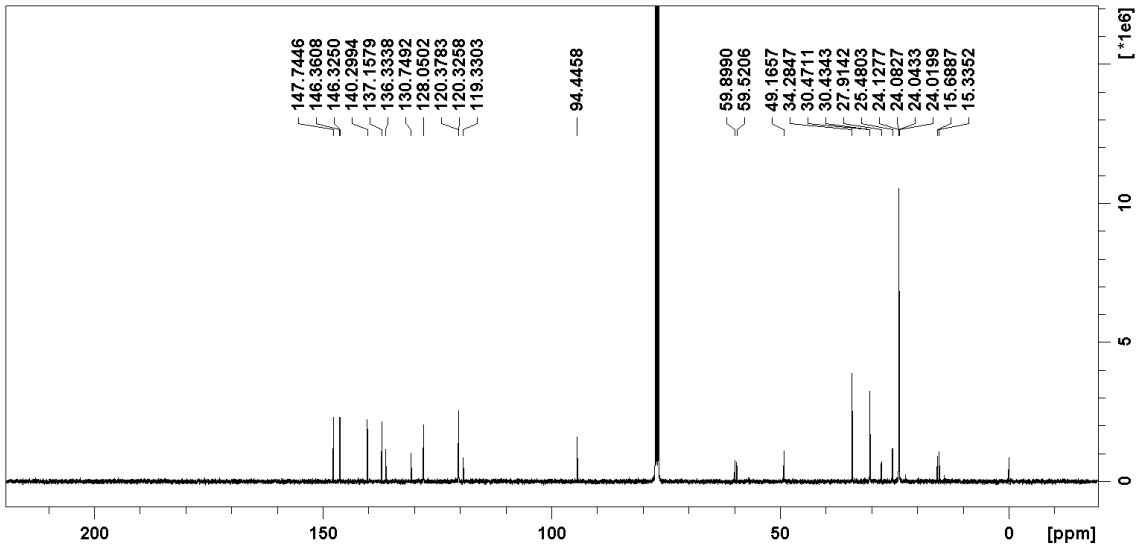

Figure 2.S60. ^{13}C NMR of **AZ3e** in $CDCl_3$ (100 MHz).

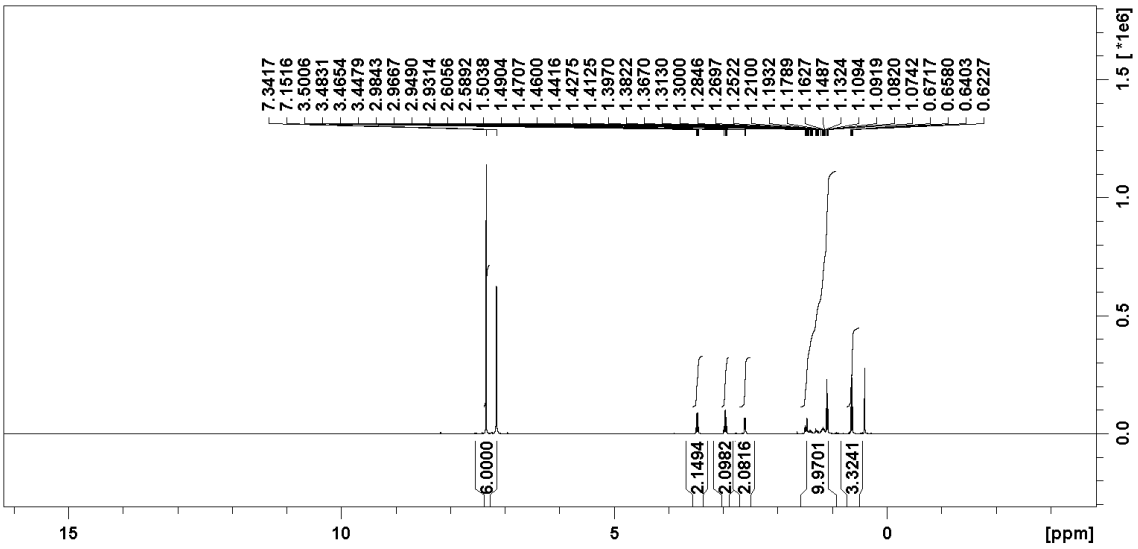

Figure 2.S61. ^{1}H NMR of *trans*-**CP3b** in C_6D_6 (400 MHz).

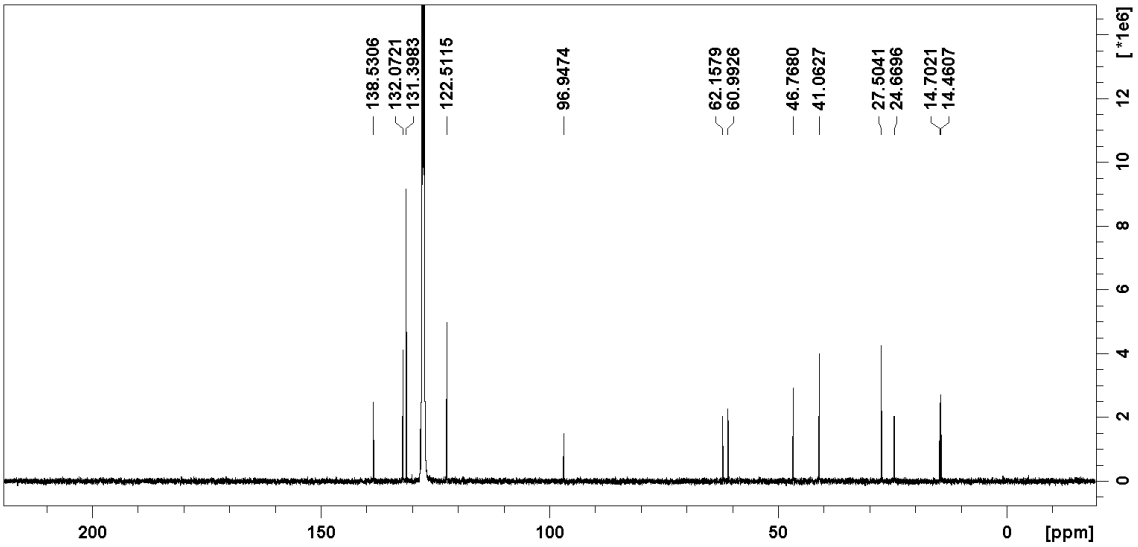

Figure 2.S62. ^{13}C NMR of *trans*-**CP3b** in C_6D_6 (100 MHz).

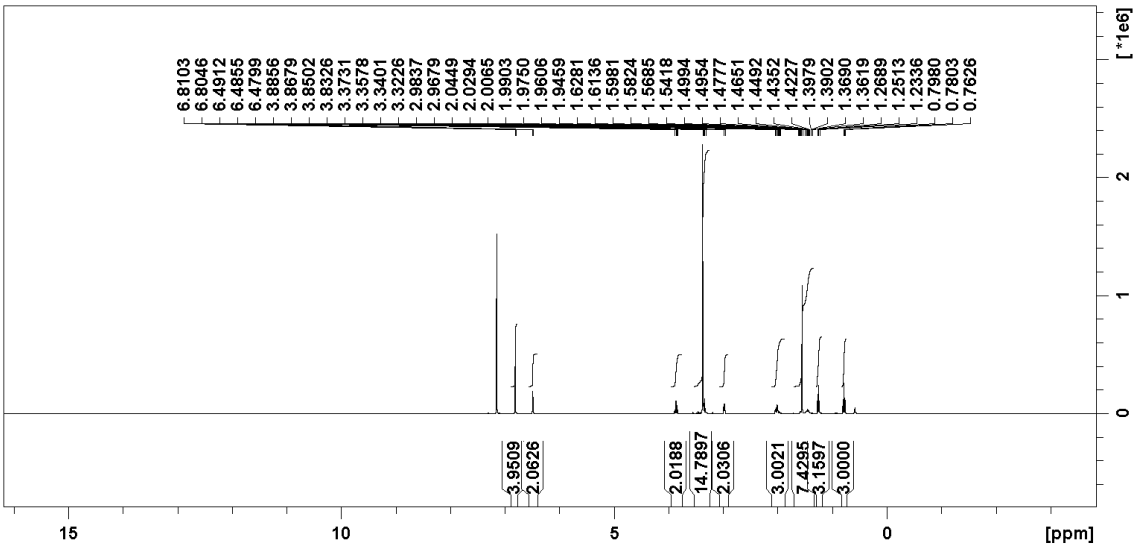

Figure 2.S63. ^{1}H NMR of *trans*-**CP3c** in C_6D_6 (400 MHz).

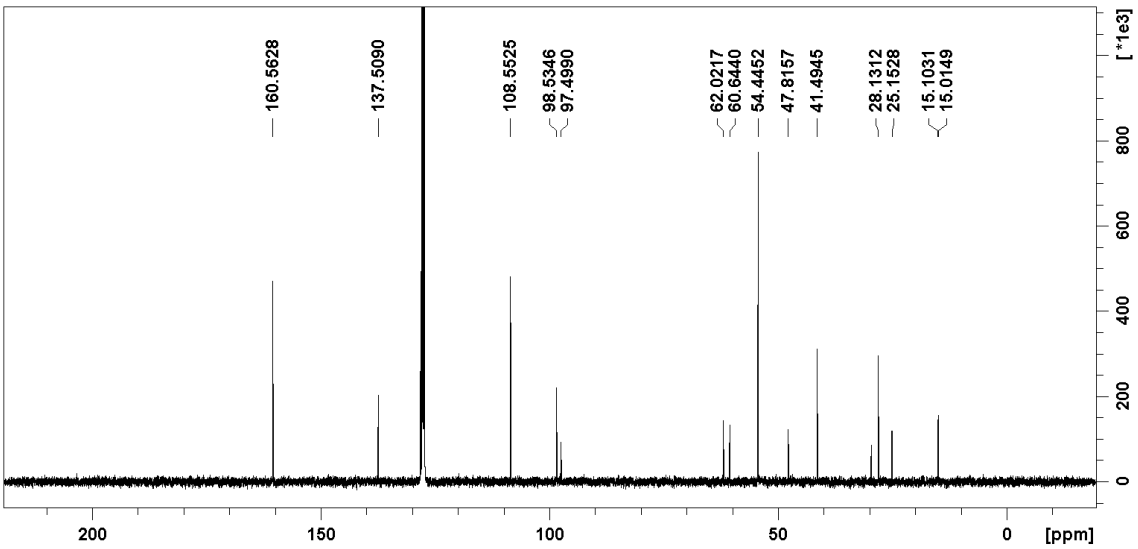

Figure 2.S64. ^{13}C NMR of *trans*-**CP3c** in C_6D_6 (100 MHz).

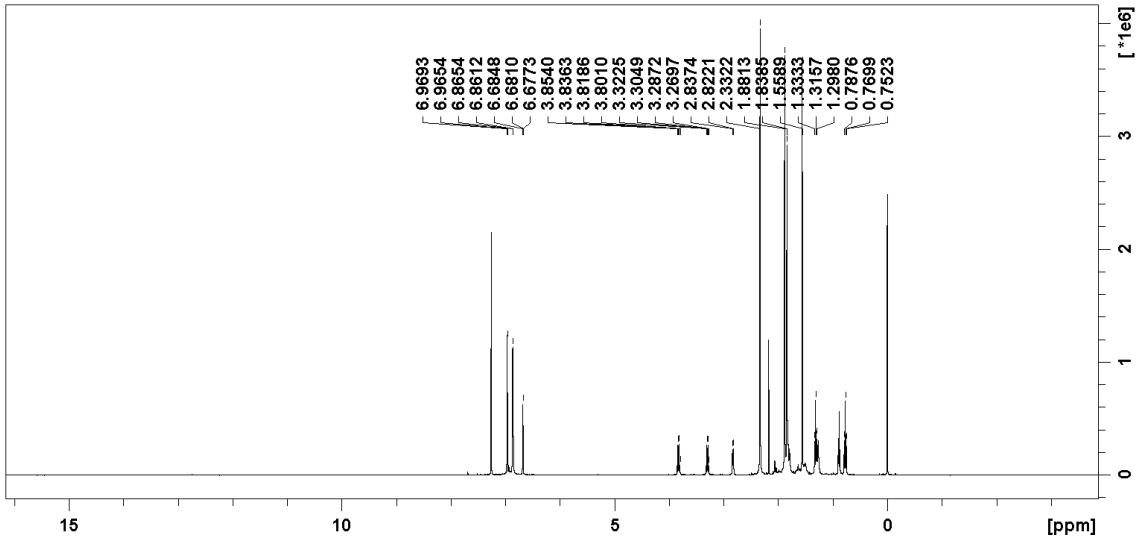

Figure 2.S65. ^{1}H NMR of *trans*-**CP3d** in $CDCl_3$ (400 MHz).

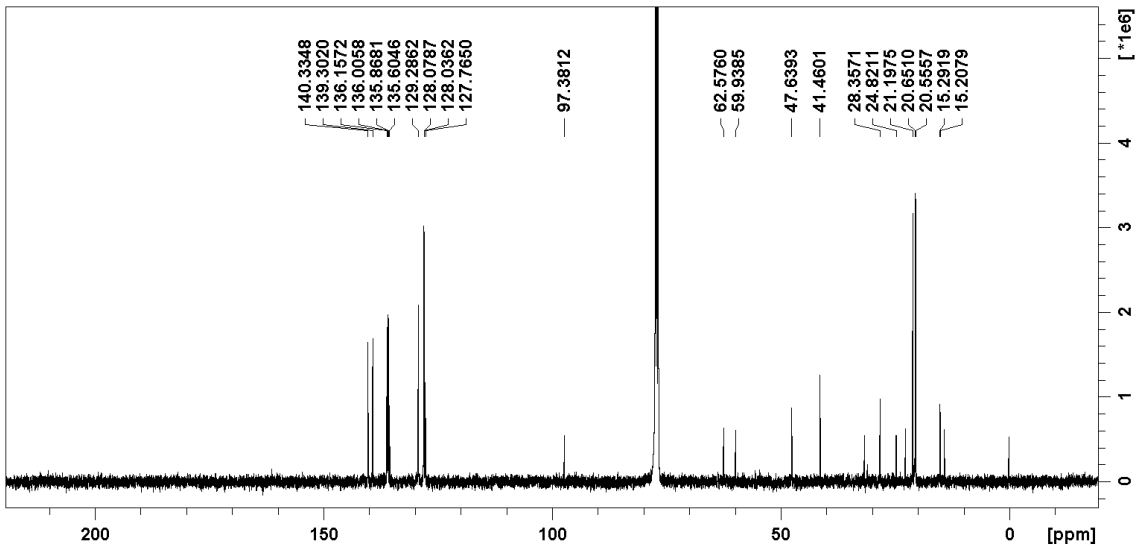

Figure 2.S66. ^{13}C NMR of *trans*-**CP3d** in $CDCl_3$ (100 MHz).

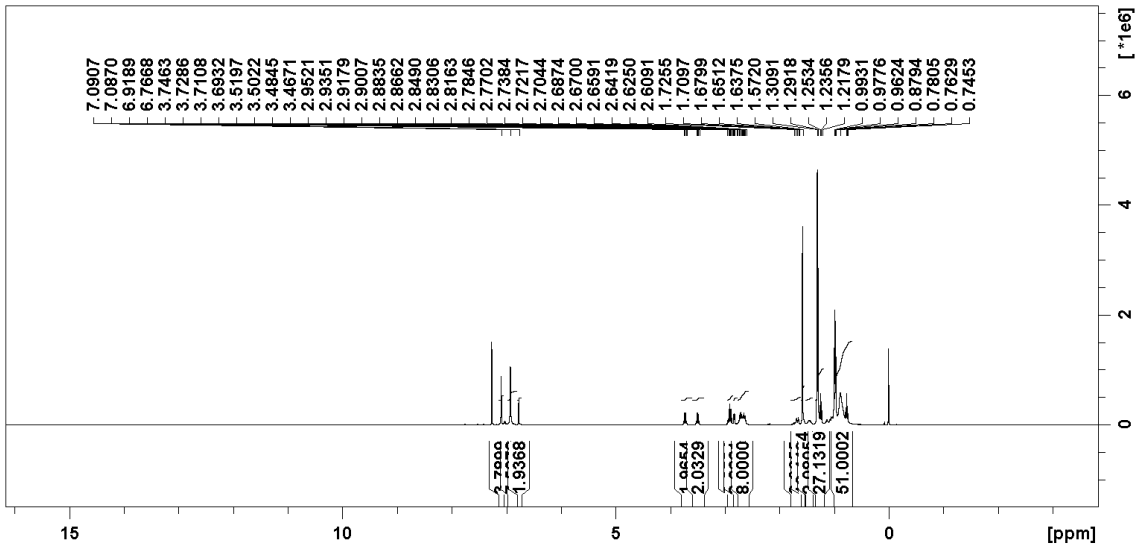

Figure 2.S67. ^{1}H NMR of *trans*-**CP3e** in $CDCl_3$ (400 MHz).

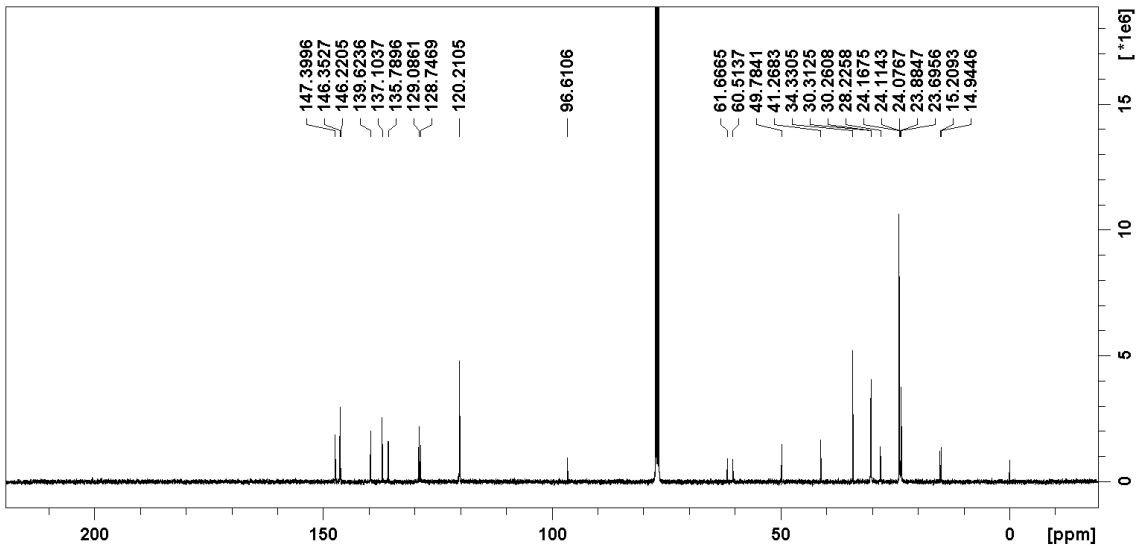

Figure 2.S68. ^{13}C NMR of *trans*-**CP3e** in $CDCl_3$ (100 MHz).

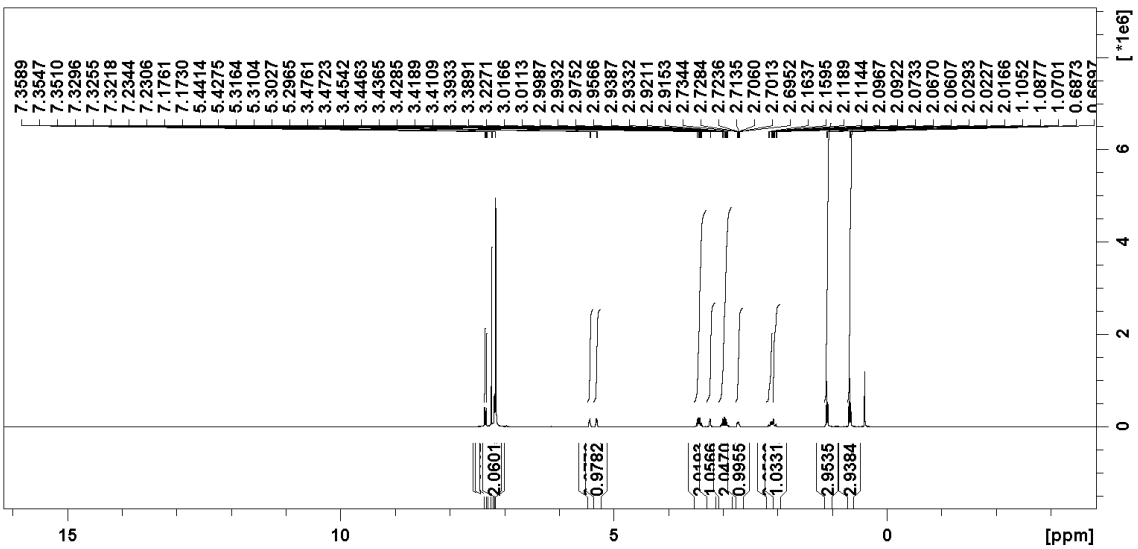

Figure 2.S69. ^{1}H NMR of *trans*-**CP4b** in C_6D_6 (400 MHz).

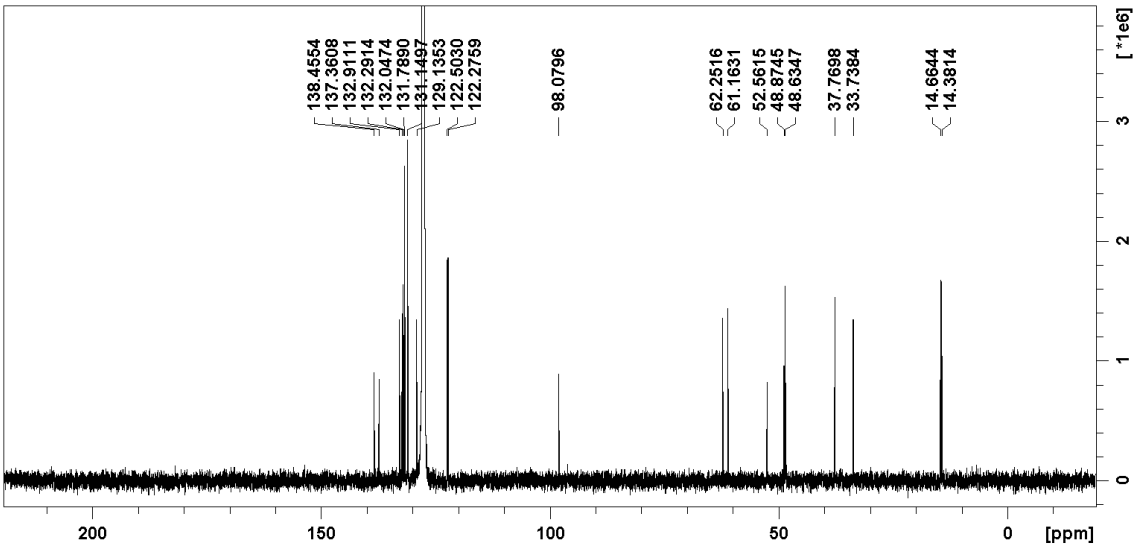

Figure 2.S70. ^{13}C NMR of *trans*-**CP4b** in C_6D_6 (100 MHz).

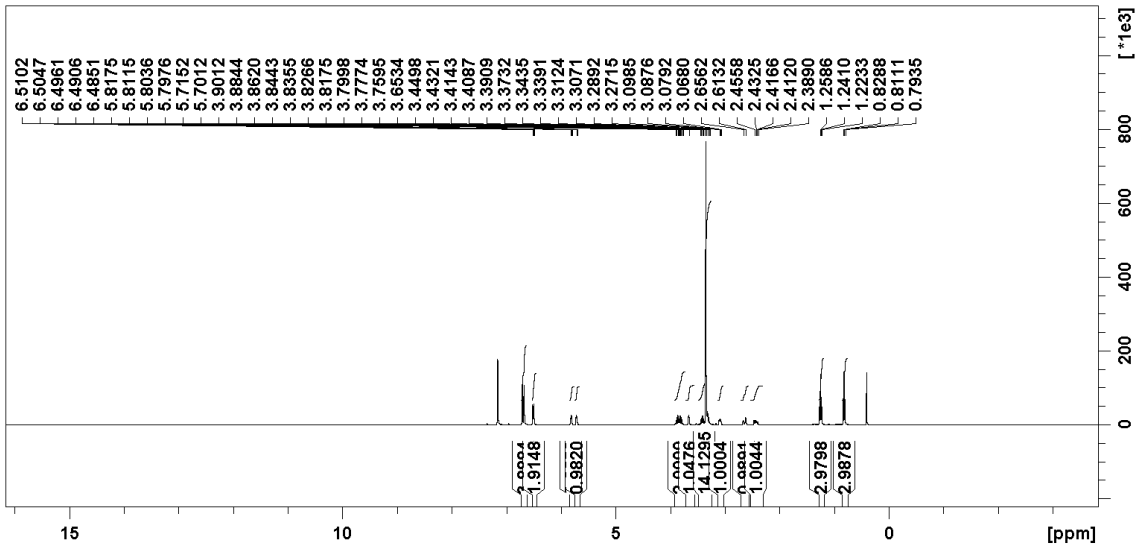

Figure 2.S71. ^{1}H NMR of *trans*-**CP4c** in C_6D_6 (400 MHz).

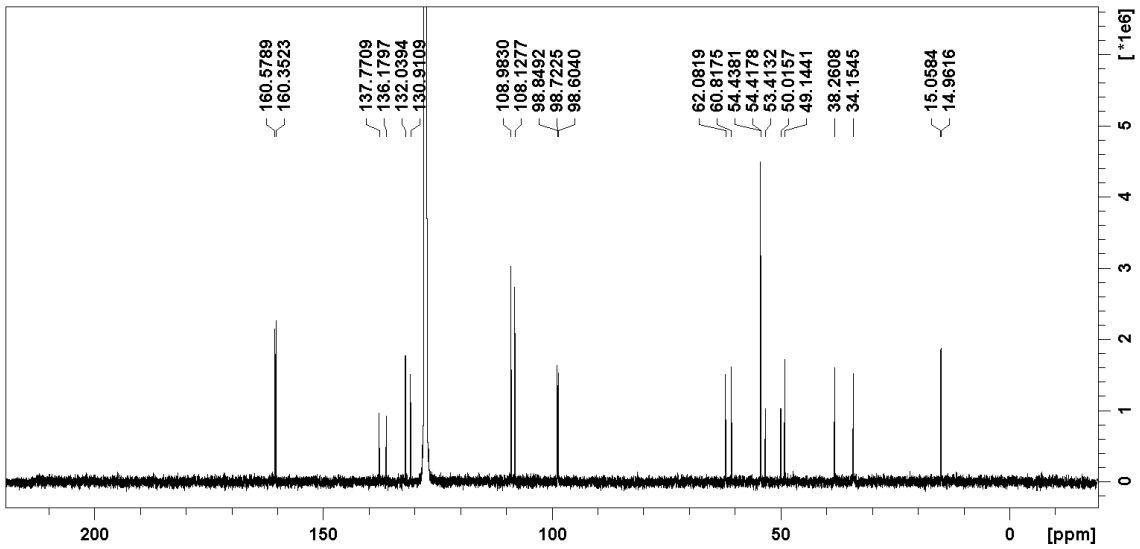

Figure 2.S72. ^{13}C NMR of *trans*-**CP4c** in C_6D_6 (100 MHz).

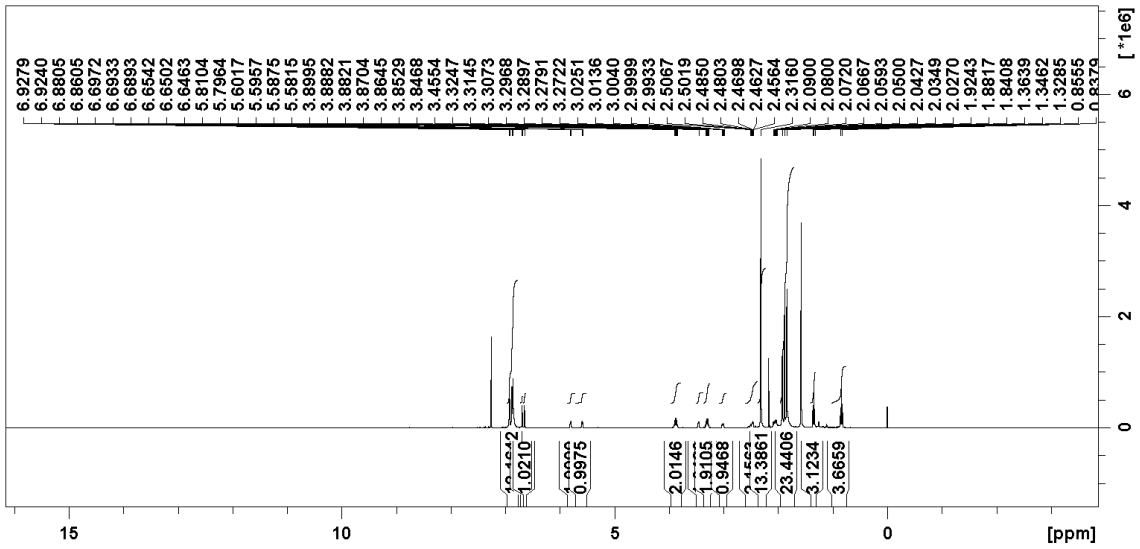

Figure 2.S73. ^{1}H NMR of *trans*-**CP4d** in $CDCl_3$ (400 MHz).

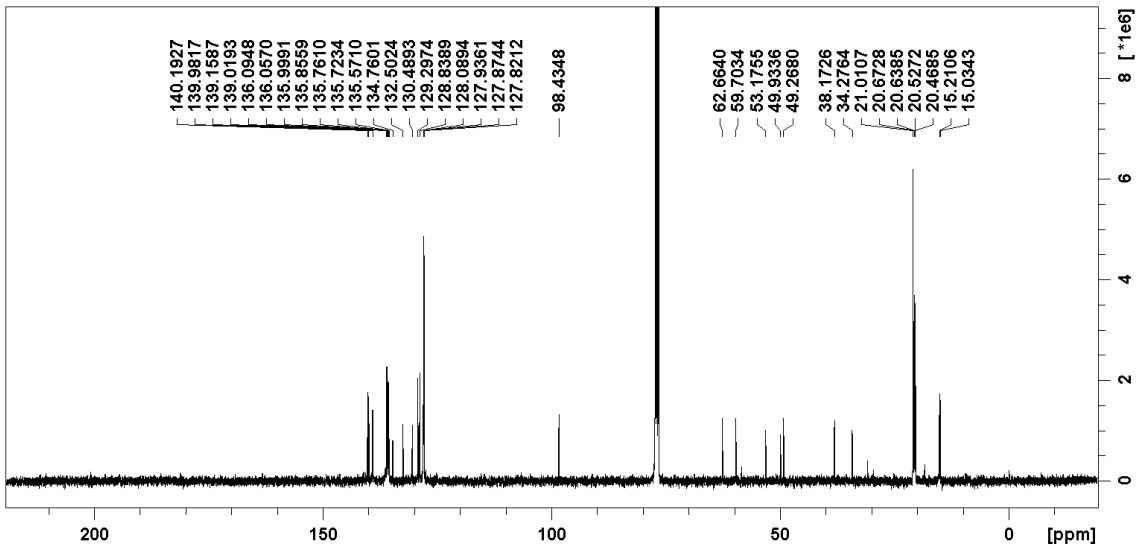

Figure 2.S74. ^{13}C NMR of *trans*-**CP4d** in $CDCl_3$ (100 MHz).

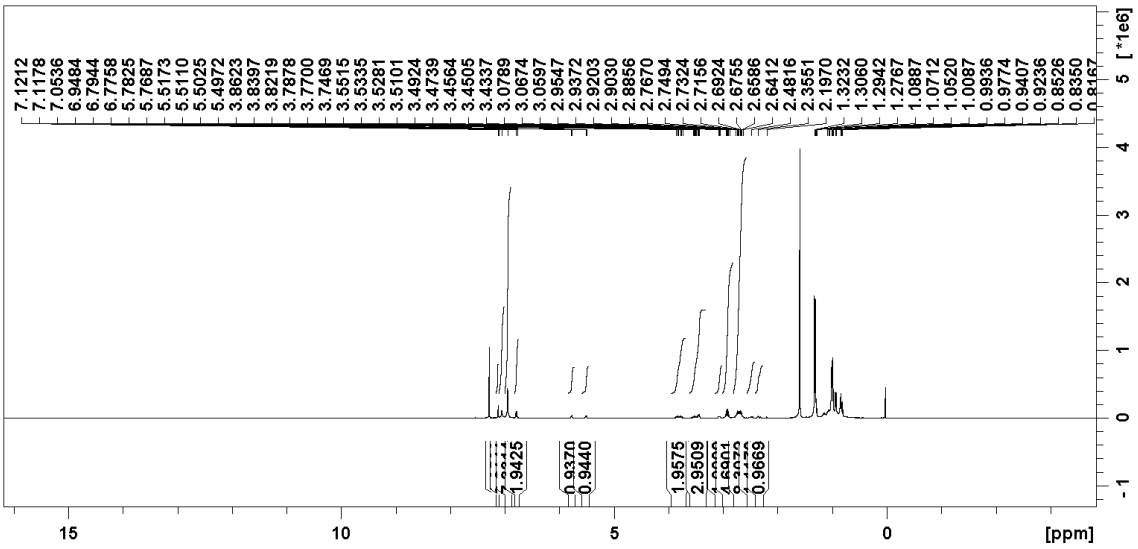

Figure 2.S75. ^{1}H NMR of *trans*-**CP4e** in $CDCl_3$ (400 MHz).

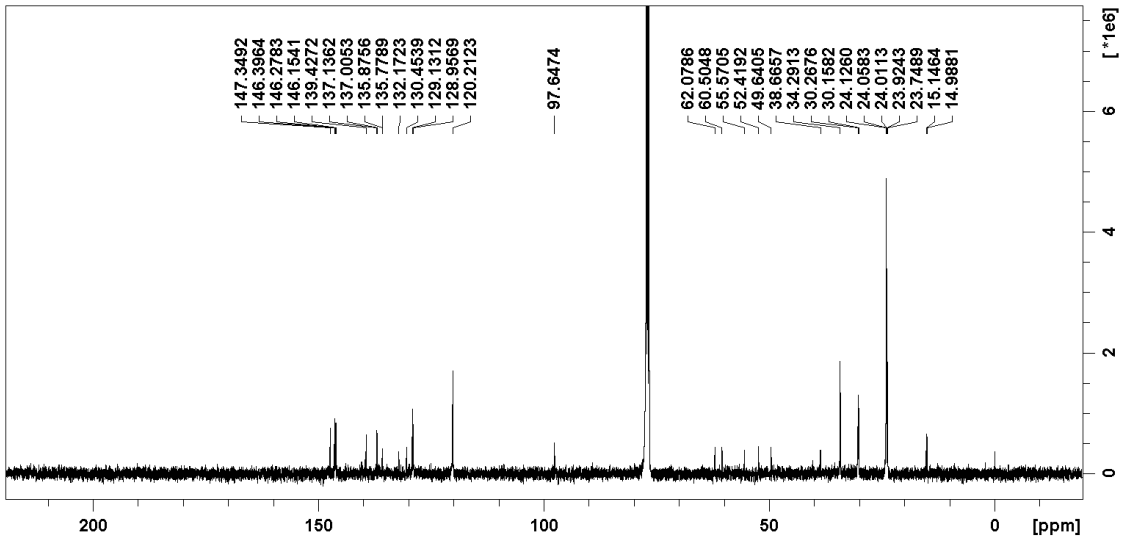

Figure 2.S76. ^{13}C NMR of *trans*-**CP4e** in $CDCl_3$ (100 MHz).

Section 2.7.11. Theoretical calculation

S-DR2a

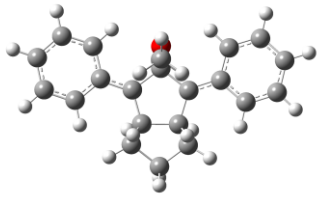

opt freq b3lyp/6-31g(d) guess=(mix,always)
Charge = 0, Multiplicity = 1
E(UB3LYP) = -1003.14830692
Sum of electronic and zero-point Energies = -1002.741055
Sum of electronic and thermal Energies = -1002.719740
Sum of electronic and enthalpy Energies = -1002.718796
Sum of electronic and thermal Free Energies= -1002.790811

T-DR2a

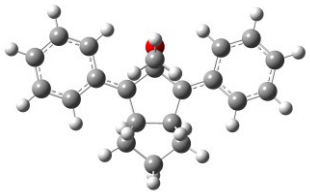

opt freq ub3lyp/6-31g(d)
Charge = 0, Multiplicity = 3
E(UB3LYP) = -1003.14465235
Sum of electronic and zero-point Energies = -1002.737613
Sum of electronic and thermal Energies = -1002.716232
Sum of electronic and enthalpy Energies = -1002.715288
Sum of electronic and thermal Free Energies = -1002.788504

***cis*-CP2a**

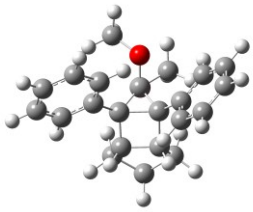

opt freq rb3lyp/6-31g(d)
Charge = 0, Multiplicity = 1
E(RB3LYP) = -1003.15523905
Sum of electronic and zero-point Energies = -1002.745940
Sum of electronic and thermal Energies = -1002.724792
Sum of electronic and enthalpy Energies = -1002.723847
Sum of electronic and thermal Free Energies = -1002.795610

***trans*-CP2a**

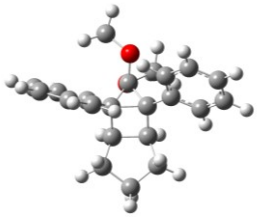

opt freq rb3lyp/6-31g(d)
Charge = 0, Multiplicity = 1
E(RB3LYP) = -1003.16123572
Sum of electronic and zero-point Energies = -1002.751984
Sum of electronic and thermal Energies = -1002.730715
Sum of electronic and enthalpy Energies = -1002.729771
Sum of electronic and thermal Free Energies = -1002.801944

cis-**TS2a**

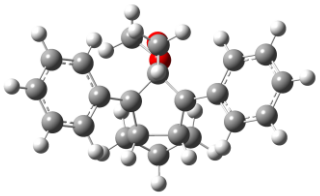

opt=ts freq ub3lyp/6-31g(d) iop(1/8=3) guess=(mix,always)

Charge = 0, Multiplicity = 1

E(UB3LYP) = -1003.13180859

Sum of electronic and zero-point Energies = -1002.723382

Sum of electronic and thermal Energies = -1002.703030

Sum of electronic and enthalpy Energies = -1002.702086

Sum of electronic and thermal Free Energies = -1002.771105

trans-**TS2a**

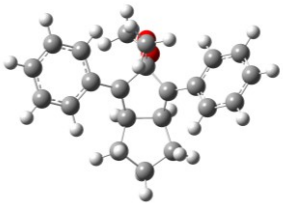

opt=ts freq ub3lyp/6-31g(d) iop(1/8=3) guess=(mix,always)

Charge = 0, Multiplicity = 1

E(UB3LYP) = -1003.12314366

Sum of electronic and zero-point Energies = -1002.715683

Sum of electronic and thermal Energies = -1002.694847

Sum of electronic and enthalpy Energies = -1002.693903

Sum of electronic and thermal Free Energies = -1002.765103

S-DR2b

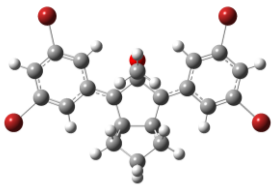

opt freq ub3lyp/6-31g(d) guess=(mix,always)

Charge = 0 Multiplicity = 1

E(UB3LYP) = -11287.56550840

Sum of electronic and zero-point Energies=-11287.199899

Sum of electronic and thermal Energies=-11287.172008

Sum of electronic and thermal Enthalpies=-11287.171064

Sum of electronic and thermal Free Energies=-11287.263693

T-DR2b

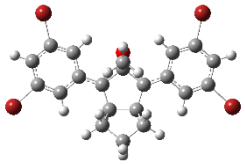

opt freq ub3lyp/6-31g(d)

Charge = 0 Multiplicity = 3

E(UB3LYP)= -11287.56233460

Sum of electronic and zero-point Energies=-11287.196963

Sum of electronic and thermal Energies=-11287.169913

Sum of electronic and thermal Enthalpies= -11287.168969

Sum of electronic and thermal Free Energies=-11287.259261

cis-**CP2b**

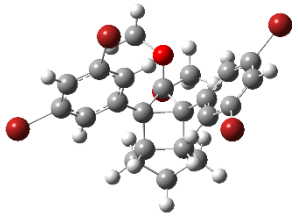	opt freq rb3lyp/6-31g(d) Charge = 0, Multiplicity = 1 E(RB3LYP)=-11287.57333260 Sum of electronic and zero-point Energies=-11287.204847 Sum of electronic and thermal Energies=-11287.177512 Sum of electronic and thermal Enthalpies=-11287.176568 Sum of electronic and thermal Free Energies=-11287.267169

trans-**CP2b**

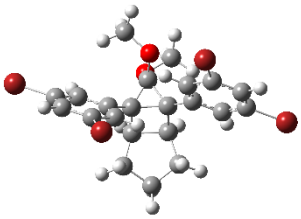	opt freq rb3lyp/6-31g(d) Charge = 0, Multiplicity = 1 E(RB3LYP) = -11287.5791855 Sum of electronic and zero-point Energies=-11287.210766 Sum of electronic and thermal Energies=-11287.183311 Sum of electronic and thermal Enthalpies=-11287.182367 Sum of electronic and thermal Free Energies=-11287.273268

cis-**TS2b**

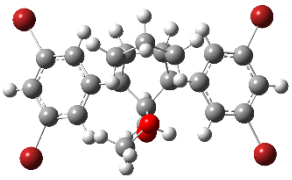	opt=ts freq ub3lyp/6-31g(d) iop(1/8=3) guess=(mix,always) Charge = 0, Multiplicity = 1 E(UB3LYP) = -11287.5484087 Sum of electronic and zero-point Energies=-11287.181645 Sum of electronic and thermal Energies=-11287.154679 Sum of electronic and thermal Enthalpies=-11287.153735 Sum of electronic and thermal Free Energies=-11287.242918

trans-**TS2b**

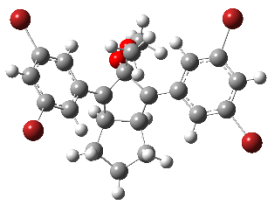	opt=ts freq ub3lyp/6-31g(d) iop(1/8=3) guess=(mix,always) Charge = 0, Multiplicity = 1 E(UB3LYP) = -11287.5400229 Sum of electronic and zero-point Energies=-11287.173397 Sum of electronic and thermal Energies=-11287.146392 Sum of electronic and thermal Enthalpies=-11287.145448 Sum of electronic and thermal Free Energies=-11287.235277

S-**DR2c**

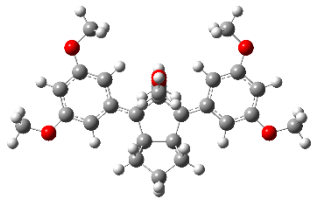

opt freq ub3lyp/6-31g(d) guess=(mix,always)

Charge = 0 Multiplicity = 1

E(UB3LYP) = -1461.24010751

Sum of electronic and zero-point Energies= -1460.702837

Sum of electronic and thermal Energies=-1460.670456

Sum of electronic and thermal Enthalpies= -1460.669512

Sum of electronic and thermal Free Energies=-1460.768134

T-**DR2c**

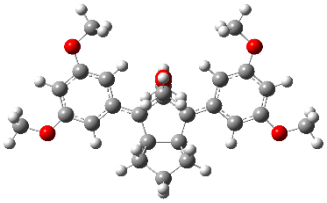

opt freq ub3lyp/6-31g(d)

Charge = 0 Multiplicity = 3

E(UB3LYP) = -1461.23627909

Sum of electronic and zero-point Energies=-1460.699236

Sum of electronic and thermal Energies=-1460.667707

Sum of electronic and thermal Enthalpies=-1460.666762

Sum of electronic and thermal Free Energies=-1460.762975

cis-**CP2c**

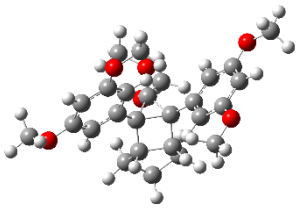

opt freq rb3lyp/6-31g(d)

Charge = 0, Multiplicity = 1

E(RB3LYP) = -1461.24682541

Sum of electronic and zero-point Energies=-1460.706854

Sum of electronic and thermal Energies=-1460.675073

Sum of electronic and thermal Enthalpies=-1460.674129

Sum of electronic and thermal Free Energies=-1460.769985

trans-**CP2c**

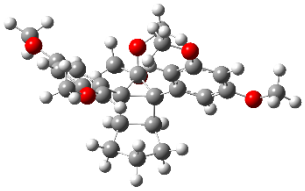

opt freq rb3lyp/6-31g(d)

Charge = 0, Multiplicity = 1

E(RB3LYP) = -1461.25746951

Sum of electronic and zero-point Energies= -1460.717306

Sum of electronic and thermal Energies= -1460.685595

Sum of electronic and thermal Enthalpies= -1460.684651

Sum of electronic and thermal Free Energies= -1460.780115

cis-**TS2c**

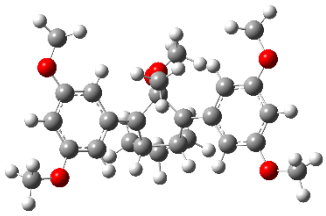

opt=ts freq ub3lyp/6-31g(d) iop(1/8=3) guess=(mix,always)

Charge = 0, Multiplicity = 1

E(UB3LYP) = -1461.22291212

Sum of electronic and zero-point Energies= -1460.683656

Sum of electronic and thermal Energies= -1460.652706

Sum of electronic and thermal Enthalpies= -1460.651762

Sum of electronic and thermal Free Energies= -1460.744288

trans-**TS2c**

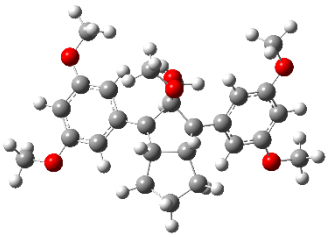

opt=ts freq ub3lyp/6-31g(d) iop(1/8=3) guess=(mix,always)

Charge = 0, Multiplicity = 1

E(UB3LYP) = -1461.21448129

Sum of electronic and zero-point Energies= -1460.676334

Sum of electronic and thermal Energies= -1460.644875

Sum of electronic and thermal Enthalpies= -1460.643931

Sum of electronic and thermal Free Energies= -1460.739089

S-**DR2d**

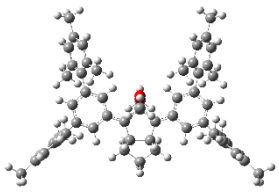

opt freq ub3lyp/6-31g(d) guess=(mix,always)

Charge = 0 Multiplicity = 1

E(UB3LYP) = -2399.16686738

Sum of electronic and zero-point Energies= -2398.105183

Sum of electronic and thermal Energies= -2398.042729

Sum of electronic and thermal Enthalpies= -2398.041785

Sum of electronic and thermal Free Energies= -2398.212696

T-**DR2d**

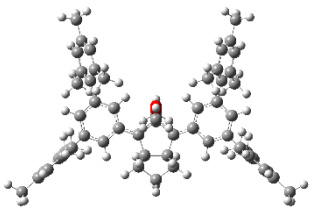

opt freq ub3lyp/6-31g(d)

Charge = 0 Multiplicity = 3

E(UB3LYP) = -2399.16317087

Sum of electronic and zero-point Energies= -2398.102029

Sum of electronic and thermal Energies= -2398.039300

Sum of electronic and thermal Enthalpies= -2398.038356

Sum of electronic and thermal Free Energies= -2398.212556

cis-**CP2d**

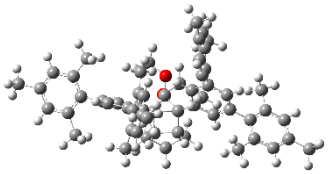

opt freq rb3lyp/6-31g(d)

Charge = 0, Multiplicity = 1

E(RB3LYP) = -2399.17120256

Sum of electronic and zero-point Energies= -2398.107454

Sum of electronic and thermal Energies= -2398.045107

Sum of electronic and thermal Enthalpies= -2398.044163

Sum of electronic and thermal Free Energies= -2398.213990

trans-**CP2d**

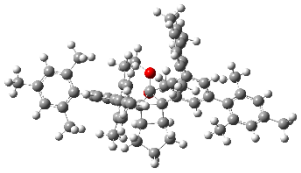

opt freq rb3lyp/6-31g(d)

Charge = 0, Multiplicity = 1

E(RB3LYP) = -2399.18081514

Sum of electronic and zero-point Energies= -2398.117022

Sum of electronic and thermal Energies= -2398.054670

Sum of electronic and thermal Enthalpies= -2398.053726

Sum of electronic and thermal Free Energies= -2398.223327

cis-**TS2d**

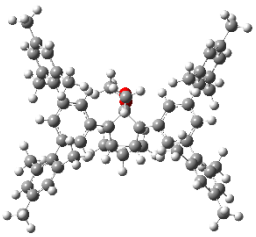

opt=ts freq ub3lyp/6-31g(d) iop(1/8=3) guess=(mix,always)

Charge = 0, Multiplicity = 1

E(UB3LYP) = -2399.15000431

Sum of electronic and zero-point Energies= -2398.086947

Sum of electronic and thermal Energies= -2398.025496

Sum of electronic and thermal Enthalpies= -2398.024552

Sum of electronic and thermal Free Energies= -2398.190960

trans-**TS2d**

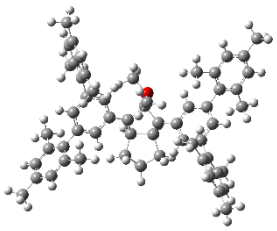

opt=ts freq ub3lyp/6-31g(d) iop(1/8=3) guess=(mix,always)

Charge = 0, Multiplicity = 1

E(UB3LYP) = -2399.14174844

Sum of electronic and zero-point Energies= -2398.079954

Sum of electronic and thermal Energies= -2398.017939

Sum of electronic and thermal Enthalpies= -2398.016995

Sum of electronic and thermal Free Energies= -2398.186966

S-**DR2e**

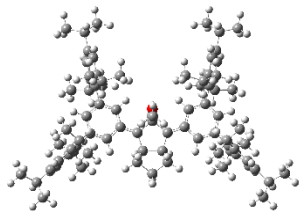

opt freq ub3lyp/6-31g(d) guess=(mix,always)

Charge = 0 Multiplicity = 1

E(UB3LYP) = -3342.67163325

Sum of electronic and zero-point Energies= -3340.924715

Sum of electronic and thermal Energies= -3340.830333

Sum of electronic and thermal Enthalpies= -3340.829389

Sum of electronic and thermal Free Energies= -3341.068407

T-**DR2e**

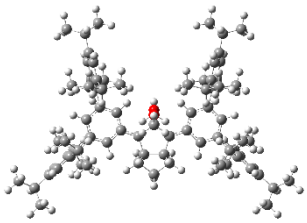

opt freq ub3lyp/6-31g(d)

Charge = 0 Multiplicity = 3

E(UB3LYP) = -3342.66801970

Sum of electronic and zero-point Energies= -3340.921433

Sum of electronic and thermal Energies= -3340.826918

Sum of electronic and thermal Enthalpies= -3340.825974

Sum of electronic and thermal Free Energies= -3341.066734

cis-**CP2e**

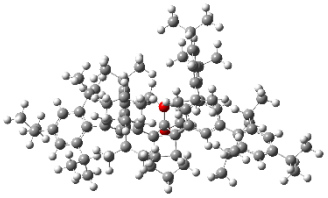

opt freq rb3lyp/6-31g(d)

Charge = 0, Multiplicity = 1

E(RB3LYP) = -3342.67344421

Sum of electronic and zero-point Energies= -3340.924054

Sum of electronic and thermal Energies= -3340.830040

Sum of electronic and thermal Enthalpies= -3340.829095

Sum of electronic and thermal Free Energies= -3341.066277

trans-**CP2e**

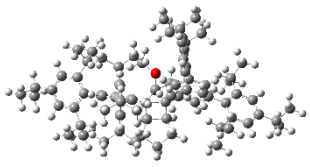

opt freq rb3lyp/6-31g(d)

Charge = 0, Multiplicity = 1

E(RB3LYP) = -3342.68306316

Sum of electronic and zero-point Energies= -3340.933211

Sum of electronic and thermal Energies= -3340.839426

Sum of electronic and thermal Enthalpies= -3340.838482

Sum of electronic and thermal Free Energies= -3341.073886

cis-**TS2e**

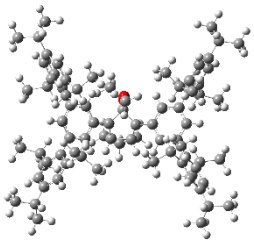

opt=ts freq ub3lyp/6-31g(d) iop(1/8=3) guess=(mix,always)

Charge = 0, Multiplicity = 1

E(UB3LYP) = -3342.65371204

Sum of electronic and zero-point Energies= -3340.905265

Sum of electronic and thermal Energies= -3340.811936

Sum of electronic and thermal Enthalpies= -3340.810992

Sum of electronic and thermal Free Energies= -3341.047399

trans-**TS2e**

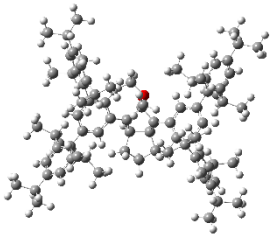

opt=ts freq ub3lyp/6-31g(d) iop(1/8=3) guess=(mix,always)

Charge = 0, Multiplicity = 1

E(UB3LYP) = -3342.64555456

Sum of electronic and zero-point Energies= -3340.898203

Sum of electronic and thermal Energies= -3340.804387

Sum of electronic and thermal Enthalpies= -3340.803442

Sum of electronic and thermal Free Energies= -3341.041903

S-**DR2d'**

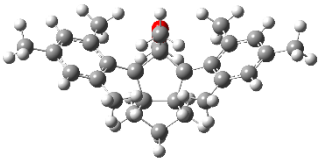

opt freq ub3lyp/6-31g(d) guess=(mix,always)

Charge = 0 Multiplicity = 1

E(UB3LYP) = -1238.99944585

Sum of electronic and zero-point Energies= -1238.424755

Sum of electronic and thermal Energies= -1238.394266

Sum of electronic and thermal Enthalpies= -1238.393322

Sum of electronic and thermal Free Energies= -1238.485067

T-**DR2d'**

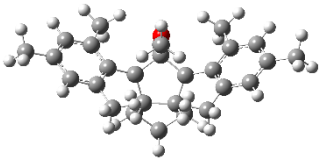

opt freq ub3lyp/6-31g(d)

Charge = 0 Multiplicity = 3

E(UB3LYP) = -1238.99202254

Sum of electronic and zero-point Energies= -1238.417514

Sum of electronic and thermal Energies= -1238.386133

Sum of electronic and thermal Enthalpies= -1238.385189

Sum of electronic and thermal Free Energies= -1238.481994

cis-**CP2d'**

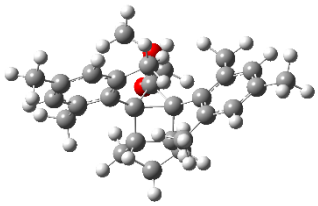	opt freq rb3lyp/6-31g(d) Charge = 0, Multiplicity = 1 E(RB3LYP) = -1239.02594492 Sum of electronic and zero-point Energies= -1238.448879 Sum of electronic and thermal Energies= -1238.418004 Sum of electronic and thermal Enthalpies= -1238.417060 Sum of electronic and thermal Free Energies= -1238.509230

trans-**CP2d'**

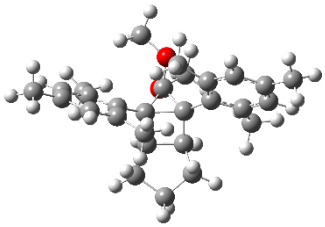	opt freq rb3lyp/6-31g(d) Charge = 0, Multiplicity = 1 E(RB3LYP) = -1239.02986044 Sum of electronic and zero-point Energies= -1238.453029 Sum of electronic and thermal Energies= -1238.422061 Sum of electronic and thermal Enthalpies= -1238.421116 Sum of electronic and thermal Free Energies= -1238.513088

Reference

1 M. Abe and R. Akisaka, *Chem. Lett.*, 2017, **46**, 1586–1592.

2 T. Nakagaki, T. Sakai, T. Mizuta, Y. Fujiwara and M. Abe, *Chem. Eur. J.*, 2013, **19**, 10395–10404.

3 M. Abe, S. Tada, T. Mizuno and K. Yamasaki, *J. Phys. Chem. B*, 2016, **120**, 7217–7226.

4 R. Akisaka and M. Abe, *Chem. – An Asian J.*, 2019, **14**, 4223–4228.

5 S. Grimme, *Wiley Interdiscip. Rev. Comput. Mol. Sci.*, 2011, **1**, 211–228.

6 J. P. Wagner and P. R. Schreiner, *Angew. Chem. Int. Ed.*, 2015, **54**, 12274–12296.

7 D. J. Liptrot and P. P. Power, *Nat. Rev. Chem.*, 2017, **1**, 0004.

8 M. Bursch, E. Caldeweyher, A. Hansen, H. Neugebauer, S. Ehlert and S. Grimme, *Acc. Chem. Res.*, 2018, **52**, 258–266.

9 S. Grimme, A. Hansen, J. Gerit Brandenburg and C. Bannwarth, *Chem. Rev.*, 2016, **116**, 5105–5154.

10 S. Grimme, J. Antony, S. Ehrlich and H. Krieg, *J. Chem. Phys.*, 2010, **132**, 154104.

11 S. Grimme, S. Ehrlich and L. Goerigk, *J. Comput. Chem.*, 2011, **32**, 1456–1465.

12 C. Quinton, S. H. Chi, C. Dumas-Verdes, P. Audebert, G. Clavier, J. W. Perry and V. Alain-Rizzo, *J. Mater. Chem. C*, 2015, **3**, 8351–8357.

13 In *IUPAC Compendium of Chemical Terminology*, IUPAC, Research Triagle Park, NC.

14 A. Pan, T. Biswas, A. K. Rakshit and S. P. Moulik, *J. Phys. Chem. B*, 2015, **119**, 15876–15884.

15 J. Ye, S. Hatano, M. Abe, R. Kishi, Y. Murata, M. Nakano and W. Adam, *Chem. Eur. J.*, 2016, **22**, 2299–2306.

16 M. Abe, K. Kanahara, N. Kadowaki, C. J. Tan and H. H. G. Tsai,

Chem. Eur. J., 2018, **24**, 7595–7600.
17 W. Siebrand and T. A. Wildman, *Acc. Chem. Res.*, 1986, **19**, 238–243.
18 C. Patoux, C. Coudret, J.-P. Launay, C. Joachim and A. Gourdon, *Inorg. Chem.*, 1997, **36**, 5037–5049.
19 M. Abe, W. Adam, T. Heidenfelder, W. M. Nau and X. Zhang, *J. Am. Chem. Soc.*, 2000, **122**, 2019–2026.

Chapter 3.
Dynamic solvent effect on the lifetime of the singlet cyclopentane-1,3-diyls

Section 3.1. The explanation of two types of solvent effect

There are two aspects of the solvent effect on the chemical reaction in solution, polarity effect and viscosity effect. The polarity effect is based on stabilizing the starting material or the transition state, which has the ionic or zwitterionic character.[1] And, it can be applied to singlet cyclopentane-1,3-diyls. The lifetime of S-**DR3a** was extended in a polar solvent, acetonitrile: τ = 1010 ns, than that in a non-polar solvent, hexane: τ = 520 ns.[2] This result was explained by stabilization of the resonance structure **ZI3a** (Scheme 3.1).[2,3]

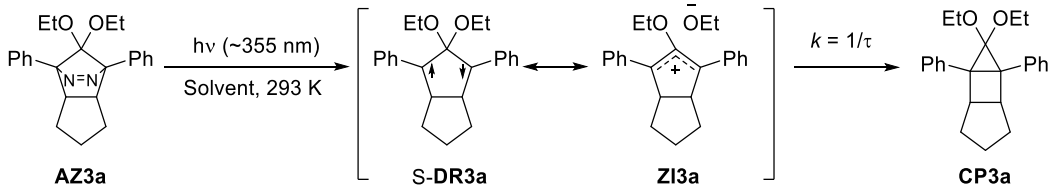

Scheme 3.1. The reactivity of S-**DR3a** and resonance structure of S-**DR3a**.

Another solvent effect, the viscosity effect, was sometimes called as dynamic solvent effect.[4] Because the reactants were solvated by the solvent molecule, the movements of both reactant and the solvent molecules is generally needed to occur reaction and to get the space for the reaction, respectively. In the viscous conditions, these movements were inhibited by the other surrounding solvent molecules. So, the reaction of reactant was retarded. The dynamic solvent effects were observed in several intramolecular reactions, such as photoisomerization of stilbene or the thermal back reaction of photochromic molecule.[4–9] And the logarithm of reaction rate k in viscosity dependent reactions were proportional to the logarithm of the inverse of the solvent viscosity η, $\ln k \propto \ln(1/\eta)$. These results

were agreed with Kuramer's explanation.[10]

In the bond formation process of the singlet diradicals S-**DR4** the aryl groups at C1 and C3 position should be moved dramatically because the radical carbons were changed from planer sp^2 carbon to pyramidalized sp^3 carbon (Scheme 3.2). And it was easily imagined that the introduction of bulky substituents at the aryl groups increase the contribution of the dynamic solvent effect to stabilize singlet diradicals.[11]

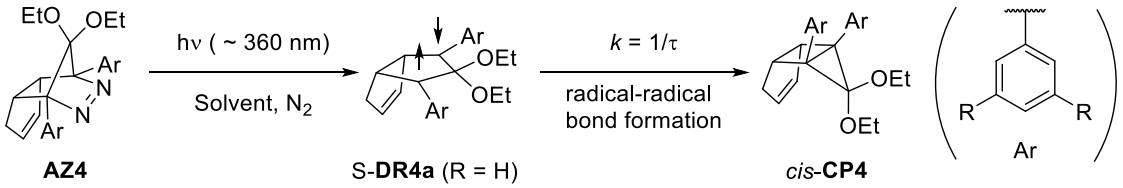

AZ4

S-**DR4a** (R = H)
S-**DR4c** (R = OMe)
S-**DR4d** (R = Mes)
S-**DR4e** (R = Tip)

cis-**CP4**

Scheme 3.2. The reactivity of S-**DR4** and stereochemistry of S-**DR4** and *cis*-**CP4**.

To disclose the combination of the dynamic solvent effect and steric effect on stabilizing the singlet diradicals, the lifetimes of S-**DR4a**,**c**-**e** were measured in several solvents in section 3.2. In section 3.3, the pressure effect on the lifetime of S-**DR4a**,**e** were conducted to consider extremely high viscous condition.

Section 3.2. The solvent effect on the lifetime of the singlet diradical S-**DR4**

First, the solvent effect on the lifetime of S-**DR4a** was investigated as the follow-up study. By the transient absorption spectroscopy technics, the lifetimes of parent S-**DR4a** were measured at five temperatures around 293 K under nitrogen in 9 solvents; pentane, hexane, cyclohexane, methylcyclohexane, benzene, toluene, 1,4-dioxane, ethyl acetate, acetonitrile (Figure 3.S1a-S9a). Same as benzene case (section 2.3), the transient species, which has absorption maximum around 560 nm, were observed and they were assigned as singlet diradical S-**DR4a** (Figure 3.S1a). From the temperature dependencies of the lifetime of S-**DR4a** in each solvent, the Eyring plots were obtained (Figure 3.S2e-S9e). The lifetime of S-**DR4a** at 293 K and the activation enthalpy and activation entropy were estimated from the linear fitting of the Eyring plots (Table 3.S1). Like the S-**DR3a** case, the lifetime of S-**DR4a** shows polarity dependency; that in hexane were 0.30 microseconds and that in acetonitrile were 0.63 microseconds.

To describe more detail of the reactivity of the singlet diradical S-**DR4a**, the logarithm of the lifetime of S-**DR4a** were plotted against the empirical solvent polarity parameters, $E_T(30)$ and π^*.[12–14] The lifetime of S-**DR4a** shows a better correlation to π^* than $E_T(30)$ (Figure 3.1). This observation was explained by the difference in the target of polarity. The $E_T(30)$ was determined by the solvatochromism of the Richard dye, a zwitterionic molecule (Figure 3.2). However, 4-nitro anisole, which has the zwitterionic resonance form, was used as the solvatochromism dye for the π^* parameter. The singlet diradical S-**DR4a** was similar to 4-nitro anisole because S-**DR4a** has resonance structure **ZI4a**, which has zwitterionic character. So, the π^* is a suitable parameter for describing the reactivity of the parent singlet diradical.

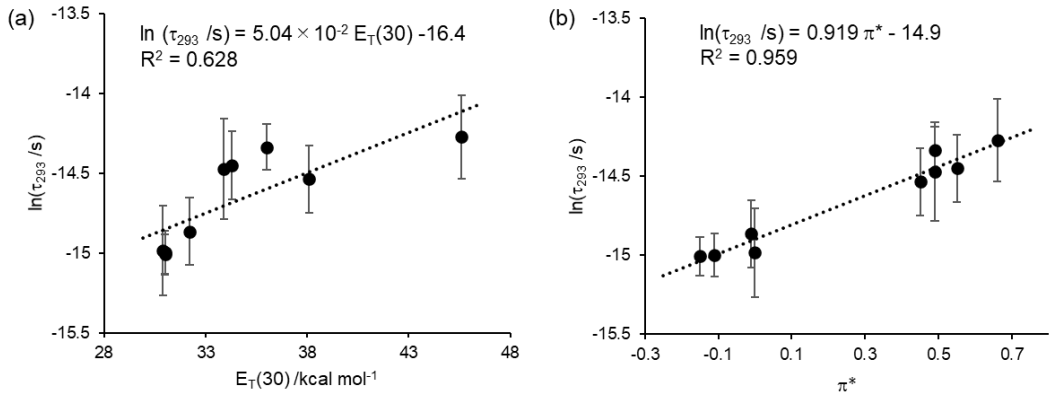

Figure 3.1. Solvent polarity dependency of the lifetime of S-**DR4a**. (a: $E_T(30)$, b:π* was used for solvent polarity parameter)

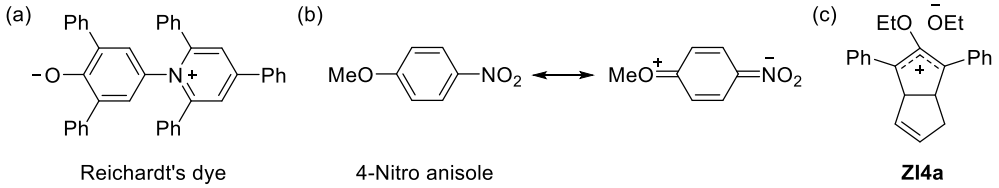

Figure 3.2. Chemical structure of (a) Reichard dye and (b) 4-nitro anisole. (c) Selected resonance structure of S-**DR4a**; **ZI4a**.

The solvent effect on the reactivity of the singlet diradical S-**DR4c**, which has the methoxy group at the meta position of the aryl group, were examined as the same procedure as that of S-**DR4a** (Figure 3.S1b-S9b and Table 3.S.2). The plot between the logarithm of the lifetime of S-**DR4c** and the solvent polarity π* does not show proper correlation (Figure 3.3a). However, the logarithm of the lifetime of S-**DR4c** was well correlated with the logarithm of the solvent viscosity (Figure 3.3b). It means the dynamic solvent effect stabilize the singlet diradical S-**DR4c**. For the more bulky substituted diradical S-**DR4d**,**e**, similar linear correlations were obtained between the log-log plot of the lifetime of S-**DR4d,e** and viscosity (Figure 3.4, Table 3.S3,4, and Figure 3.S.12)

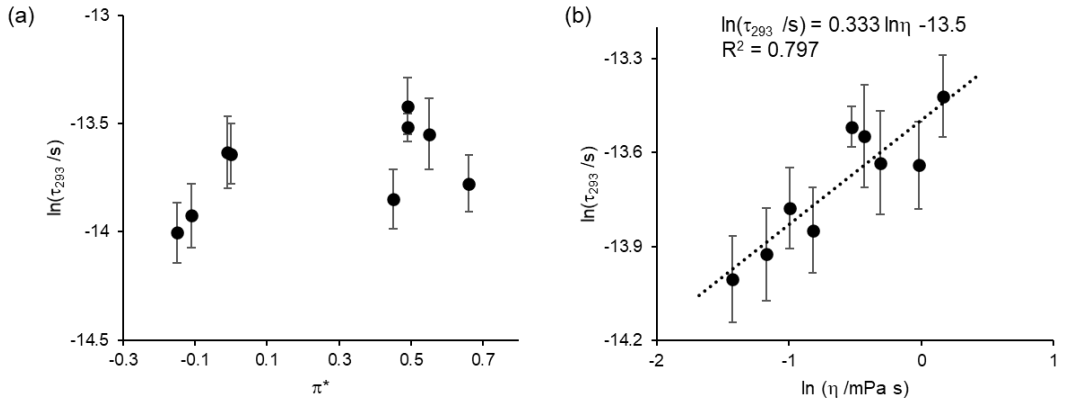

Figure 3.3. (a) Solvent polarity dependency and (b) viscosity dependency of the lifetime of S-**DR4c**.

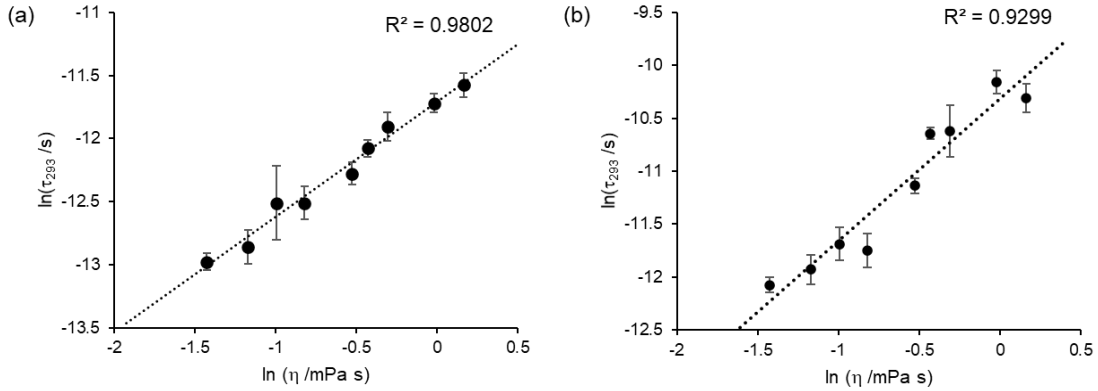

Figure 3.4. Viscosity dependency of the lifetime of (a) S-**DR4d** (R = Mes) and (b) S-**DR4e** (R = Tip).

To get more long-lived singlet diradical, the reactivities of the S-**DR4** in more high viscous media than typical organic solvents were interested. The glycerol triacetate (GTA) and 2,4-dicyclohexyl-2-methyl pentane (DCMP) were chosen as high viscous media (Figure 3.5); the viscosity (η /mPa s) of GTA, DCMP, and cyclohexane were 23, 39, and 0.98, respectively.[15,16] The lifetime of S-**DR4c-e** in GTA and DCMP were investigated from transient absorption of **AZ4c-e** (Figure 3. S.10, S.11). As expected, the lifetimes of S-**DR4c-e** were extended in GTA and DCMP (for S-**DR4e** in Figure 3.6a). The lifetime of S-**DR4e** was reached to sub

milliseconds time scale, 0.29 milliseconds, in DCMP (Table 3.S.4).

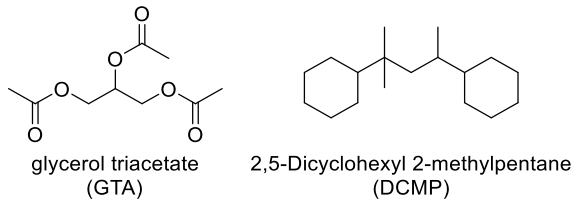

Figure 3.5. Chemical structure of GTA and DCMP.

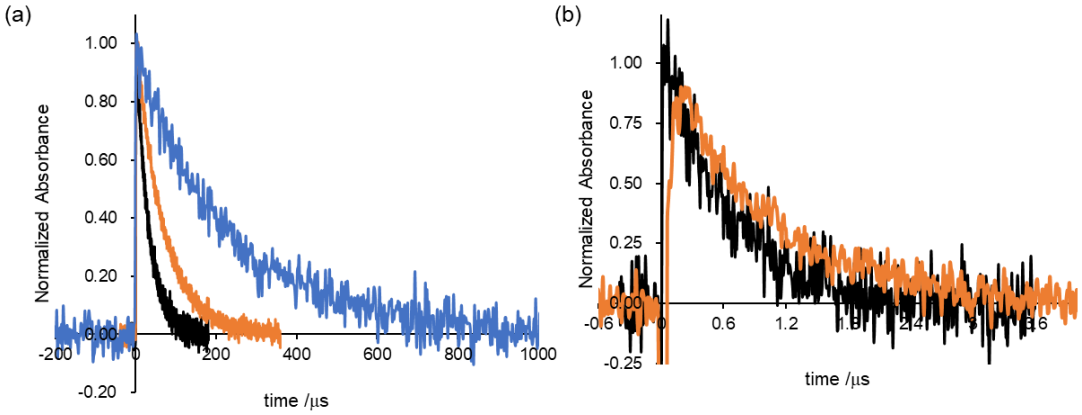

Figure 3.6. (a) Time profiles of the singlet diradical S-**DR4e** in DCMP (Blue), GTA (orange), cyclohexane (black). (b) Time profiles of the singlet diradical S-**DR4a** in DCMP (Blue), GTA (orange), acetonitrile (black).

The logarithm of the lifetime of S-**DR4c-e,** including all solvents, were linearly correlated to the logarithm of the solvent viscosity (Figure 3.7a and Table 3.1). Furthermore, non-substituted singlet diradical S-**DR4a** were longer lived in GTA than in acetonitrile (Figure 3.6b). Unfortunately, the solubility of **AZ4a** in DCMP was too low to conduct the laser flash photolysis measurements, so the lifetime of S-**DR4a** was not measured in DCMP. The solvent polarity is almost the same for acetonitrile and GTA; the π^* of GTA and acetonitrile is 0.63 and 0.66, respectively. It means the reason for the extension of the lifetime of S-**DR4a** in GTA was not coming from the solvent polarity. When the lifetime of S-**DR4a** was

plotted against the combined parameter of η and π*, a better correlation was observed than plotted with only η or π*(Figure 3.7b and Figure 3.S12a). This observation suggests that both solvent viscosity and polarity were suppressing the degradation of S-**DR4a**.

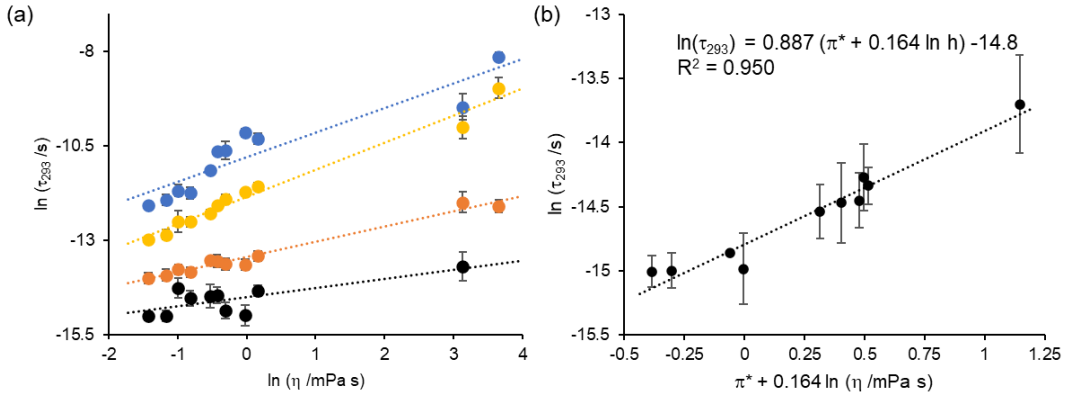

Figure 3.7. (a) viscosity dependency of the lifetime of S-**DR4a**,**c-e** in various solvents. (Black: S-**DR4a**, Orange: S-**DR4c**, Yellow: S-**DR4d**, Blue: S-**DR4e**.) (b) Combined parameter (π* and ln η) fitting of the lifetime of S-**DR4a**.

Table 3.1. Viscosity dependency on the lifetime of S-**DR4**.

Singlet diradical	slope β[a]	R^2 value[a]
S-**DR4a**	0.24 ± 0.08	0.55
S-**DR4c**	0.40 ± 0.02	0.97
S-**DR4d**	0.72 ± 0.04	0.98
S-**DR4e**	0.65 ± 0.09	0.86

a: Slope (β) and coefficient of determination (R^2) calculated from Figure 3.8a by regression analysis. Mean errors from regression analysis are shown as errors for the β.

Comparing the viscosity dependency of the lifetime of singlet diradical S-**DR4** between different substituents, the notable phenomena was observed (Table 3.1). The effects of solvent viscosity on the lifetime of S-**DR4** are presented as the slope β of Figure 3.7a.

Same as previous observed viscous depended reaction,[7,10,16] slope β indicated between 0 and 1. Between S-**DR4a**,**c**,**d**, the bulkier substituents increase the effect of the solvent viscosity. Although S-**DR4e** has bigger Tip groups than S-**DR4d** and the lifetime of S-**DR4e** were longer than that of S-**DR4d** in all solvents, the viscosity dependency on the lifetime of S-**DR4e** was almost the same as that of S-**DR4d**. These results imply that both the solvent rearrangements and the bulky aryl group's steric effects have a contribution to determining the lifetime of singlet diradicals S-**DR4d**,**e**.

To confirm the reaction path of the singlet diradical S-**DR4e** in high viscous condition, the product analysis of the photoreaction of **AZ4e** in DCMP under nitrogen were conducted (Figure 3.8). When the azoalkane **AZ4e** were irradiated by a 365 nm LED lamp, the signals around 6.7 and 5.7 ppm were generated with the degradation of the peaks corresponded to **AZ4e** (Figure 3.8b-d). The obtained signals were matched with the signal of the photoproduct in deuterium benzene, *trans*-**CP4e** (Figure 3.8e). So, the decay of the singlet diradical S-**DR4e** in DCMP should be the same as benzene, the radical-radical bond formation process.

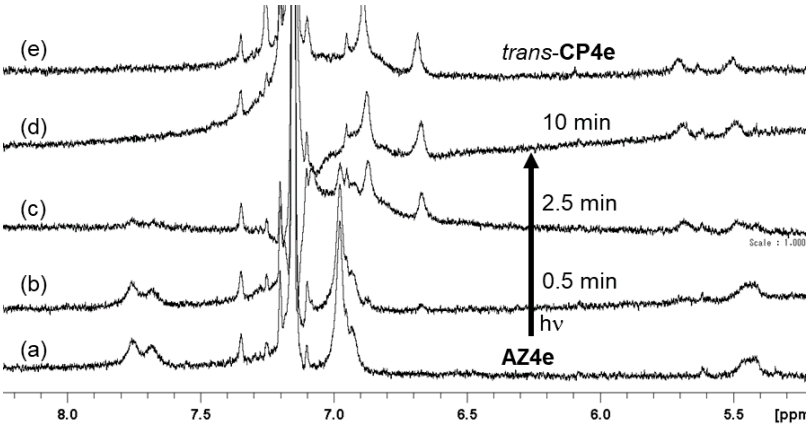

Figure 3.8. ^{1}H NMR (400 MHz) of **AZ4e**(a), photo irradiation with LED lamp (365 nm) after (b) 30 sec, (c) 150 sec and (d) 600 sec, and (e) *trans*-**CP4e** in DCMP. C_6D_6 was used as an external standard for the lock.

To gain further information, the activation enthalpy $\Delta H^{\ddagger}$ and the activation entropy $\Delta S^{\ddagger}$ of the decay process of the singlet diradical S-**DR4a**,**c-e** in all solvents were plotted as the enthalpy-entropy compensation plot (Figure 3.9a). The obtained plot shows a linear correlation. This linear correlation also informed that the reaction path of singlet diradical S-**DR4a**,**c-e** in all solvents were the same; the bond formation reaction. Furthermore, to clarify the viscosity effect on the reactivity of the singlet diradical S-**DR4e**, the enthalpy and entropy term of the activation free energy ($\Delta H^{\ddagger}$ and $-\Delta S^{\ddagger}_{293} = -293 \times \Delta S^{\ddagger}$) were plotted against the logarithm of the viscosity (Figure 3.9b). The activation enthalpy was increased by increasing the solvent viscosity. It was explained by the increase of the activation energy of the solvent rearrangements. The activation entropy term ($-\Delta S^{\ddagger}_{293}$) shows a negative linear correlation with the logarithm of the solvent viscosity. It was understood as the compensation of the activation enthalpy and activation entropy.

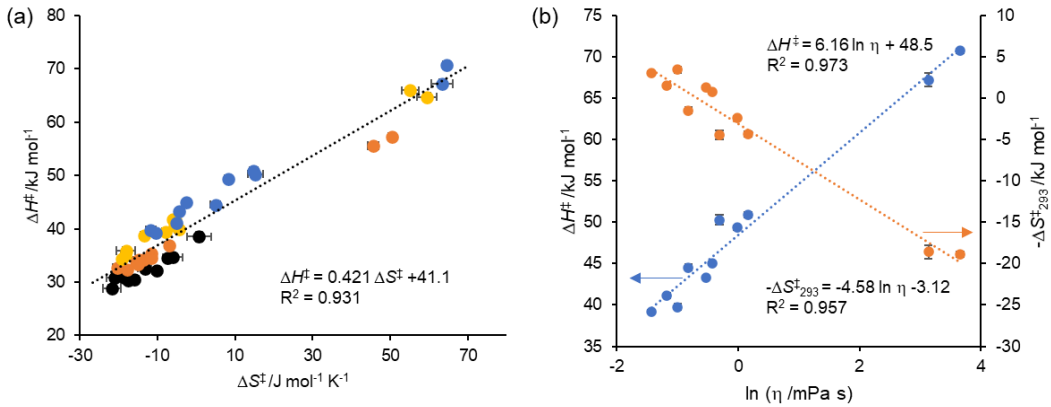

Figure 3.9. (a) Enthalpy entropy compensation graph. (Black: S-**DR4a**, Orange: S-**DR4c**, yellow: S-**DR4d**, Blue: S-**DR4e**. Black dot line: linear fitting for all singlet diradical S-**DR4.**) (b) The viscosity dependency of the activation enthalpy ($\Delta H^{\ddagger}$, Blue) and the activation entropy term of the activation Gibbs energy at 293 K ($-\Delta S^{\ddagger}_{293}$, orange).

As mentioned in chapter 2, the lifetimes of S-**DR4e** in benzene were the same under air and nitrogen. However, that was affected by the concentration of molecular oxygen especially in DCMP. Increasing the oxygen concentration shortens the observed lifetime of S-**DR4e** (Figure 3.10a). When the inverse of the lifetime of S-**DR4e**, rate constants k_{obs}, were plotted against the concentration of oxygen, the linear relationship was observed (Figure 3.10b).

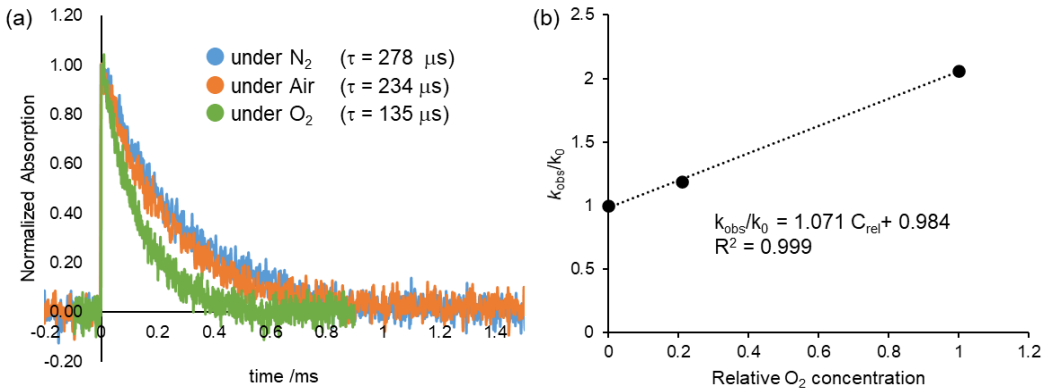

Figure 3.10. (a) The time trace of the singlet diradical S-**DR4e** in DCMP under nitrogen (blue), air (orange), and oxygen (green). (b) The relative oxygen concentration dependency of the reaction rate for the decay of the singlet diradical S-**DR4e**. The relative O_2 concentration was presented as C_{rel} in the equation.

To estimate the quenching constants k_q, the saturated oxygen concentration in DCMP was needed. But this value was not reported. On the other hand, that in hexane, cyclohexane, and paraffin oil at 293 K were calculated as 15.0, 11.2, and 6.05 mM, respectively (see section 3.5.7). From these values, the author assumed the saturated oxygen concentration in DCMP to 5 ~ 30 mM. From the linear regression, the quenching constants k_q of singlet diradical S-**DR4e** in DCMP were estimated to 7.7×10^5 ~ 1.3×10^5 M^{-1} s^{-1}. These values were consistent with the estimation for the quenching constants between S-**DR3a** and molecular oxygen, less than 4×10^5 M^{-1} s^{-1}.[2]

There are two possibilities for the reaction mechanism to this observation; one is the direct reaction between oxygen and singlet diradical (Scheme 3.3). Another hypothesis is triplet diradical T-**DR4e** were equilibrated with S-**DR4e** and react with oxygen. More detail analysis, such as temperature dependency of k_q, is needed for a decision of plausible mechanism.

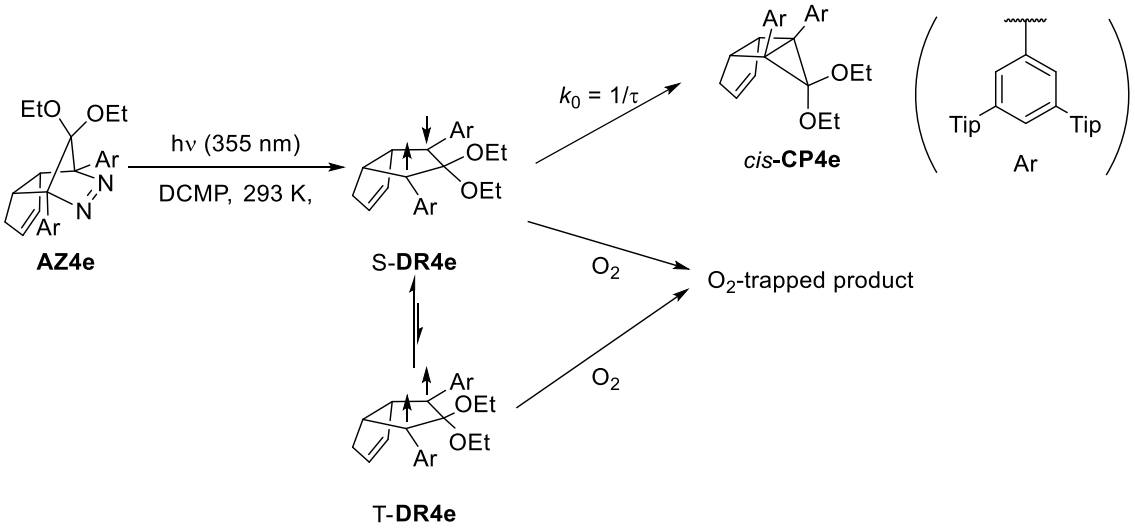

Scheme 3.3. A plausible mechanism for the decay of the singlet diradical S-**DR4e** presence of the molecular oxygen.

Section 3.3. Pressure effect on the lifetime of the singlet diradical S-**DR4**

The generation of the singlet diradical S-**DR4e** under high-pressure conditions was conducted because the limitation of the viscosity effect on the reactivity of the singlet diradical was still unclear. Generally, the viscosities of the organic solvents were increased under high pressure and written as an equation, $\ln \eta = \ln \eta_0 + \alpha P$.[4] The parameter η_0 and α means the viscosity under atmospheric pressure and the pressure dependency of the solvent viscosity, respectively. So, these values are dependent on the solvent. Significantly, the high viscous solvent, GTA and DCMP, has an immense values for both η_0 and α than ordinary organic solvents.[15,16] Taking advantage of this, the pressure dependency of the lifetime of S-**DR4e** was examined, and it was expected that the lifetime was increased by increasing the pressure.

The 355 nm laser irradiated the precursor **AZ4e** dissolved in DCMP under argon in the cell for high-pressure experiments. Although the lifetime of S-**DR4e** was about 0.3 ms at atmospheric pressure, it was extended to 2000 ms (2.0 seconds) at 4000 atm (Figure 3.11). The lifetimes of S-**DR4e** were also determined to 4.65, 53.9, and 352 ms at 1000, 2000, and 3000 atm, respectively (Figure 3.S13). When the logarithm of the lifetime of S-**DR4e** was plotted against the pressure, a linear correlation was observed between these (Figure 3.12a).

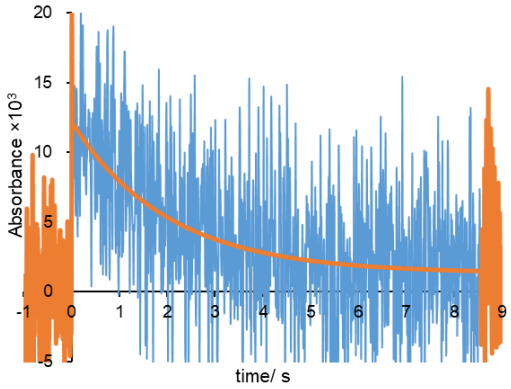

Figure 3.11. The time trace of the singlet diradical S-**DR4e** in DCMP at 4000 atm. (Blue: experiment data, Orange: fitting)

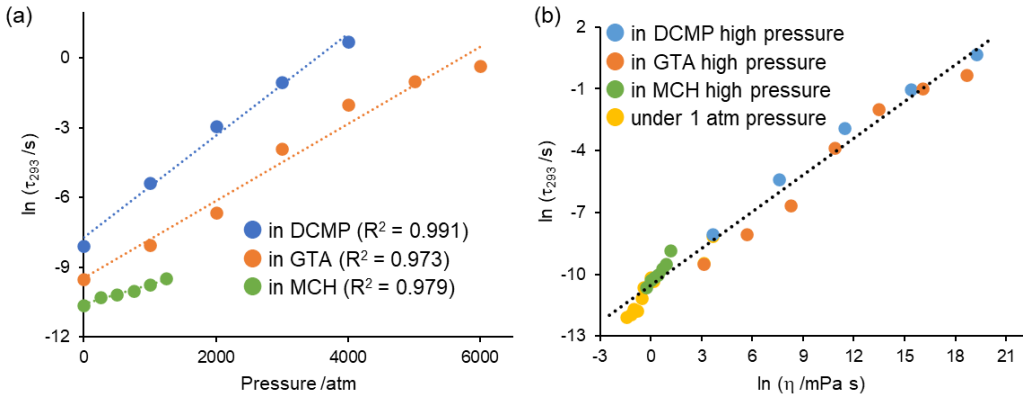

Figure 3.12. (a) The pressure dependency of the lifetime of S-**DR4e** in DCMP(blue), GTA(orange), and MCH(green). (b) The viscosity dependency of the lifetime of S-**DR4e** in DCMP(blue), GTA(orange), and MCH(green) under high pressure and in the various solvents at ambient pressure (yellow).

The pressure dependencies of the lifetime of S-**DR4e** were also examined in other solvents, GTA, and methylcyclohexane (MCH). DCMP has a high viscosity and low polarity, so GTA was selected as the high viscous and high polarity solvent. MCH was chosen as the low viscous and low polar solvent. In both solvents, the logarithm of the lifetime of S-**DR4e** was correlated linearly with the pressure

(Figure 3.12a and Figure 3.S14, S15). Using the linear relationship between the logarithm of the viscosity and the pressure, $\ln \eta = \ln \eta_0 + \alpha P$, the viscosities were calculated at each pressure. The viscosity dependency of the lifetime of the singlet diradical S-**DR4e,** including high-pressure conditions, were obtained from the estimated viscosity (Figure 3.12b). The positive correlation in the log-log plot of the viscosity and the lifetime of the singlet diradical S-**DR4e** stated that the bond formation process in S-**DR4e** was greatly influenced by the molecular motions of the singlet diradical and solvent molecule.

In the atmospheric pressure, the viscosity effect on the lifetime of the parent singlet diradical S-**DR4a** was observed between that in GTA and that in acetonitrile (see section 3.2). So, the pressure effects on the lifetime of the parent singlet diradical S-**DR4a** were also investigated to describe more detail of the bulky substituents group influence. The longer lifetimes of the singlet diradical S-**DR4a** were observed by increasing the pressure in both GTA and MCH (Figure 3.13a and Figure 3.S16-S18). When the lifetime of S-**DR4a**,**e** were compared simultaneously, the Tip groups effectively suppress the bond formation not only under atmospheric pressure but also under high pressure. Concretely, the lifetime of S-**DR4a** and S-**DR4e** in GTA at 5000 atm was 3.6 and 371 ms, respectively; the lifetime of S-**DR4a** and S-**DR4e** in MCH at 1000 atm was 0.54 and 59.5μs, respectively. Although the logarithm of the lifetime of S-**DR4a** in MCH was linearly increased by increasing pressure, that in GTA shows the singular point for the slope against the pressure around 2000 atm. Like the S-**DR4e**, the log-log plot between the viscosity and the lifetime of S-**DR4a** were prepared (Figure 3.13b). The lifetime's viscosity dependency was refracted around 670 mPa s, $\ln \eta \sim 6.5$, the same as the pressure dependency in GTA.

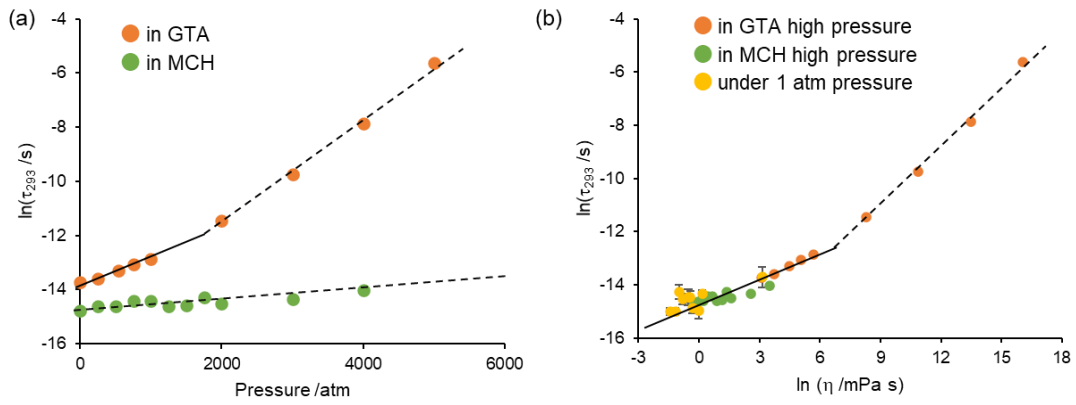

Figure 3.13. (a) The pressure dependency of the lifetime of S-**DR4a** in GTA(orange) and MCH(green). (b) The viscosity dependency of the lifetime of S-**DR4a** in GTA(orange) and MCH(green) under high pressure and various solvent at ambient pressure (yellow).

There were two possibilities for this observation. One is the effect of the activation volume could be ignored by increasing the effect of the solvent fluctuation. A similar situation, in which the viscosity effect was more influenced to determine the reaction kinetics than the traditional pressure effect, had been observed previously for the thermal back reaction of the photochromic molecule or thermal *cis-trans* isomerization for analogous of azobenzene.[4,9,15,16] Another is the polarity increased induced by pressure. The singlet diradical S-**DR4a** were long-lived by increasing solvent polarity, which was mentioned in section 3.2. Furthermore, the polarity of several solvents was increased by high pressure.[17] So, the singlet diradical S-**DR4a** would be stabilized by the high polarity induced pressure. However, the author in the reference commented that the pressure dependency of the solvent polarity becomes smaller during increasing pressure. Therefore, the former description seems more reasonable than the latter. Nevertheless, to conduct the pressure effect on the absorption maximum of the 4-nitro anisole in GTA is needed for confirming the reason.

Section 3.4. Summary of this chapter

It was summarized that the steric and viscosity effect on the lifetime of singlet diradicals S-**DR4** in this chapter. For the non-substituted case, the lifetime of singlet diradical S-**DR4a** was affected by both the solvent polarity and solvent viscosity. However, by increasing the bulkiness of the aryl group at C1, C3 position just a little, the lifetime of singlet diradical S-**DR4c-e** were almost solely defined by the solvent viscosity. The bulkiness of the aryl groups in singlet diradicals S-**DR4** influenced the viscosity dependency of the lifetime of that. The product analysis and the enthalpy-entropy plot support that the singlet diradical's decay processes are the bond-formation process in all substituents under nitrogen. However, highly long-lived singlet diradical S-**DR4e** in DCMP were trapped by molecular oxygen. To obtain more longer-lived singlet diradical, the singlet diradical were generated in extremely high viscous conditions induced by high pressure. The lifetime of singlet diradical S-**DR4e** was reached to 2 seconds in DCMP at 4000 atm. Further experiments satisfy that the viscosity of reaction media also influences the lifetime of singlet diradical S-**DR4a**. On the other hand, the viscosity dependency of the lifetime of singlet diradical S-**DR4a** was described by two crossed lines at around 670 mPa s.

Section 3.5. Experimental section

Section 3.5.1 General information

AZ4a,c-e were synthesized by the same procedure as chapter 2.[18] Solvents used for laser flash photolysis (LFP) measurements were purchased from commercial suppliers and used without further purification. The concentrations of samples for LFP measurements under atmospheric pressure were adjusted to 5 mM, and its optical densities were around 0.4 at the exciting wavelength (355 nm). The excitation source for the LFP system was an Nd: YAG laser (λ_{exc} = 355 nm, 5 ns pulse, 7 mJ). The monitoring system consisted of a 150 W xenon lamp as a light source, Unisoku-MD200 monochromator, and a photomultiplier. The temperature was controlled with a CoolSpek USP-203-B (Unisoku). The concentration of samples for LFP measurements under high pressure was adjusted to 10 mM. Details of high-pressure kinetics were described elsewhere [19] while Nd: YAG laser, 150 W xenon lamp, and Unisoku-MD200 were used as the excitation source, light source, and monochromator, respectively. The solvent polarity parameter, π^* and $E_T(30)$, were cited from corresponding articles.[12,20] And π^* for methylcyclohexane and 2,4-dicyclohexyl-2-methyl-pentane were determined by the measurements of UV-vis absorption of 4-nitro-anisole (section 3.5.9). The solvent viscosity, η, were cited from corresponding articles. [7,15,16,21–26] Pressure dependency of solvent viscosity for glycerol triacetate and 2,4-dicyclohexyl-2-methyl-pentane were calculated from corresponding articles using $\ln \eta = \ln \eta_0 + \alpha P$.[15,16] And that for methylcyclohexane were estimated from the previous report (section 3.5.10).

Section 3.5.2. Transient Absorption spectra

Transient Absorption spectra of **AZ4a,c-e** were measured at around 293 K in each solvent under N_2 atmosphere. In all cases, transient species, which has absorption maximum at around 560 – 600 nm, were observed like Figure 3.S1. Moreover, these absorptions were corresponding to HOMO-LUMO transition of S-**DR4a,c-e**.

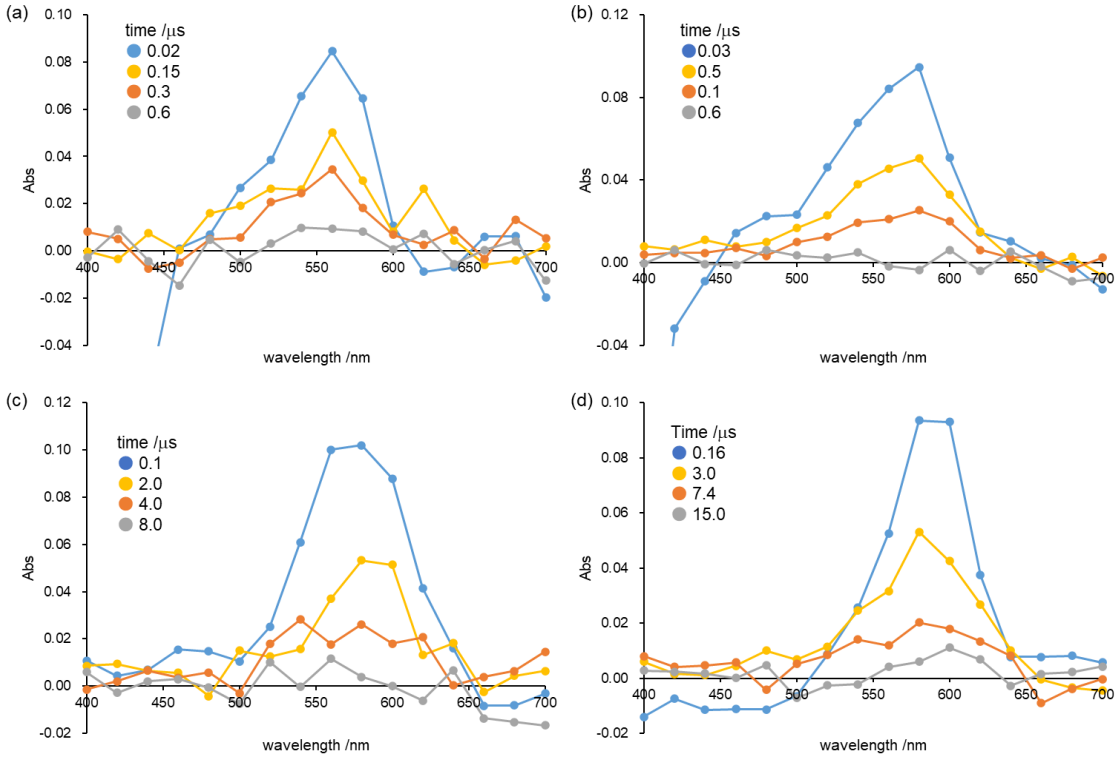

Figure 3.S1. Transient Absorption of S-DR4 in hexane (a) S-**DR4a** at 294.1 K (b) S-**DR4c** at 295.5 K (c) S-**DR4d** at 291.7 K (d) S-**DR4e** at 295.3 K.

Section 3.5.3. Temperature dependency of the lifetime of S-**DR4a**,**c-e**

Temperature dependency of the lifetime of S-**DR4a,c-e** in hexane, benzene, toluene, cyclohexane, methylcyclohexane, acetonitrile, ethyl acetate, 1,4-dioxane, glycerol triacetate (GTA) and 2,4-dicyclohexyl-2-methyl pentane (DCMP) were measured at 5 temperature between 283 K to 323 K under N_2 atmosphere. Temperature dependency of the lifetime of S-**DR4a,c-e** in pentane were measured at 5 temperature between 263K to 303 K under N_2 atmosphere. Measurements were conducted 5 times at each temperature. The decay profile were monitored at 560 nm(S-**DR4a**), 580 nm(S-**DR4c, d**), and 600 nm (S-**DR4e**).

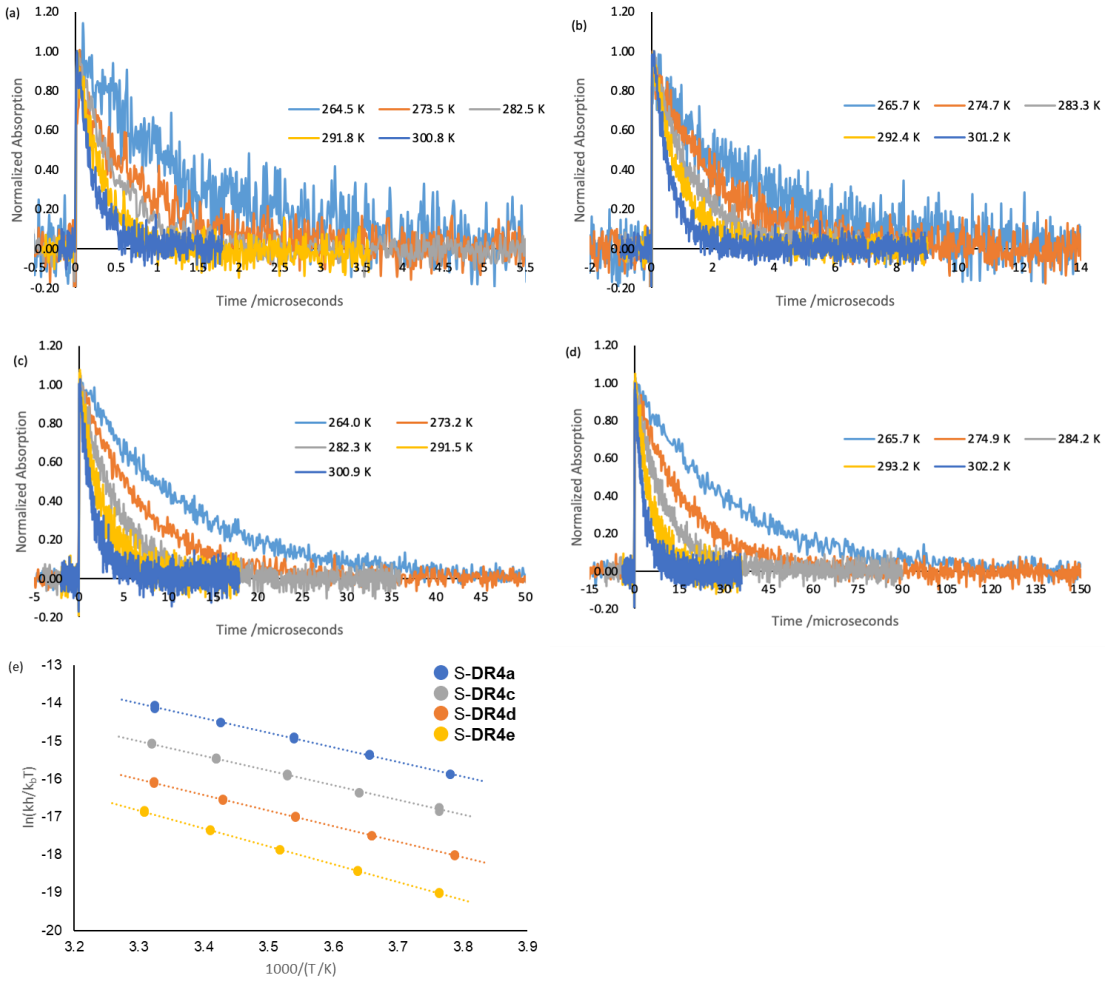

Figure 3.S2. Decay profile of (a)S-**DR4a**, (b)**4c**, (c)**4d** and (d)**4e** in pentane at each temperature and (e)Eyring plot of ring closing reaction of S-**DR4a**,**c-e** in pentane.

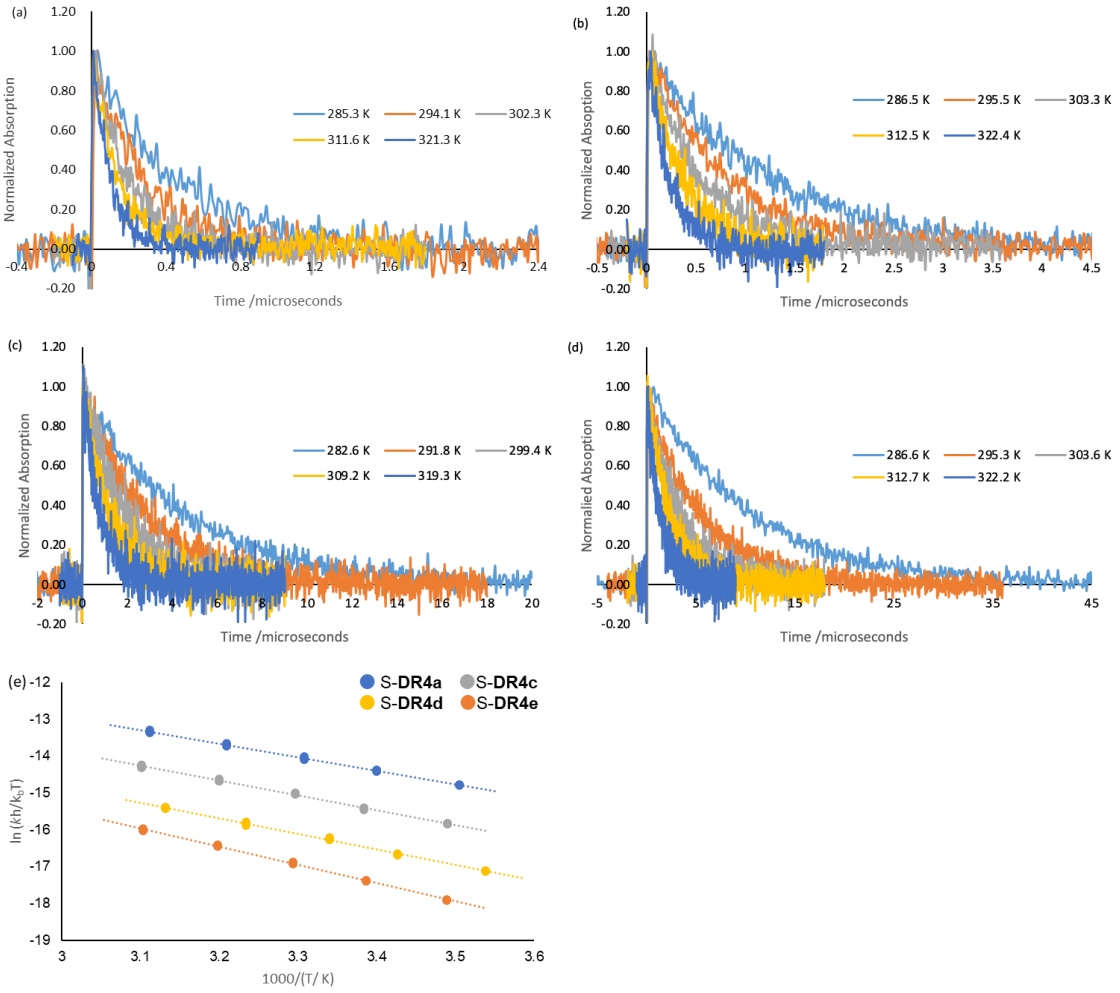

Figure 3.S3. Decay profile of (a)S-**DR4a**, (b)**4c**, (c)**4d** and (d)**4e** in hexane at each temperature and (e)Eyring plot of ring closing reaction of S-**DR4a**,**c-e** in hexane.

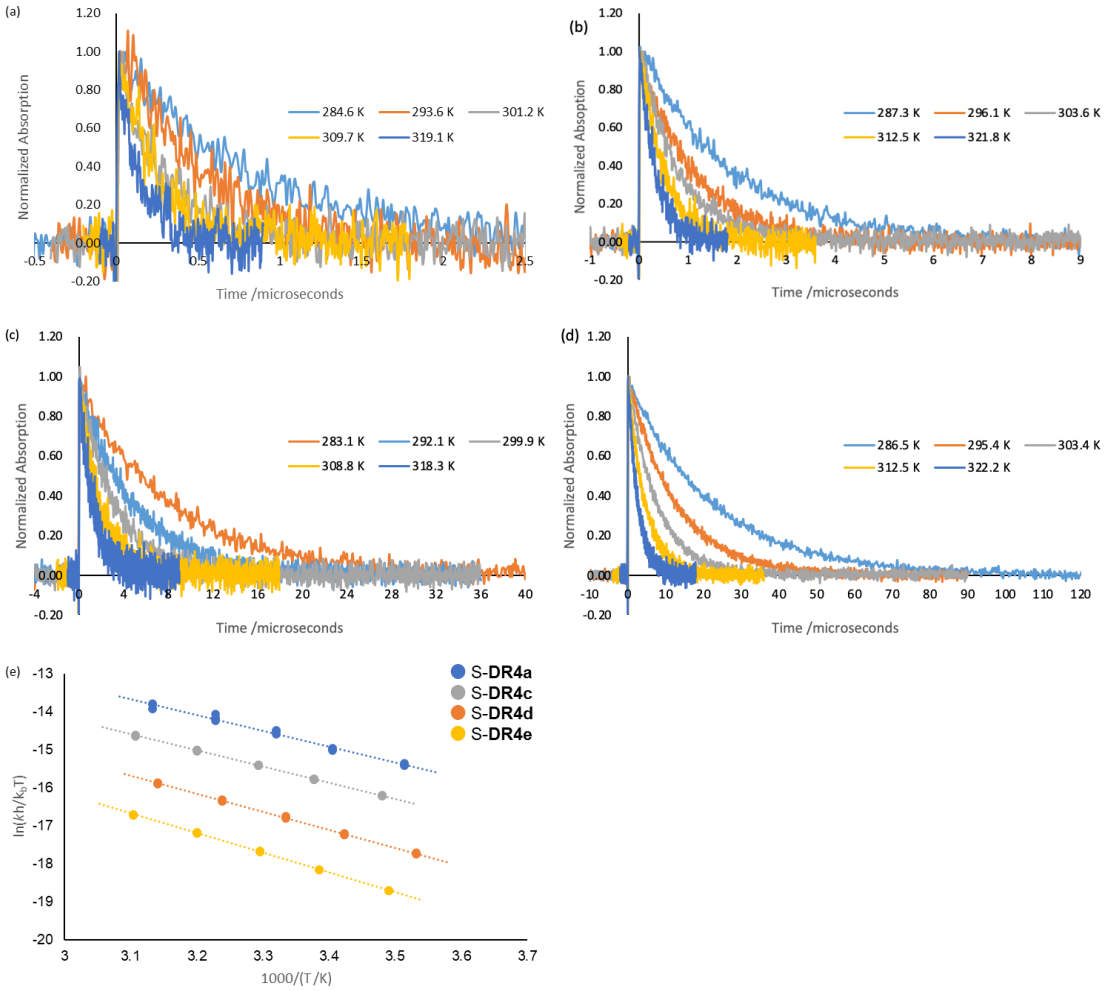

Figure 3.S4. Decay profile of (a)S-**DR4a**, (b)**4c**, (c)**4d** and (d)**4e** in toluene at each temperature and (e)Eyring plot of ring closing reaction of S-**DR4a**,**c-e** in toluene.

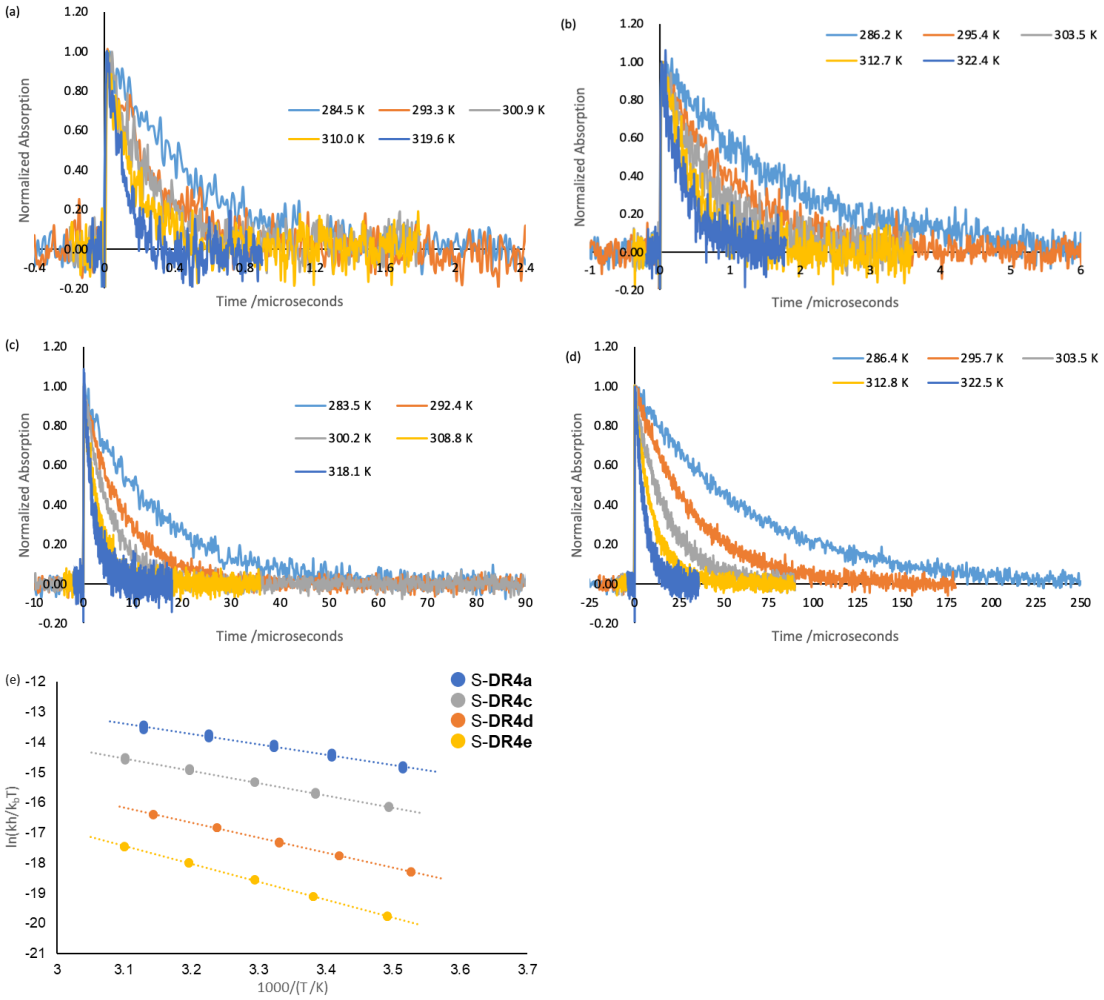

Figure 3.S5. Decay profile of (a)S-**DR4a**, (b)**4c**, (c)**4d** and (d)**4e** in cyclohexane at each temperature and (e)Eyring plot of ring closing reaction of S-**DR4a**,**c-e** in cyclohexane.

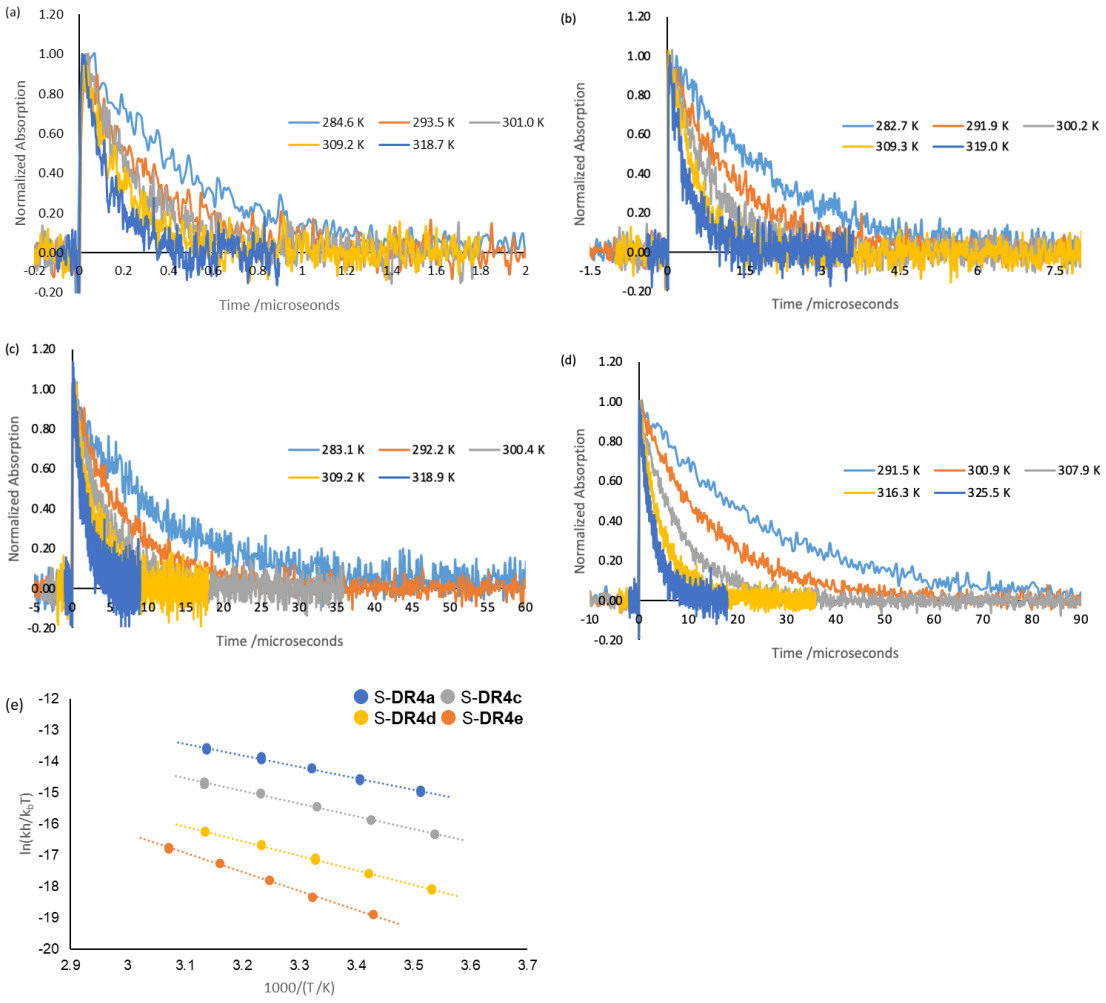

Figure 3.S6. Decay profile of (a)S-**DR4a**, (b)**4c**, (c)**4d** and (d)**4e** in methylcyclohexane at each temperature and (e)Eyring plot of ring closing reaction of S-**DR4a**,**c-e** in methylcyclohexane.

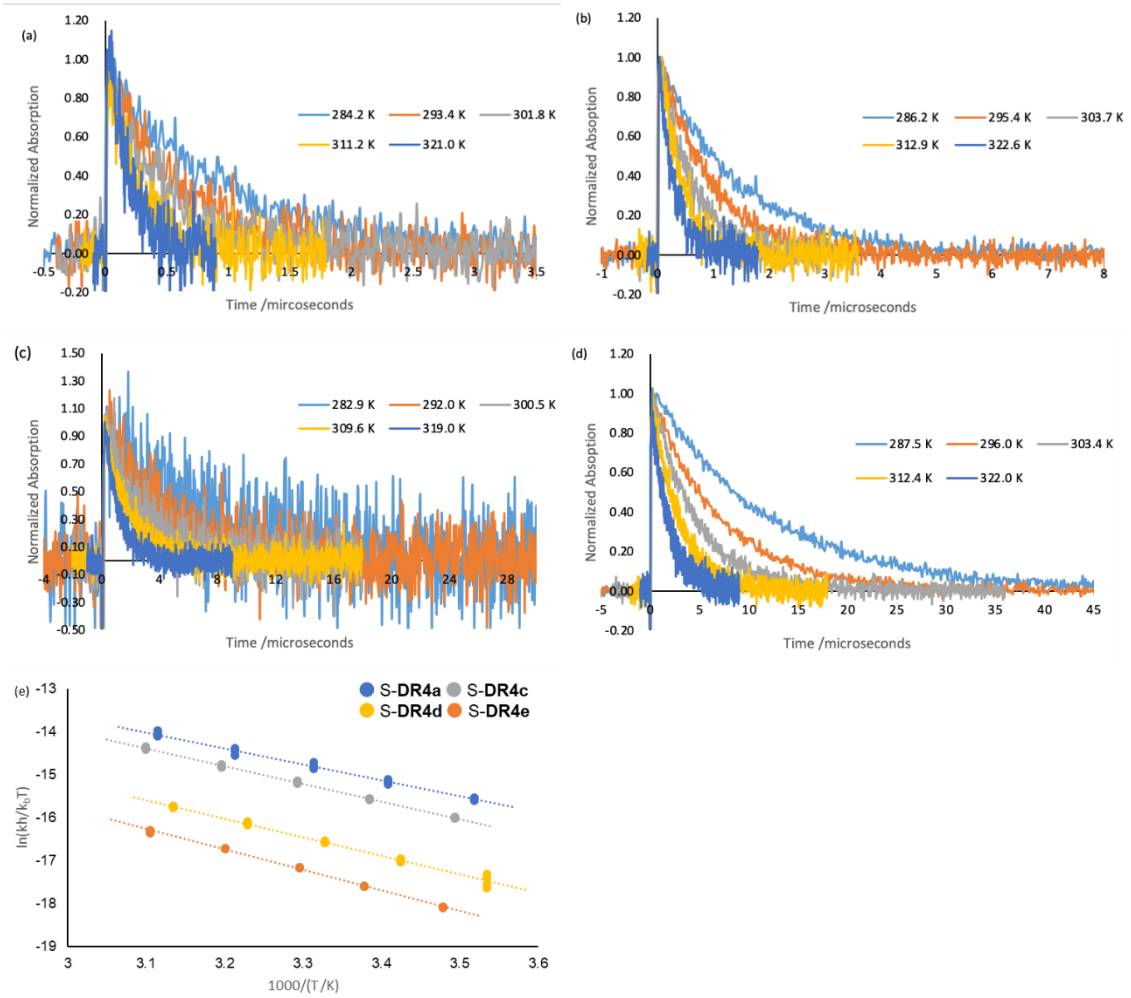

Figure 3.S7. Decay profile of (a)S-**DR4a**, (b)**4c**, (c)**4d** and (d)**4e** in acetonitrile at each temperature and (e)Eyring plot of ring closing reaction of S-**DR4a**,**c-e** in acetonitrile.

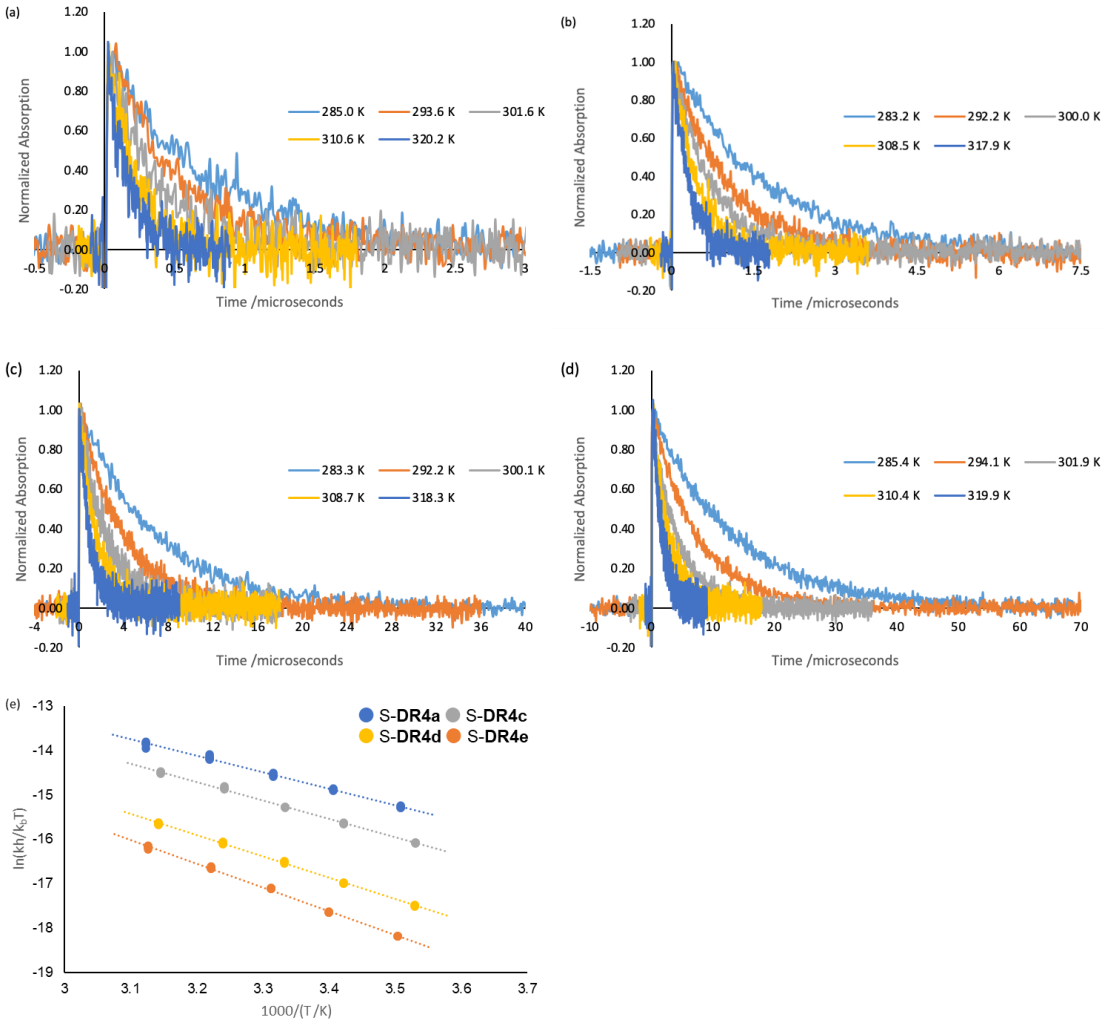

Figure 3.S8. Decay profile of (a)S-**DR4a**, (b)**4c**, (c)**4d** and (d)**4e** in ethyl acetate at each temperature and (e)Eyring plot of ring closing reaction of S-**DR4a**,**c-e** in ethyl acetate.

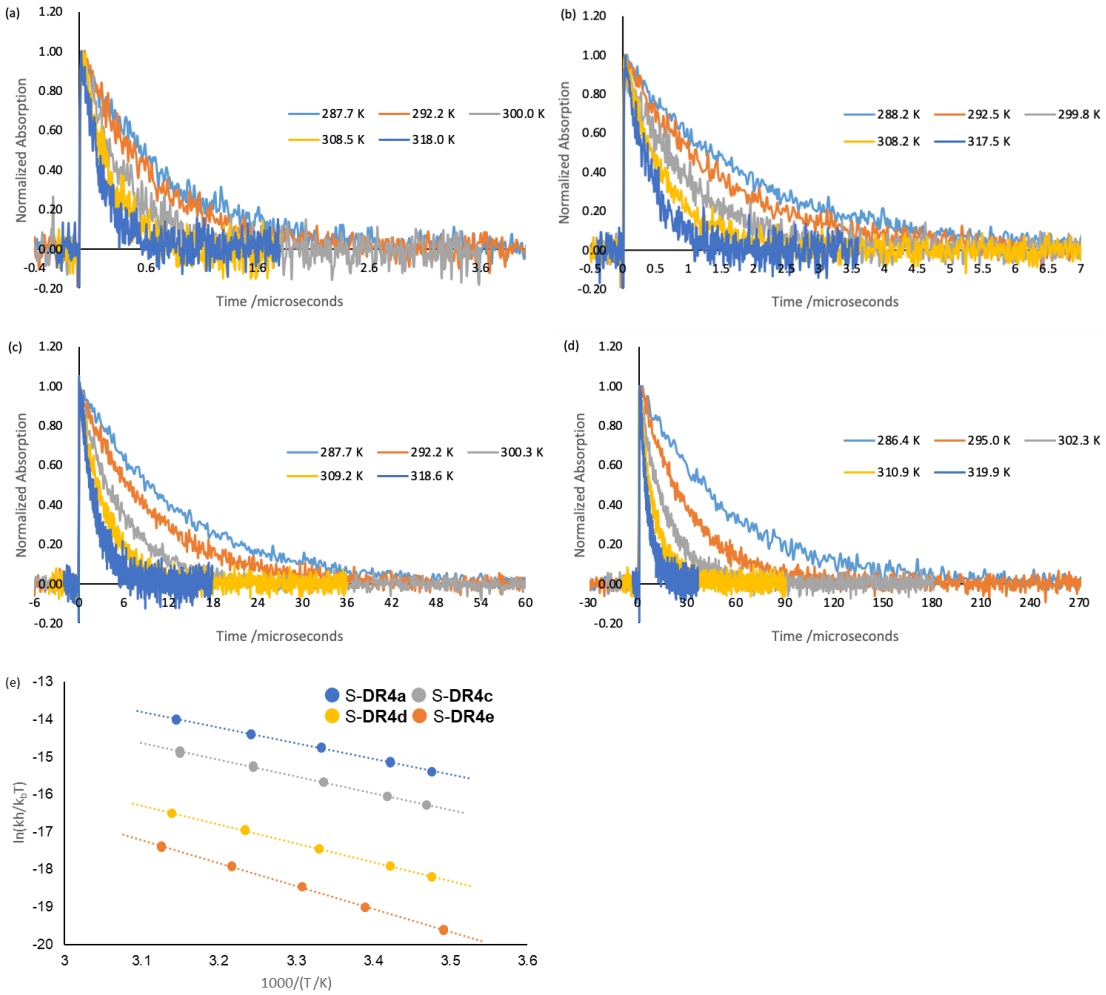

Figure 3.S9. Decay profile of (a)S-**DR4a**, (b)**4c**, (c)**4d** and (d)**4e** in 1,4-dioxane at each temperature and (e)Eyring plot of ring closing reaction of S-**DR4a**,**c-e** in 1,4-dioxane.

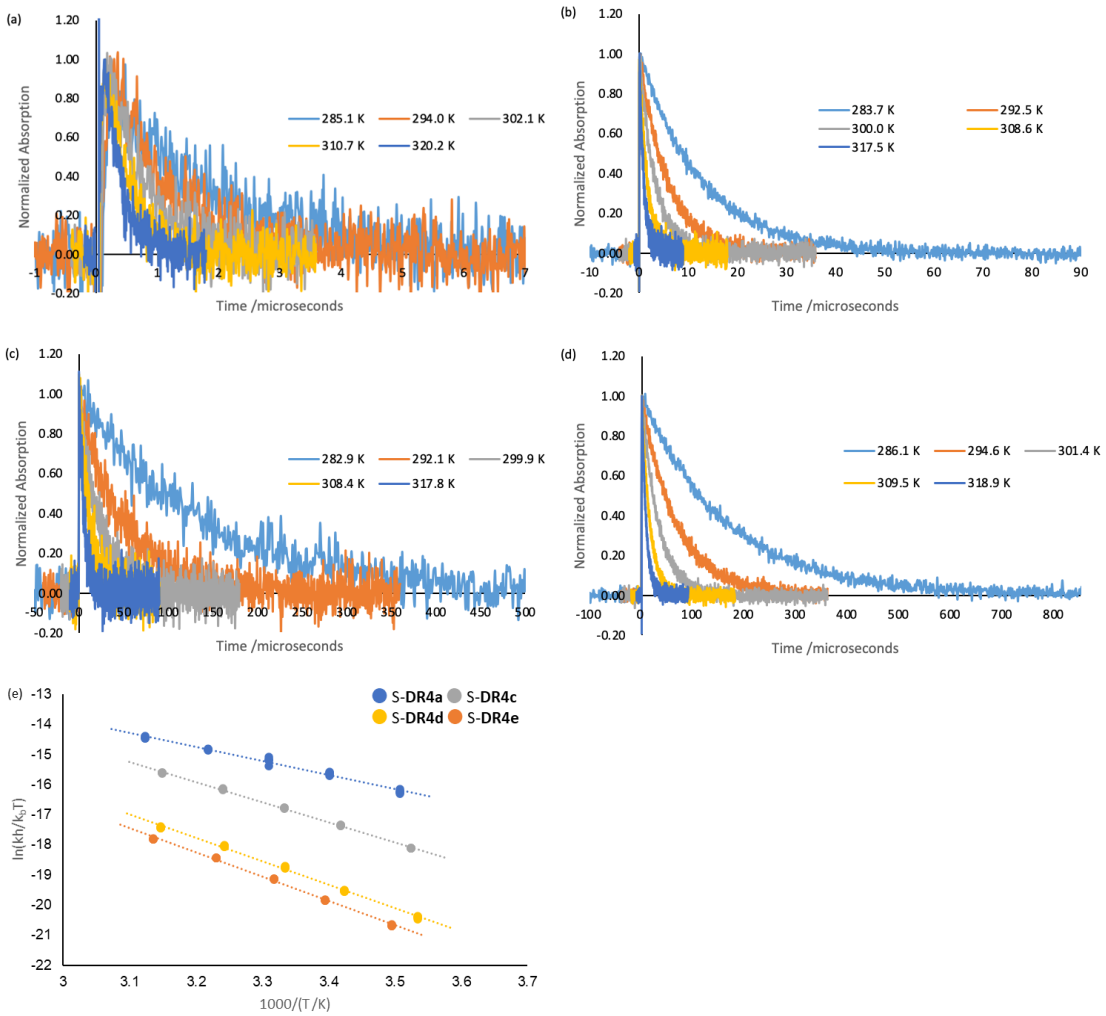

Figure 3.S10. Decay profile of (a)S-**DR4a**, (b)**4c**, (c)**4d** and (d)**4e** in GTA at each temperature and (e)Eyring plot of ring closing reaction of S-**DR4a**,**c-e** in GTA.

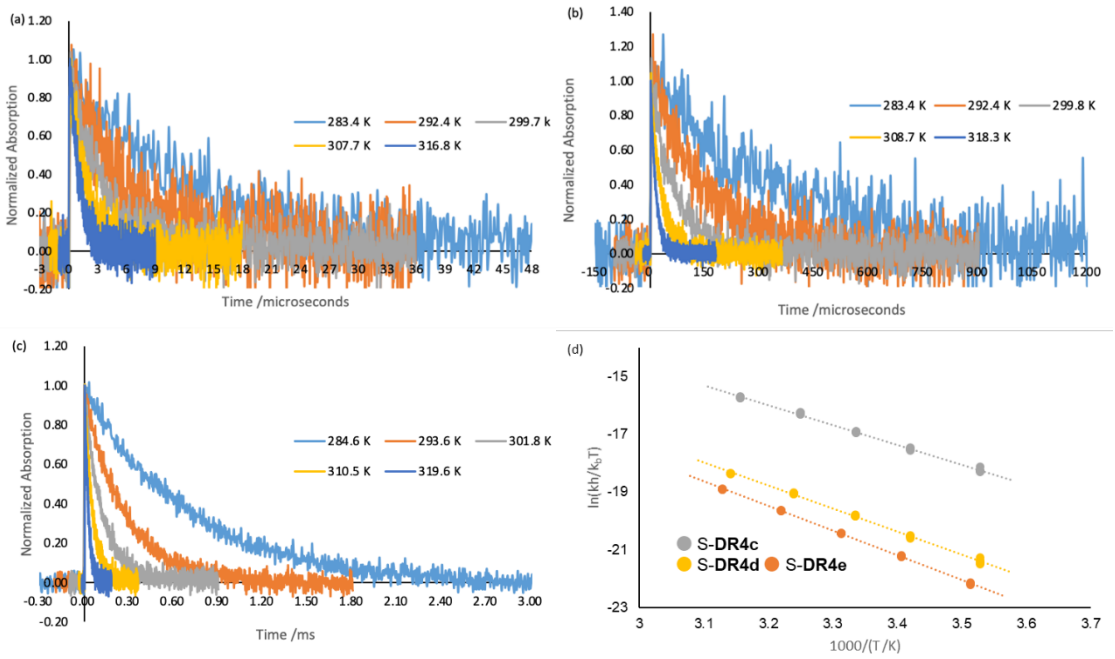

Figure 3.S11. Decay profile of (a)S-**DR4c**, (b)**4d**, and (c)**4e** in DCMP at each temperature and (d)Eyring plot of ring closing reaction of S-**DR4c**-**e** in DCMP

Section 3.5.4. The lifetime of S-**DR4a**,**c-e** at 293 K and the activation parameter for ring closing reaction of S-**DR4a**,**c-e**

The lifetime τ_{293} of S-**DR4a**,**c-e** at 293 K, the activation enthalpy $\Delta H^{\ddagger}$ and activation entropy $\Delta S^{\ddagger}$ were determined from the Eyring plot (Figure 3.S2-S11) by regression analysis

Table 3.S1. Solvent parameters, lifetime of S-**DR4a,** and activation parameters of ring closing reaction from S-**DR4a** in each solvent.

Solvent	π*	$E_T(30)$/ kcal mol^{-1}	η /mPa s	τ_{293} / μs [a]	$\Delta H^{\ddagger}$ /kJ mol^{-1} [b]	$\Delta S^{\ddagger}$ /kJ mol^{-1} T^{-1}[b]
Pentane	–0.15	31.0	0.24	0.30 ± 0.04	32.2 ± 0.3	–10.3 ± 1.1
Hexane	–0.11	31.0	0.31	0.31 ± 0.04	30.5 ± 0.3	–15.9 ± 1.1
Benzene	0.55	34.3	0.65	0.53 ± 0.12	32.6 ± 0.5	–13.2 ± 1.7
Toluene	0.49	33.9	0.59	0.52 ± 0.2	34.6 ± 0.8	–6.2 ± 2.5
Cyclohexane	0	30.9	0.98	0.31 ± 0.10	28.8 ± 0.7	–21.7 ± 2.3
Methyl Cyclohexane	–0.01	32.2	0.73	0.35 ± 0.08	30.3 ± 0.5	–17.7 ± 1.7
Acetonitrile	0.66	45.6	0.37	0.63 ± 0.19	30.8 ± 0.6	–21.0 ± 2.1
Ethyl Acetate	0.45	38.1	0.44	0.49 ± 0.11	30.9 ± 0.5	–18.4 ± 1.7
1,4-dioxane	0.49	36.0	1.18	0.59 ± 0.09	34.5 ± 0.4	–7.4 ± 1.2
GTA	0.63	43.3	23	1.12 ± 0.5	38.5 ± 0.9	0.68 ± 3.1

[a] τ_{293} were estimated from Eyring plot. The mean error obtained from regression analysis is shown as errors. [b] $\Delta H^{\ddagger}$ and $\Delta S^{\ddagger}$ were calculated from Eyring plot. The mean error obtained from regression analysis is shown as errors.

Table 3.S2. Solvent parameters, lifetime of S-**DR4c,** and activation parameters of ring closing reaction from S-**DR4c** in each solvent.

Solvent	π*	$E_T(30)$ /kcal mol^{-1}	η /mPa s	τ_{293} /μs [a]	$\Delta H^{\ddagger}$ /kJ mol^{-1} [b]	$\Delta S^{\ddagger}$ /kJ mol^{-1} T^{-1} [b]
Pentane	–0.15	31.0	0.24	0.83 ± 0.12	32.4 ± 0.3	–17.8 ± 1.2
Hexane	–0.11	31.0	0.31	0.90 ± 0.14	33.4 ± 0.4	–15.0 ± 1.2
Benzene	0.55	34.3	0.65	1.30 ± 0.23	32.7 ± 0.4	–20.3 ± 1.3
Toluene	0.49	33.9	0.59	1.34 ± 0.09	35.4 ± 0.2	–11.6 ± 0.5
Cyclohexane	0	30.9	0.98	1.19 ± 0.17	33.9 ± 0.3	–15.5 ± 1.1
Methyl Cyclohexane	–0.01	32.2	0.73	1.19 ± 0.21	34.2 ± 0.4	–14.8 ± 1.3
Acetonitrile	0.66	45.6	0.37	1.04 ± 0.14	34.1 ± 0.3	–13.7 ± 1.0
Ethyl Acetate	0.45	38.1	0.44	0.97 ± 0.14	34.6 ± 0.3	–11.5 ± 1.1
1,4-dioxane	0.49	36.0	1.18	1.49 ± 0.21	36.9 ± 0.3	–7.0 ± 1.1
GTA	0.63	43.3	23	5.53 ± 1.0	55.6 ± 0.4	45.6 ± 1.4
DCMP	0.14	30.1	38.7	6.19 ± 1.9	57.2 ± 0.7	50.3 ± 2.2

[a] τ_{293} were estimated from Eyring plot. The mean error obtained from regression analysis is shown as errors. [b] $\Delta H^{\ddagger}$ and $\Delta S^{\ddagger}$ were calculated from Eyring plot. The mean error obtained from regression analysis is shown as errors.

Table 3.S3. Solvent parameters, lifetime of S-**DR4d,** and activation parameters of ring closing reaction from S-**DR4d** in each solvent.

Solvent	π*	$E_T(30)$/ kcal mol^{-1}	η /mPa s	τ_{293} / μs [a]	$\Delta H^{\ddagger}$ /kJ mol^{-1} [b]	$\Delta S^{\ddagger}$ /kJ mol^{-1} T^{-1} [b]
Pentane	–0.15	31.0	0.24	2.32 ± 0.2	34.4 ± 0.2	–19.3 ± 0.6
Hexane	–0.11	31.0	0.31	2.61 ± 0.4	35.0 ± 0.3	–18.4 ± 1.1
Benzene	0.55	34.3	0.65	5.68 ± 0.4	40.6 ± 0.2	–5.6 ± 0.5
Toluene	0.49	33.9	0.59	4.65 ± 0.4	39.4 ± 0.2	–8.0 ± 0.7
Cyclohexane	0	30.9	0.98	8.12 ± 0.6	41.6 ± 0.2	–5.4 ± 0.6
Methyl Cyclohexane	–0.01	32.2	0.73	6.76 ± 0.8	38.8 ± 0.3	–13.4 ± 0.9
Acetonitrile	0.66	45.6	0.37	3.70 ± 1.2	35.9 ± 0.7	–18.1 ± 2.4
Ethyl Acetate	0.45	38.1	0.44	3.69 ± 0.5	39.9 ± 0.3	–4.5 ± 1.0
1,4-dioxane	0.49	36.0	1.18	9.39 ± 0.9	41.7 ± 0.2	–6.0 ± 0.8
GTA	0.63	43.3	23	44.8 ± 16	64.7 ± 0.7	59.4 ± 2.5
DCMP	0.14	30.1	38.7	127 ± 40	66.0 ± 0.7	55.1 ± 2.2

[a] τ_{293} were estimated from Eyring plot. The mean error obtained from regression analysis is shown as errors. [b] $\Delta H^{\ddagger}$ and $\Delta S^{\ddagger}$ were calculated from Eyring plot. The mean error obtained from regression analysis is shown as errors.

Table 3.S4. Solvent parameters, lifetime of S-**DR4e,** and activation parameters of ring closing reaction from S-**DR4e** in each solvent.

Solvent	π*	$E_T(30)$/ kcal mol^{-1}	η /mPa s	τ_{293} / μs [a]	$\Delta H^{\ddagger}$ /kJ mol^{-1} [b]	$\Delta S^{\ddagger}$ /kJ mol^{-1} T^{-1} [b]
Pentane	–0.15	31.0	0.24	5.68 ± 0.4	39.2 ± 0.2	–10.4 ± 0.6
Hexane	–0.11	31.0	0.31	6.59 ± 1.0	41.1 ± 0.3	–5.1 ± 1.1
Benzene	0.55	34.3	0.65	23.8 ± 1.4	45.0 ± 0.1	–2.5 ± 0.5
Toluene	0.49	33.9	0.59	14.6 ± 1.1	43.3 ± 0.2	–4.5 ± 0.6
Cyclohexane	0	30.9	0.98	38.8 ± 4.5	49.4 ± 0.3	8.2 ± 0.9
Methyl Cyclohexane	–0.01	32.2	0.73	24.4 ± 6.8	50.3 ± 0.6	15.2 ± 2.0
Acetonitrile	0.66	45.6	0.37	8.38 ± 1.4	39.8 ± 0.4	–11.8 ± 1.3
Ethyl Acetate	0.45	38.1	0.44	7.89 ± 1.4	44.5 ± 0.4	4.97 ± 1.3
1,4-dioxane	0.49	36.0	1.18	33.3 ± 4.8	50.9 ± 0.3	14.7 ± 1.1
GTA	0.63	43.3	23	77.2 ± 31.5	67.2 ± 0.8	63.4 ± 2.8
DCMP	0.14	30.1	38.7	289 ± 37	70.7 ± 0.3	64.4 ± 1.0

[a] τ_{293} were estimated from Eyring plot. The mean error obtained from regression analysis is shown as errors. [b] $\Delta H^{\ddagger}$ and $\Delta S^{\ddagger}$ were calculated from Eyring plot. The mean error obtained from regression analysis is shown as errors.

Section 3.5.5. The dependency of the lifetime of S-**DR4a**,**c-e** on the solvent polarity

The polarity dependency on the lifetime of S-**DR4a**, R^2 value in Figure 3.S12a, was decreased by adding the result of the lifetime of S-**DR4a** in GTA to the plot. This result also supports the viscosity dependency of the lifetime of S-**DR4a**. The logarithm of the lifetime of S-**DR4c-e** in all solvent in Table S2-4 were also plotted against the solvent polarity, π* (Figure 3. S12b-d). Nevertheless, linear relationship was not observed for S-**DR4c-e** cases.

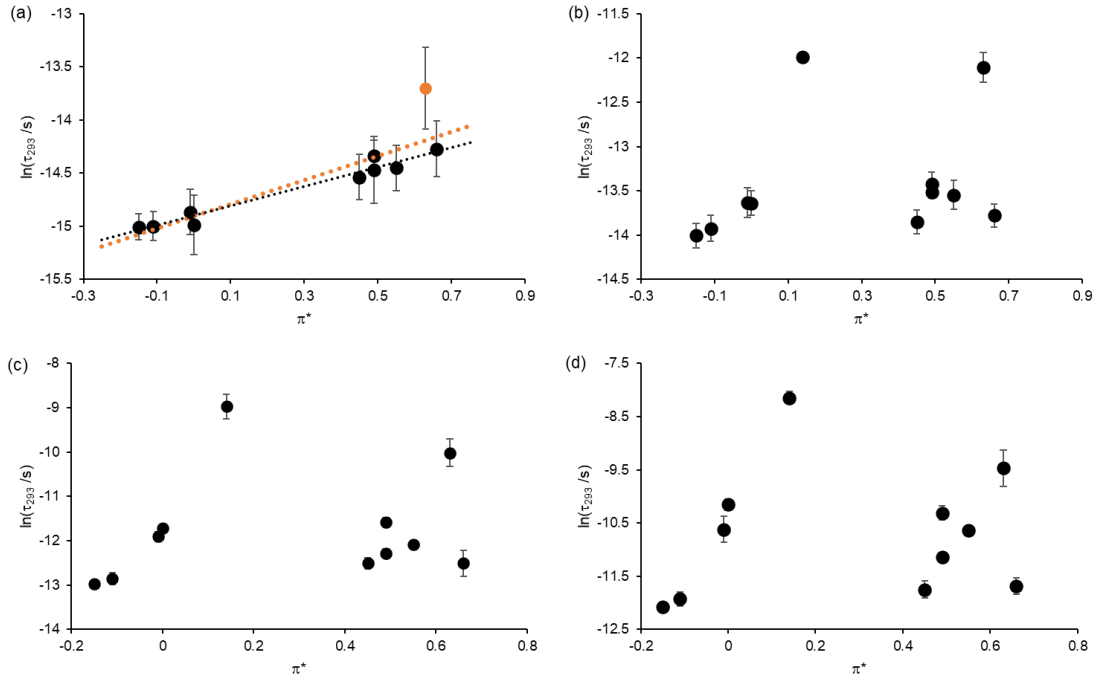

Figure 3.S12. (a) Solvent polarity (π*) dependency of the lifetime of S-**DR4a**. Black: all solvent in Table 3. S1 except GTA (same as Figure 3.1b), R^2 = 0.9594, Orange: all solvent in Table S1, R^2 = 0.7865. (b-d) Solvent polarity dependency of the lifetime of (b) S-**DR4c**, (c) S-**DR4d**, and (d) S-**DR4e**.

Section 3.5.6. NMR analysis of photoproduct of S-**DR4e** in DCMP

AZ4e (3 mg, 3 μmol) were dissolved in degassed DCMP (0.3 ml). This solution was irradiated by the 365 nm LED lamp, and the reaction was monitored by ^{1}H-NMR. To compare the photo product in benzene, which is *trans*-**CP4e**, **AZ4e** were irradiated in C_6D_6 by the 365 nm LED lamp. Then photo product in C_6D_6 were evaporated and dissolved in DCMP. Obtained ^{1}H NMR spectra were described as *trans*-**CP4e** in Figure 3.9e. These ^{1}H NMR spectra were measured on a Bruker ASCENDTM 400 spectrometer.

Section 3.5.7. Estimation the quenching constants of S-**DR4e** with molecular oxygen

The molecular fraction of oxygen x_1 in hexane, cyclohexane and paraffin were reported 1.96 $\times 10^{-3}$, 1.21×10^{-3} and 2.78×10^{-3} at 1 atm of oxygen.[27,28] Assuming the solvent density does not change with the dissolution of oxygen, the author estimated the saturated dissolution concentration of oxygen from the density of the solvent and the molecular weight of the solvent (Table 3. S5).

Table 3.S5. The molecular fraction and concentration of oxygen in solvents at saturated condition.

Solvent	$x_1 \times 10^3$	Density /g ml^{-1}	Molecular weight / g mol^{-1}	O_2 conc /mM
Hexane	1.96	0.66	86.18	15.0
Cyclohexane	1.21	0.78	84.16	11.2
Paraffin oil	2.78	0.88	405	6.05

By mathematical transformation, the result of regression analysis for Figure 3.11b was transformed to $k_{obs} = k_0 + 1.071\ (k_0/C_{sat}) \times C$: saturated oxygen concentration in DCMP and oxygen concentration at the condition was presented as C_{sat} and C, respectively. From this equation, quenching constant k_q were assigned to $1.071(k_0/C_{sat})$. The rate constant k_0 were calculated to 3.60×10^3 s^{-1} from the lifetime of S-**DR4e** under nitrogen condition in DCMP. When the saturated oxygen concentration in DCMP were estimated to 5, 10, 20 and 30 mM, quenching constant k_q were calculated to 7.71×10^5, 3.85×10^5, 1.93×10^5, and 1.28×10^5 M^{-1} s^{-1}, respectively.

Section 3.5.8. High pressure experiments

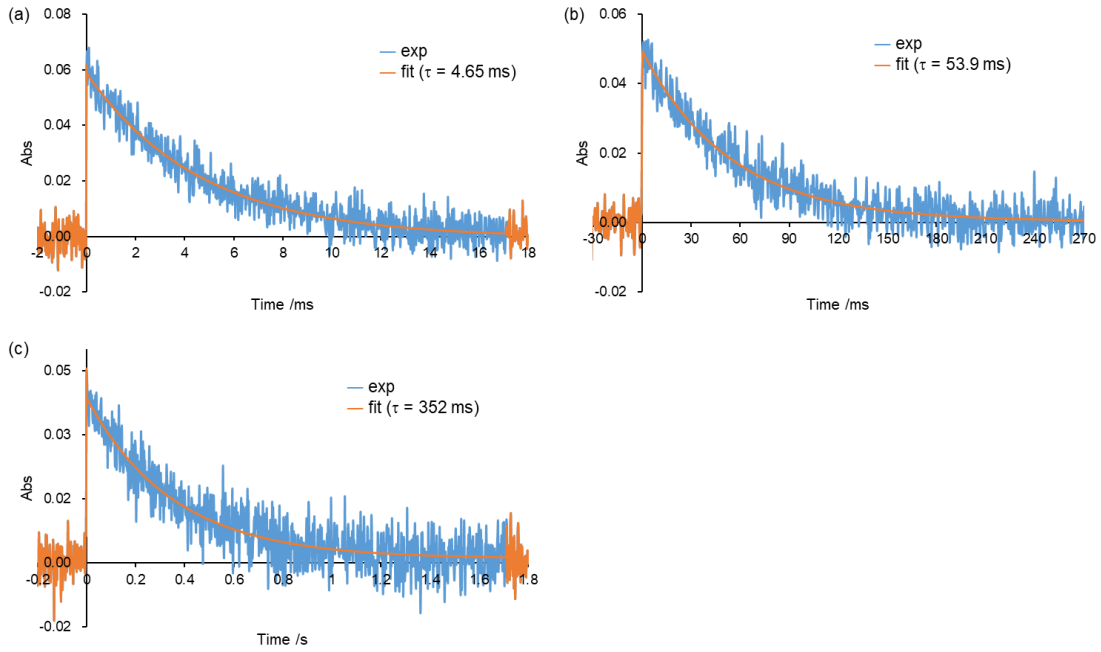

Figure 3.S13. Time profile of S-**DR4e** in DCMP under (a) 1000 , (b) 2000, (c) 3000 atm at 293 K.

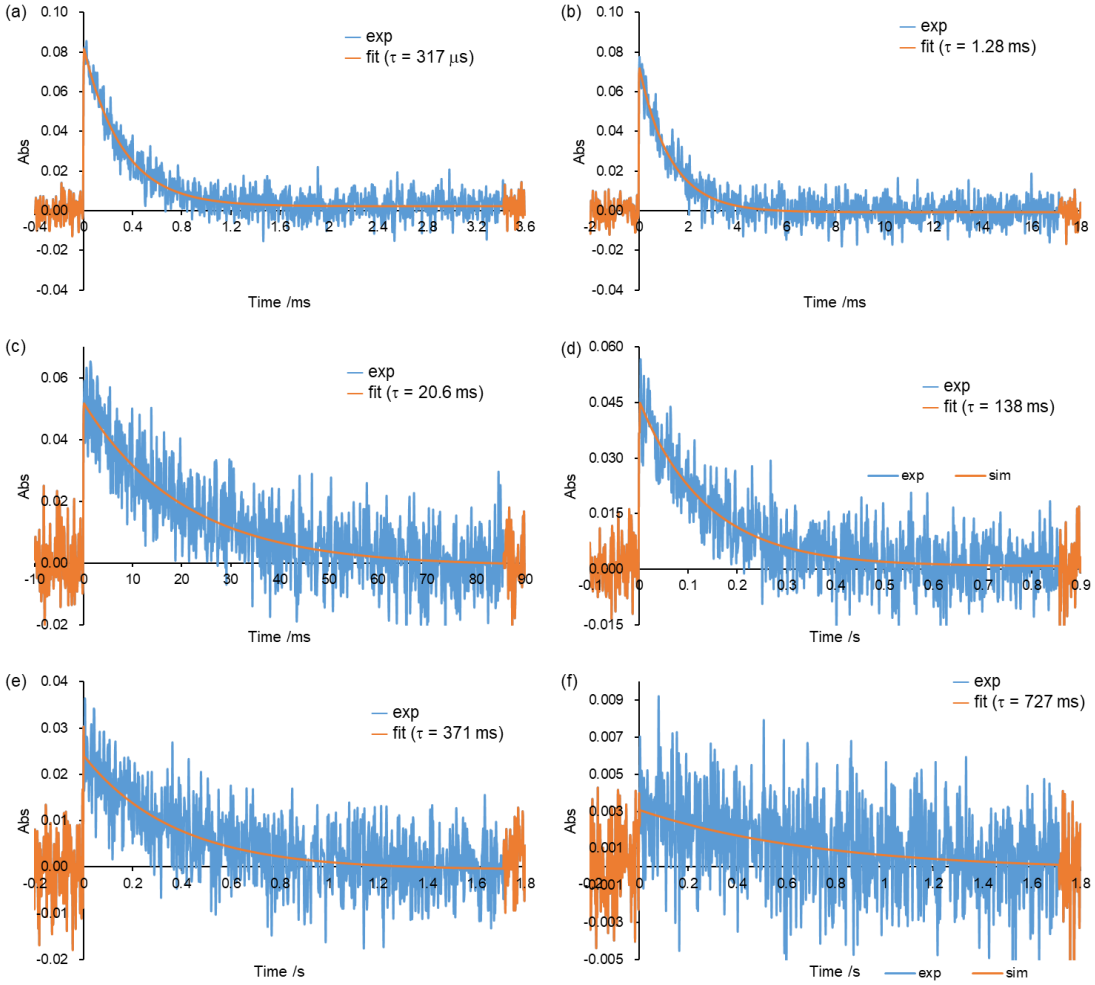

Figure 3.S14. Time profile of S-**DR4e** in GTA under (a) 1000 , (b) 2000, (c) 3000, (d) 4000 , (e) 5000, (f) 6000 atm at 293 K.

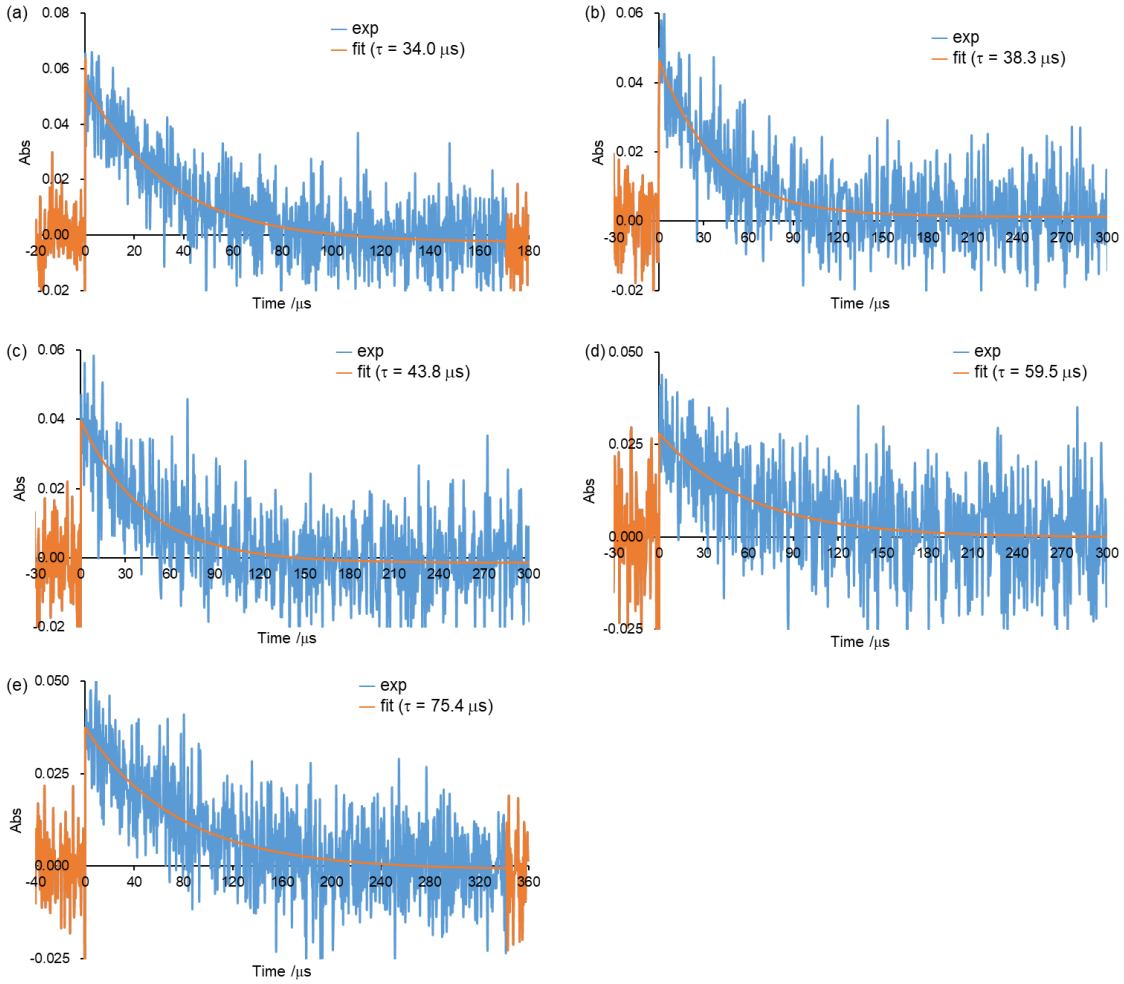

Figure 3.S15. Time profile of S-**DR4e** in MCH under (a) 250, (b) 500, (c) 750, (d) 1000, (e) 1250 atm at 293 K.

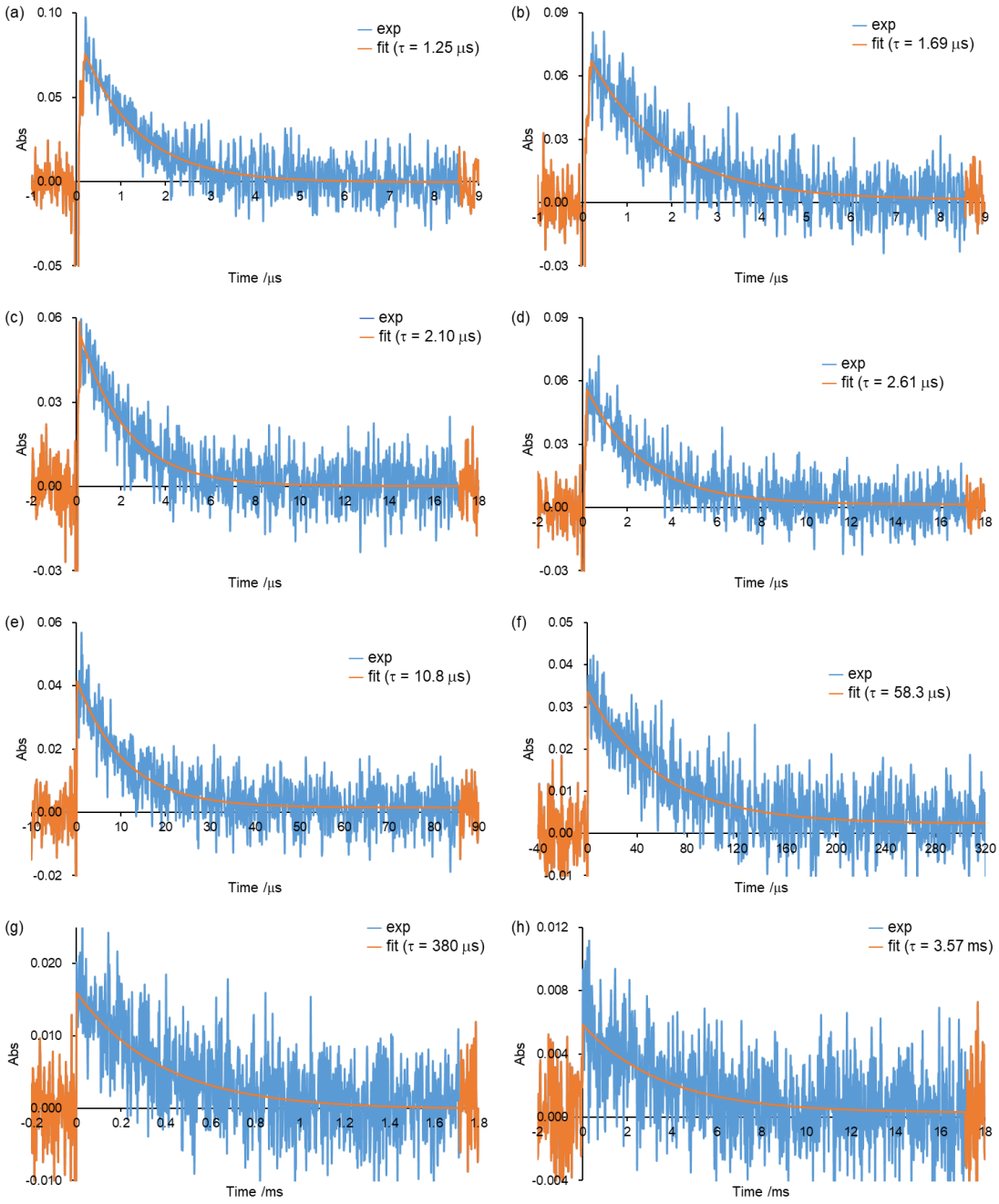

Figure 3.S16. Time profile of S-**DR4a** in GTA under (a) 250, (b) 535, (c) 750, (d) 1000, (e) 2000, (f) 3000, (g) 4000, (h) 5000 atm at 293 K.

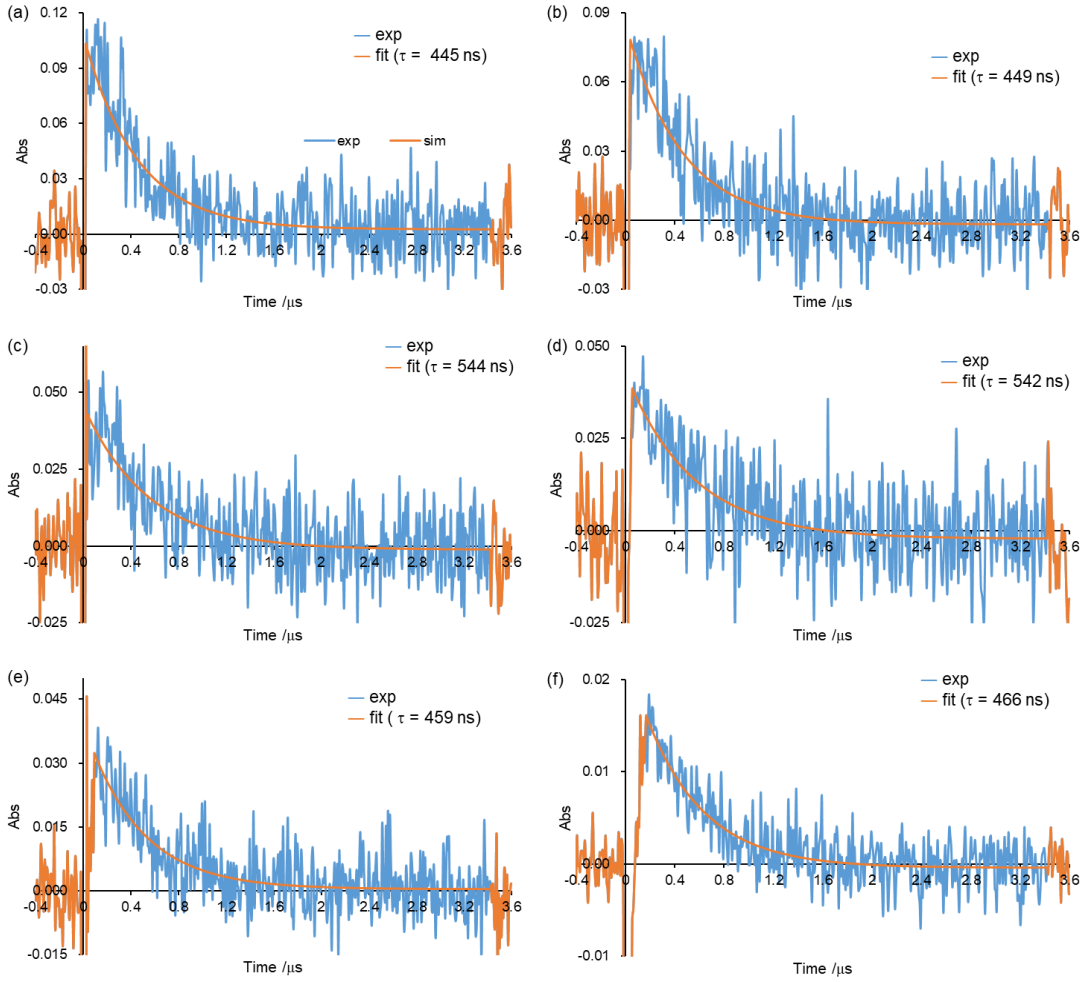

Figure 3.S17. Time profile of S-**DR4a** in MCH under (a) 250, (b) 535, (c) 750, (d) 1000, (e) 1250, (f) 1500 atm at 293 K.

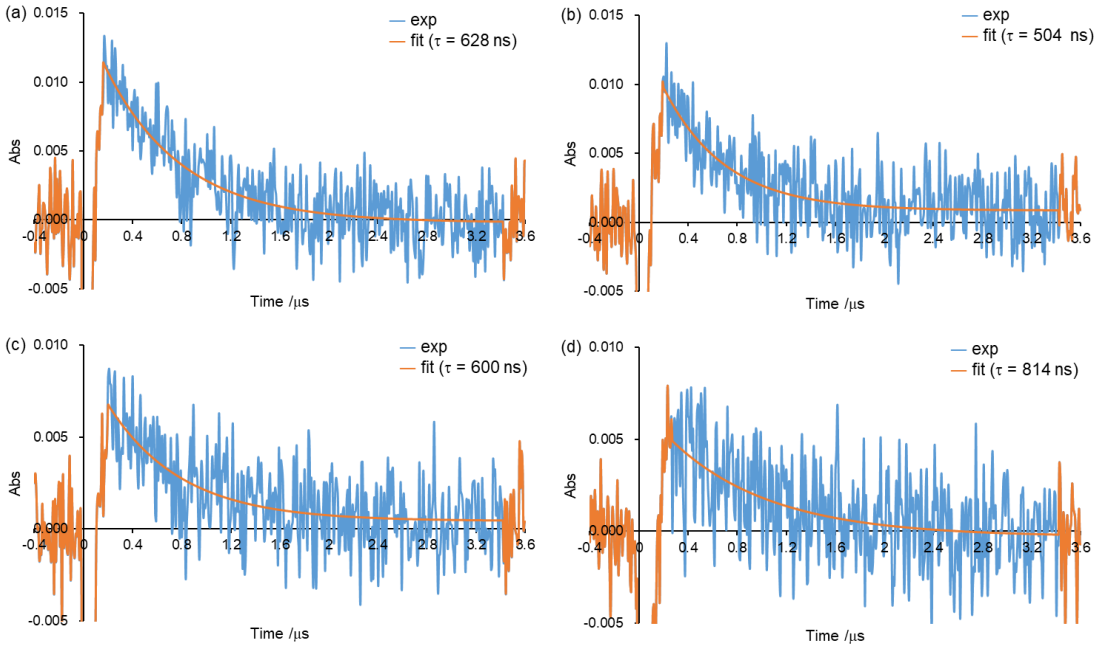

Figure 3.S18. Time profile of S-**DR4a** in MCH under (a) 250, (b) 535, (c) 750, (d) 1000, (e) 1250, (f) 1500 atm at 293 K.

Section 3.5.9. Determination of solvent polarity parameter, π*

The UV-vis absorption spectra of 4-nitro-anisole were measured in MCH (Methyl Cyclohexane) and DCMP (Figure 3. S18). From the wavelength of absorption maximum, λ_{max}, π* values of each solvent were calculated from the literature equation, $10^4/\lambda_{max} = 34.17 - 2.41\ \pi^*$. [12] These UV-vis absorption measurements were recorded on a SHIMADZU UV-3600 Plus spectrometer.

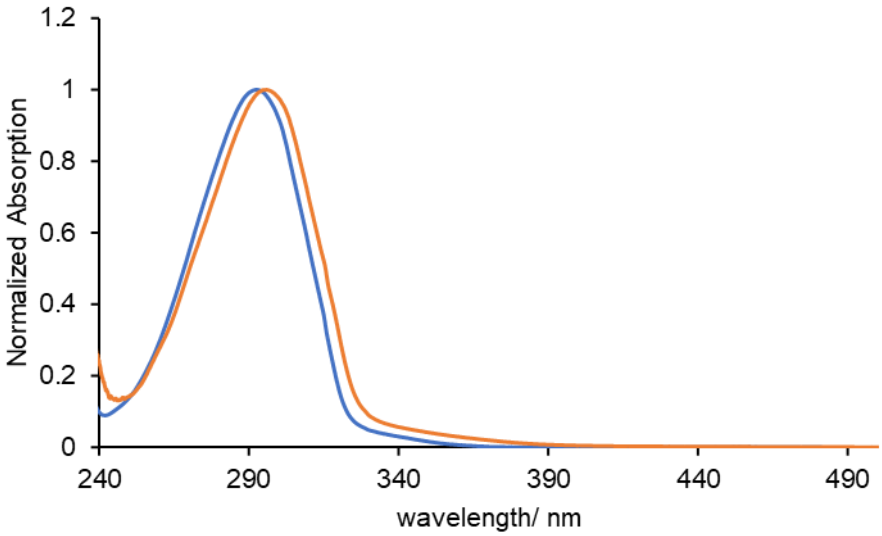

Figure 3.S19. UV-vis absorption spectra of 4-nitro-anisole in MCH (Blue), and DCMP(Orange).

Table 3.S6. Determination of π* for MCH and DCMP.

Solvent	λ_{max} /nm[a]	π*
MCH	292.55	–0.01
DCMP	295.55	0.14

[a] Absorption maximum λ_{max} of 4-nitro-anisole in each solvents.

Section 3.5.10. Calculation of the pressure dependency of solvent viscosity for methyl cyclohexane

The pressure dependency of the solvent viscosity for methyl cyclohexane at 293 K were examined by Zéberg-Mikkelsen *et. al*.[22] And these data were fitted with equation, $\ln \eta = \ln \eta_0 + \alpha P$, by regression analysis (Figure 3. S19). From these parameters, α and η_0, solvent viscosity for each pressure were calculated (Table S6).

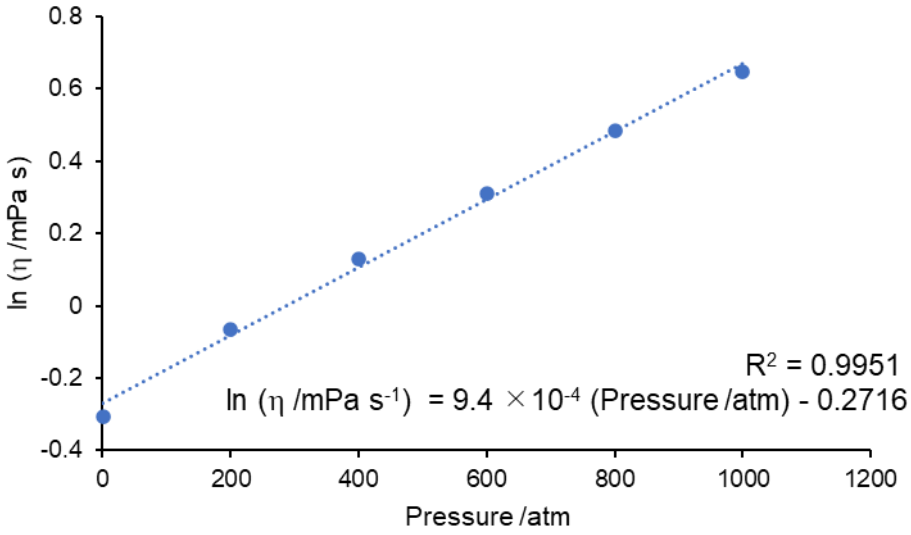

Figure 3.S20. Pressure dependency of the viscosity for methyl cyclohexane.

Table 3.S7. Estimated Viscosity for methyl cyclohexane at each Pressure.

Pressure /atm	1	250	500	750	1000	1250
ln (η /mPa s)	–0.2707	–0.0359	0.1999	0.43566	0.67142	0.90718
η /mPa s	0.763	0.965	1.22	1.54	1.96	2.48

References

1 E. D. Hughes and C. K. Ingold, *J. Chem. Soc.*, 1935, 244.

2 M. Abe, W. Adam, T. Heidenfelder, W. M. Nau and X. Zhang, *J. Am. Chem. Soc.*, 2000, **122**, 2019–2026.

3 M. Abe and R. Akisaka, *Chem. Lett.*, 2017, **46**, 1586–1592.

4 T. Asano, *Pure Appl. Chem.*, 1999, **71**, 1691–1704.

5 J. Schroeder, J. Troe and P. Vöhringer, *Chem. Phys. Lett.*, 1993, **203**, 255–260.

6 L. Nikowa, D. Schwarzer, J. Troe and J. Schroeder, *J. Chem. Phys.*, 1992, **97**, 4827–4835.

7 J. C. M. Kistemaker, A. S. Lubbe, E. A. Bloemsma and B. L. Feringa, *ChemPhysChem*, 2016, **17**, 1819–1822.

8 A. S. Lubbe, J. C. M. Kistemaker, E. J. Smits and B. L. Feringa, *Phys. Chem. Chem. Phys.*, 2016, **18**, 26725–26735.

9 Y. Goto, T. Takahashi, Y. Ohga, T. Asano, M. Hildebrand and N. Weinberg, *Phys. Chem. Chem. Phys.*, 2003, **5**, 1825–1830.

10 H. A. Kramers, *Physica*, 1940, **7**, 284–304.

11 R. Akisaka, Y. Ohga and M. Abe, *Phys. Chem. Chem. Phys.*, 2020, **22**, 27949–27954.

12 M. J. Kamlet, J. L. Abboud and R. W. Taft, *J. Am. Chem. Soc.*, 1977, **99**, 6027–6038.

13 K. Dimroth, C. Reichardt, T. Siepmann and F. Bohlmann, *Justus Liebigs Ann. Chem.*, 1963, **661**, 1–37.

14 C. Reichardt, *Solvents and Solvent Effects in Organic Chemistry*, Wiley, 2003.

15 T. Asano, K. Cosstick, H. Furuta, K. Matsuo and H. Sumi, *Bull. Chem. Soc. Jpn.*, 1996, **69**, 551–560.

16 T. Asano, K. Matsuo and H. Sumi, *Bull. Chem. Soc. Jpn.*, 1997, **70**, 239–244.

17 K. Tamura, Y. Ogo and T. Imoto, *Chem. Lett.*, 1973, **2**, 625–628.

18 R. Akisaka and M. Abe, *Chem. – An Asian J.*, 2019, **14**, 4223–4228.

19 T. Asano and T. Okada, *J. Phys. Chem.*, 1984, **88**, 238–243.
20 C. Reichardt, *Chem. Rev.*, 1994, **94**, 2319–2358.
21 G. Li, H. Chi, Y. Guo, W. Fang and S. Hu, *J. Chem. Eng. Data*, 2013, **58**, 3078–3086.
22 C. K. Zéberg-Mikkelsen, M. Barrouhou, A. Baylaucq and C. Boned, *Int. J. Thermophys.*, 2003, **24**, 361–374.
23 N. G. Tsierkezos, M. M. Palaiologou and I. E. Molinou, *J. Chem. Eng. Data*, 2000, **45**, 272–275.
24 F. Chen, Z. Yang, Z. Chen, J. Hu, C. Chen and J. Cai, *J. Mol. Liq.*, 2015, **209**, 683–692.
25 H. Djojoputro and S. Ismadji, *J. Chem. Eng. Data*, 2005, **50**, 727–731.
26 N. F. Gajardo-Parra, M. I. Campos-Franzani, A. Hernández, N. Escalona and R. I. Canales, *J. Chem. Eng. Data*, 2020, **65**, 2032–2043.
27 R. Battino, H. L. Clever and C. L. Young, in *Oxygen and Ozone*, Elsevier, 1981, vol. 7, pp. xiii–xviii.
28 In *Oxygen and Ozone*, Elsevier, 1981, pp. 214–260.

Chapter 4.
Summary and outlook

The construction of the original π system is the key to developing organic molecules with a notable feature. Generally, ethylene, the smallest π bonding molecule, has a fixed two carbon bond length because they have a rigid σ bond. It was expected that the π bonding without σ bonding, π single bond, would have an extremely small HOMO-LUMO gap and play role in organic chemistry. Theoretically, the generation of π single bond molecules was estimated using 1,3-diradical in four or five-membered ring systems with substitution of electron withdrawing group at the C2 position. Furthermore, several researchers reported the isolation of π single bonding molecules. However, these isolated π single-bonded molecules had hetero atoms at radical centers. To expand the chemistry of π single bonds in pure organic chemistry, the author tried to stabilize singlet cyclopentane 1,3-diyls with bulky substituents.

The effect of introducing the bulky groups to phenyl ring in cyclopentane-1,3-diradical, S-**DR2**-**4** was examined theoretically and experimentally. The theoretical calculation for the singlet diradical S-**DR2** allows the author to introduce the bulky Tip groups at the phenyl rings' meta position. The azo alkane **AZ3**,**4** were synthesized via two essential reactions, [4+1] cycloaddition reaction between tetrazine and diethoxy carbene, and Suzuki-Miyamura cross-coupling. The generation of singlet diradical S-**DR3**,**4** in benzene by photo denitrogenation reaction was confirmed by the transient absorption spectra, which have an absorption maximum around 600 nm. The NMR measurements, cryogenic experiment, and detail analysis of activation energy confirmed the decay process of S-**DR3**,**4** should be the radical-radical bond formation process forming *cis*-**CP3**,**4**. The introduction of bulky substituents extended the lifetime of S-**DR3**,**4**. Among them, the replacement of hydrogen to Tip groups extended the lifetime of S-**DR4** at 293 K by 45 times. The increasing of activation energy and activation enthalpy concluded the kinetic stabilization of singlet diradical S-**DR3**,**4**. The differences between the activation energy of S-**DR3** and S-**DR4** were decreased by increasing the bulkiness of the aryl groups. This result implies the change of the activation energy's main contribution from the steric

repulsion between the extra cyclopentane ring and alkoxy group to that between the aryl group and alkoxy group. The low-temperature NMR experiment helps the understanding of another reactivity of S-**DR4e**, the bond formation via *trans*-**TS4e**.

The stabilization of S-**DR4** was also observed by unusual solvent effect, dynamic solvent effect. In general organic solvents, the lifetime of parent singlet diradical S-**DR4a** were following the solvent polarity. It is because the singlet diradical S-**DR4a** has a zwitterionic resonance structure **ZI4a**. However, by introducing the bulky substituents at the meta position of the phenyl ring, the lifetimes of S-**DR4** were changed to follow the solvent viscosity. By using a highly viscous solvent, glycerol triacetate (GTA), the lifetime of S-**DR4a** was also affected by solvent viscosity. Especially in 2,4-dicyclohexyl-2-methyl pentane (DCMP), the lifetime of S-**DR4e** was reached to sub milliseconds scale, 0.29 ms, and depends on the concentration of oxygen. Although the viscosity dependencies of the lifetime of S-**DR4d**,**e** were almost the same, the difference between the lifetime of S-**DR4d** and that of S-**DR4e** inform the importance of the bulky substituents under high viscous conditions. The detail analysis of the activation parameter and product analysis confirm that the degradation process of the singlet diradical S-**DR4** in high viscous conditions under inert atmosphere was still the bond formation process. The pressure dependency on the lifetime of S-**DR4a**,**e** were also explained the solvent dynamic effect on that because the solvent viscosities were increased by increasing pressure. Finally, the lifetime of S-**DR4e** beyond the milliseconds time scale, τ = 2000 ms, in extreme viscous condition, in DCMP under 4000 atm.

These studies encourage further experiments for the 2,2-dialkoxy-cyclopentane-1,3-diradical and other reactive molecules. Because the lifetime of S-**DR3**,**4e** was still longer than that of S-**DR3**,**4d**, the introducing bulkier groups than Tip groups at the meta position of the phenyl ring in S-**DR3** or **4** will extend the lifetime of that. Other measurements, such as IR or Raman spectroscopy analysis, under the intense viscous condition for S-**DR4e** will help understand the chemistry of π single bonding. The

stabilization by dynamic solvent will adopt the other unstable molecule, which was decomposed by the intramolecular reaction.

Acknowledgement

The studies described in this thesis have been performed under the direction of Professor Manabu Abe at the Department of Chemistry, Graduate School of Science, Hiroshima University, from April 2016 to March 2021.

The author is deeply grateful to Professor Manabu Abe for his helpful discussions, experimental guidance, hearty advice, contribution to revising the author's manuscripts and encouragement through the course of the studies. The author would like to express his deep gratitude to Dr. Sayaka Hatano and Dr. Ryukichi Takagi for the helpful discussions, experimental guidance, and considerate suggestions.

The author wishes to thank the member of Reaction Organic Chemistry laboratory. Especially, Dr. Jianfei Xue, Dr. Shouhei Yoshidomi, Mr. Yoshiki Fujita, Mr. Keita Ohnishi, Mr. Misaki Matsumoto, Mr. Youhei Chitose, Mr. Norito Kadowaki, Mr. Ayato Yamada, Mr. Zhe Wang, Ms. Ryoko Oyama, Mr. Yuki Miyazawa, Mr. Kazunori Okamoto, Mr. Masaki Matsui, and Mr. Ryo Murata are appreciated for their technical advice, sudden discussions, and helpful suggestion.

The author thankful to Professor Junji Ichikawa, Associate Professor Kohei Fuchibe and Dr. Takeshi Fujita for teaching him the research of organic synthesis at the University of Tsukuba as bachelor course students.

The author thankful to Professor Yasushi Ohga and Mr. Toru Takahashi for their helpful discussion about the dynamic solvent effect and kind assistance of pressure experiments at Oita University.

The author appreciates the suggestion and discussion about this research from Professor Takeharu Haino, Professor Tsutomu Mizuta and Emeritus Professor Yohsuke Yamamoto in the organic group seminars of Hiroshima University.

The author also thanks Ms. Tomoko Amimoto from N-BARD, Hiroshima University, who did the contribution to the HRMS measurements.

The author wishes to thank Dr. Naoto Suzuki, Dr. Yota Watabe, Dr. Shogo Morisako, Dr. Daisuke Shimoyama, Dr. Tomohito Morosaki, Dr. Yuki Suda, Mr. Yohsuke Ito, Mr. Takumi Oishi, Mr. Kazuki Nakanishi, Mr. Taiki Imagawa, Mr. Naoyuki Hisano, Ms. Natsumi Nitta, Mr. Junichi Usuba and Mr. Tomohiro Hidano for their fruitful discussion, kind encouragement and continuous friendship.

The author thanks Mr. Taiki Yoshikawa, Mr. Keisuke Yoshinami, Mr. Yuji Takagi, Ms. Rio Maruyama, Mr. Kei Maruyama, Mr. Kazuki Nishida, Mr. Yasutaka Irie, Ms. Saki Iwai, Mr. Takuya Date and Ms. Saya Aoki for their kind friendship.

Finally, I wish to express my deepest gratitude to my parent, Tomonori Akisaka and Noriko Akisaka, and my sister, Hikari Akisaka, for their kindly continuous encouragement and for providing a very comfortable environment, which allows me to concentrate on my research.

March 2021
Rikuo Akisaka

List of Publication

Articles

(1) Bulky Substituent Effect on Reactivity of Localized Singlet Cyclopentane-1,3-diyls with π-Single Bonding (C-π-C) Character. Rikuo Akisaka and Manabu Abe, *Chem. Asian J.*, **2019**, *14*, 4223-4228.

(2) Dynamic solvent effect in radical–radical coupling reactions: an almost bottleable localised singlet diradical. Rikuo Akisaka, Yasushi Ohga and Manabu Abe, *Phys. Chem. Chem. Phys.* **2020**, *22*, 27949-27954.

Supplemental Articles

(1) Is π-Single Bonding (C-π-C) Possible? A Challenge in Organic Chemistry. Manabu Abe and Rikuo Akisaka, *Chem. Lett.* **2017**, *46*, 1586-1592.

(2) Pinpoint-fluorinated polycyclic aromatic hydrocarbons (F-PAHs): Syntheses of difluorinated subfamily and their Properties. Kohei Fuchibe, Kento Shigeno, Nan Zhao, Hiromichi Aihara, Rikuo Akisaka, Toshiyuki Morikawa, Takeshi Fujita, Kie Yamakawa, Toshihiro Shimada, Junji Ichikawa, *J. Fluor. Chem.* **2017**, *203*, 173–184.

(3) Kinetic Stabilization of Localized Singlet Diradicaloids With π Single Bonding Character. Rikuo Akisaka and Manabu Abe, In *Kinetic Control in Synthesis and Self-Assembly;* Elsevier, **2019**; 1–20.

(4) Impact of the macrocyclic structure and dynamic solvent effect on the reactivity of a localised singlet diradicaloid with π-single bonding character. Zhe Wang, Rikuo Akisaka, Sohshi Yabumoto, Tatsuo Nakagawa, Sayaka Hatano and Manabu Abe, *Chem. Sci.* **2021**. *12*, 613-625.